Application of Low Melt Alloys as Compliant Thermal Interface Materials: A Study of Performance and Degradation under Thermal Duress

by

Chandan Kumar Roy

A dissertation submitted to the Graduate Faculty of
Auburn University
in partial fulfillment of the
requirements for the Degree of
Doctor of Philosophy

Auburn, Alabama
August 6, 2016

Keywords: Thermal interface material, Thermal conductivity; Thermal resistance; Thermal aging; Thermal cycling

Approved by

Daniel K. Harris, Chair, Associate Professor, Mechanical Engineering
Roy W. Knight, Assistant Professor, Mechanical Engineering
Daniel Mackowski, Associate Professor, Mechanical Engineering
Bertram Zinner, Associate Professor, Mathematics and Statistics
Vishwani Agrawal, Professor, Electrical and Computer Engineering

Abstract

Thermal interface materials (TIMs) are a crucial part of thermal management in micro-electronics and often can account for a significant portion of the overall thermal budget. Generally, materials with high thermal conductivities and low thermal resistances are ideal candidates for the application as a TIM. Low melt alloys (LMAs) are promising TIM candidate materials due their inherent high thermal conductivities, good wetting properties, and their mechanical compliance addressing the coefficient of thermal expansion mismatch concerns. In this work, the interstitial thermal performance of three different alloys, alloy 1 (75.5 Ga, 24.5 In, melting point (MP): 16^{o}C), alloy 2 (100 Ga, MP: 30^{o}C), and alloy 3 (51 In, 32.5 Bi, 16.5 Sn, MP: 60^{o}C) has been tested using widely accepted ASTM D-5470 standard methodology. The thermal performance of LMAs was measured in terms of thermal resistance (temperature drop across the LMA joint per unit heat flux). The effect of interfacial pressure on the thermal resistance was also investigated within the range of 34.5 to 345 kPa. The reliability of LMA interfaces was investigated in terms of high temperature aging (130^{o}C), thermal cycling (-40^{o}C to +80^{o}C and -40^{o}C to +125 ^{o}C), and highly accelerated stress testing (85^{o}C and 85% relative humidity). The interactions of alloys with various substrate materials (copper, nickel, and tungsten) were studied by coating a thin layer of nickel (about 5 µm) and a thin layer of tungsten (about 2 µm) onto the bare copper surfaces comprising the interfacial joint. Finally, to compare the performance of LMAs, some commercial TIMs (greases, phase change materials, and thermal pads) were also tested using the same methodology and apparatus.

Acknowledgments

I would like to thank my advisory committee Dr. Roy Knight, Dr. Daniel Mackowski, Dr. Bertram Zinner and Dr. Vishwani Agrawal.

It is an honor for me to thank my advisor and mentor Dr. Daniel Harris for providing me the opportunity to work in this project and believing in me. His proper guidance and amicable disposition encouraged me all the time throughout my dissertation work. Without his support, this work would not have been possible.

I would like to thank Dr. Roy Knight and Dr. Sushil Bhavnani for their important suggestions and feedback during this research.

Finally, I would like to thank my family members specially my wife and parents. Without their love and encouragement, I could not able to continue my study.

Table of Contents

List of Tables

List of Figures

List of Abbreviations

BLT	Bond Line Thickness
CNT	Carbon Nanotube
CTE	Coefficient of Thermal Expansion
HAST	Highly Accelerated Stress Testing
IHS	Integrated Heat Spreader
IMC	Intermetallic Compound
LMA	Low Melt Alloy
MWCNT	Multi-walled Carbon Nanotube
PCM	Phase Change Material
PEG	Polyethylene Glycol
RSD	Relative Standard Deviation
RT	Room Temperature
TIM	Thermal Interface Material

Symbols

A	Area (m^2)
d	Distance (m)
I	Current (amp)
k	Thermal Conductivity (W/m^oC)

L	Thickness (m)
l	Location of Probe (mm)
q	Heat Flow (W)
q"	Heat Flux (W/cm^2)
R	Thermal Resistance ($cm^{2o}C/W$)
T	Temperature (^oC)
U	Uncertainty
V	Electric Potential (Volts)

Subscripts

avg	Average
cond	Conduction
th	Thermal

Chapter 1 : Introduction

1.1 Thermal interface material

When two solid surfaces are brought into contact, surface asperities (roughness, flatness) limit their actual contact to 1-2% of the apparent contact at a lower pressure [1]. The remaining interspace is filled mostly with air which has a poor thermal conductivity (0.026 W/m^{o}C at room temperature). A magnified bare contact between two solid surfaces is shown in Figure 1.1a. Heat transfer across these solid contacts would result in significant temperature drop at the interface. By improving the quality of these contacts, the heat transfer can be enhanced. One option is to apply a very high pressure, which would crush much of the peaks and increase the area of contact; however, the application of pressure is somewhat restricted considering the load constraints of the components attached [2]. Furthermore, mating surfaces can be polished to a high degree to remove much of the roughness and waviness. This is not a good option from an economic point of view because the surface preparation would make the components expensive. Another feasible option is to place a highly conductive material at the interface, which would fill those gaps at a lower pressure by displacing air from the interface as shown in Figure 1.1b. This material, which is placed at the interface between two objects to facilitate the heat transfer, is known as thermal interface material (TIM). An ideal TIM would fill all the microscopic irregularities that exist at the interface. However, an actual TIM will leave some air gaps at the interface depending on the conformability of the TIM.

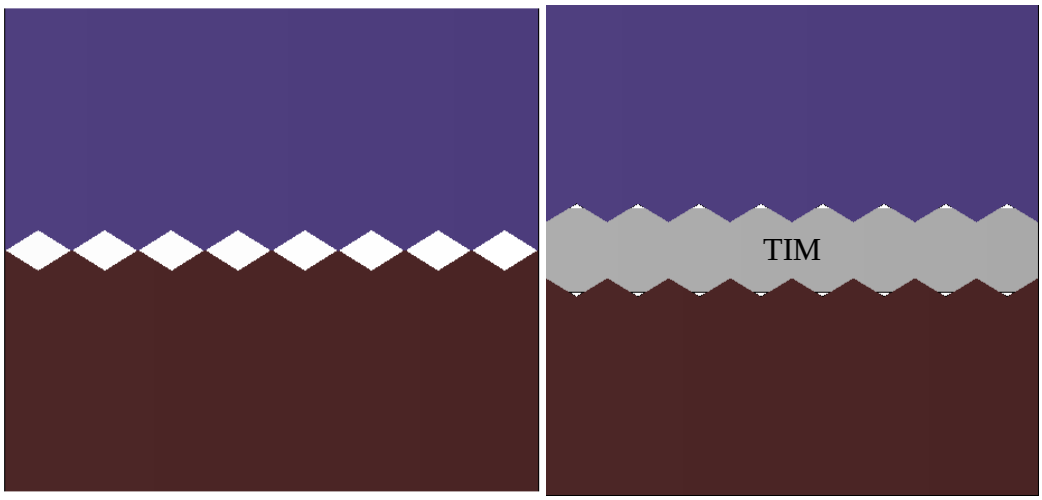

(a) (b)

Figure 1.1: (a) A magnified view of bare contact between two solid surfaces (b) Contact between two solid surfaces using a TIM

1.2 Contact resistance

Contact resistance arises due the incomplete contact between two solid objects. Because of the insufficient contact (mostly due to the surface asperities), the heat transfer at the interface is hindered. Heat can transfer in two ways through such interface. One way is the conduction through the actual contact points and the other way is the conduction and/or radiation through the gaps. Thus, the contact resistance is viewed as the equivalent of two parallel resistances due to two heat flow paths [3]. In general, rough and non-flat surfaces induce more contact resistance compared to the smooth and flat surfaces. As such, the contact resistance can be minimized by increasing the area of contact, which in turn enhances the heat transfer.

1.3 Thermal resistance to heat conduction

It is well known that for one dimensional, steady state heat transfer in a plane wall with no internal heat generation and constant thermal conductive, the temperature varies linearly with the distance as shown in Figure 1.2 [3]. The Fourier's law can be written as

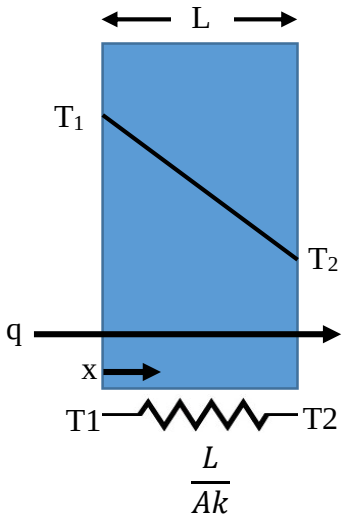

Figure 1.2: Heat transfer and the temperature distribution through a plane wall

$$q = -\mathrm{kA}\frac{\mathrm{dT}}{\mathrm{dx}} = \mathrm{kA}\frac{\mathrm{T_1} - \mathrm{T_2}}{\mathrm{L}} \tag{1-1}$$

Where: k is the thermal conductivity of the wall material, A is the area available for heat transfer, T_1 and T_2 are the temperature of the wall, and L is the thickness of the wall. From the Fourier's law, the thermal resistance to heat conduction (R_{cond}) is defined as

$$\mathrm{R_{cond}} = \frac{\mathrm{L}}{\mathrm{Ak}} = \frac{\mathrm{T_1} - \mathrm{T_2}}{\mathrm{q}} \tag{1-2}$$

The conduction resistance is analogous to electrical resistance for flow of current. The conduction resistance arises due to the finite thermal conductivity of the material through which heat flows. The material resist the flow of heat depending on its thermal conductivity.

1.4 Performance of TIM

The thermal performance of the TIM is characterized by the thermal conductivity and thermal resistance. The total thermal resistance at the interface is the combination of conduction resistance of the TIM and the two contact resistances at two mating surfaces as shown in Figure 1.3.

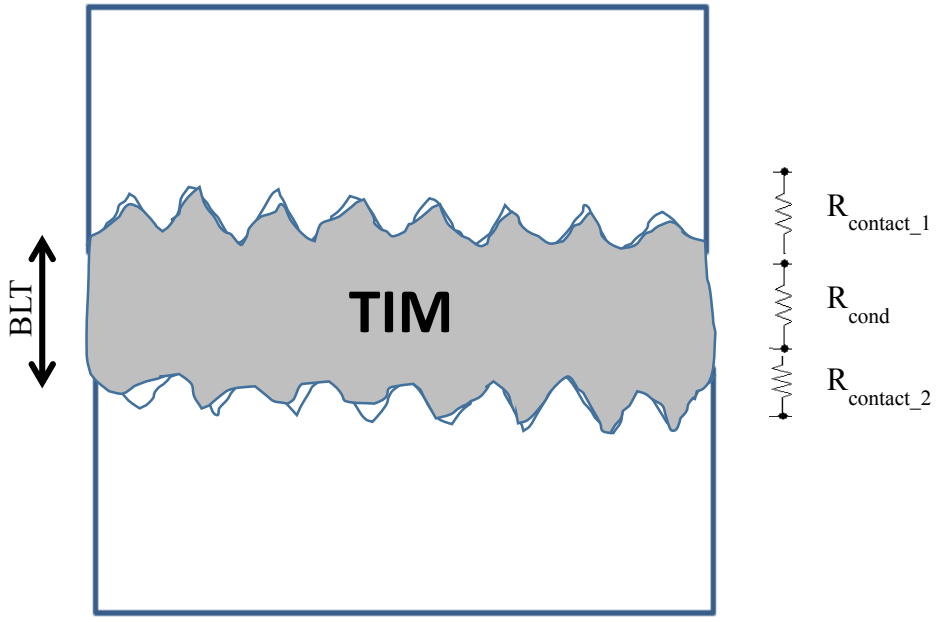

Figure 1.3: Interfacial thermal resistance between two solid objects after the application of TIM

The total interfacial thermal resistance can be expressed as,

$$R_{interface} = R_{contact\_1} + R_{contact\_2} + R_{cond} \quad (1\text{-}3)$$

Where: $R_{contact\_1}$ and $R_{contact\_2}$ are the contact resistances of two contact surfaces with the TIM and $R_{cond.}$ is the conduction resistance of the TIM which can be expressed as,

$$R_{cond} = \frac{BLT}{k} \quad (1\text{-}4)$$

Combining the two contact resistances into one, the interfacial thermal resistance is expressed as,

$$R_{interface} = R_{contact} + \frac{BLT}{k} \quad (1\text{-}5)$$

Where: k is the thermal conductivity of the TIM and bond line thickness (BLT) is the thickness of TIM under operation. The ultimate goal is to find a TIM material that is compatible, reliable and offers lower interfacial thermal resistance. It is evident from the above relation (1-5) that a high conductivity material at a thin BLT would lower conduction resistance. For this reason, it is always expected for a TIM to be highly conductive and have a thin BLT. The contact resistances are highly dependent on the quality of the mating surfaces (surface roughness, flatness). In general, a rough, non-flat surface would result in a high contact resistance. In addition, the contact resistances also are a function of how well the TIM flows at the interface, filling the microscopic voids and other irregularities.

A desirable TIM should offer low thermal resistance at a thin BLT, high thermal conductivity, conformability at low to moderate pressures, good wetting properties, ease of manufacturing, and reasonable cost while also being environmentally and health friendly [2]. In addition to these properties, compliant TIMs must also be able to withstand the mechanical stresses resulting from the coefficient of thermal expansion (CTE) mismatches that occur between the adjoining materials (e.g. silicon-copper for processor-heat sink attachment). If the CTE strain overwhelms the mechanical properties of the TIM, the joint will ultimately fail. Therefore, high performing compliant TIMs are an essential design option for better thermal performance and improved reliability.

1.5 Application of TIM in thermal management

Thermal management plays a key role in electronics cooling as the power density continues to escalate and is expected to exceed 100 W/cm^2 (1 W/mm^2) [4].Therefore, international electronics manufacturing initiative (iNEMI) declared thermal management a research priority in

2013 [5]. One of the thermal management areas in electronics involves reducing the thermal resistance between the microprocessor chip and heat sink using TIMs. The function of the TIM is to transfer the heat effectively from the silicon die (or chip) to the heat sink. For lower power applications (<30 watts of power, typically used in laptops), the silicon die is directly attached to the heat sink via TIM as shown in Figure 1.4a. However, for medium to higher power (>30 watts of power, used in desktop and server applications), the die is connected with the heat sink via an integrated heat spreader (IHS), where two TIMs are used (Figure 1.4b). One is placed in between the die and IHS referred to as TIM1 and the other is in between IHS and the heat sink, known as TIM2 [1,4,6].

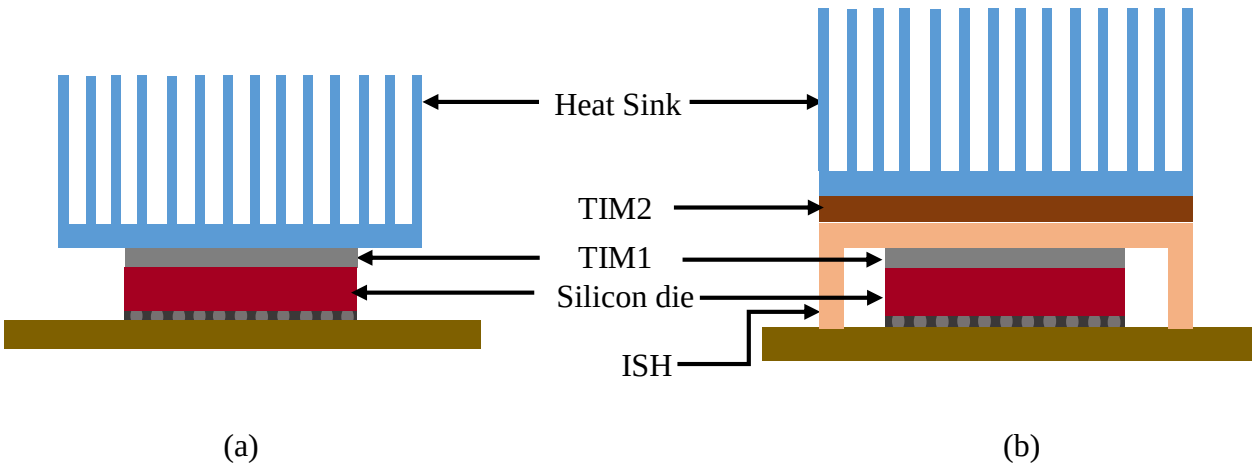

Figure 1.4: Low and high power electronics architecture (a) low power, typically used in laptop applications (b) high power, typically used in desktop and server applications

Chapter 2 : Literature Review

2.1 Traditional TIMs

In this section, thermal performance and practical concerns of conventional TIMs such as thermal grease, phase change material, thermal gel, and thermal pad are discussed.

2.1.1 Thermal grease

Greases are usually made by mixing silicone or hydrocarbon oil with conductive particles such as silver, zinc oxide, aluminum oxide, or boron nitride to enhance the thermal conductivity. Greases flow quite well at the interface and fill most of the interstitial voids and irregularities which would otherwise be filled with air. Traditional greases have thermal resistance ranging from 0.1 to 0.55 $cm^{2o}C/W$ [1,7]. Today's high performing grease such as ShinEtsu X23-7921-5, has a thermal conductivity >6 W/m^oC [8] and can offer thermal resistance as low as 0.065 $cm^{2o}C/W$ [8]. Dow Corning claimed the thermal resistance of their grease, TC 5026, to be as low as 0.032 $cm^{2o}C/W$; however, Wasniewski *et al*. [7] found the thermal resistance of the same compound to be about 0.2 $cm^{2o}C/W$ at a thickness of 38 μm. Gwinn and Web [2] reported thermal resistance of Arctic Silver grease was 0.018 $cm^{2o}C/W$. However, Wasniewski *et al*. [7] and Roy *et al*. [8] could not reproduce that result with the same grease; the reported thermal resistance was about 0.1 $cm^{2o}C/W$. Thus, there is a large discrepancy between the manufacturer's claimed resistance and experimental results by different investigators. Chung [9] reported that polyethylene glycol (PEG) based thermal pastes are superior to silicone-based pastes due to the low viscosity of PEG. PEG-

based paste can offer thermal resistance as low as 0.053 cm^{2}°C/W when mixed with boron nitride particles (optimum concentration was found as 18 vol.%). Although greases offer low thermal resistance, there are practical concerns with greases. Greases are messy, difficult to apply and remove during re-work, and have reliability issues such as pump out, phase separations, and dry out, which limit the use of greases as an efficient TIM over a nominal lifespan of use [1,2]. In addition, greases can be electrically conductive; excess grease that extrudes out of the interface can cause electrical shorts [2].

2.1.2 Phase change material

Phase change materials (PCMs) are made of highly conductive particles suspended in a base material, which can be a natural material such as fully refined paraffin, a polymer, a co-polymer, or a combination of these [10]. PCMs soften and start to flow above a certain temperature. The temperature at which the phase change occurs is called the phase change temperature or the transition temperature. When the temperature is below the transition point, PCMs act like solid materials, and above the transition point, the materials start to flow like greases as they begin to fill the irregularities exist at the interface. The typical phase change temperature of the commercial PCMs ranges from 50-90^{o}C [10]. Gwinn and Web [2] reported the thermal resistance of PCMs was in the range 0.14-0.58 cm^{2o}C/W, while Blezie [11] reported in the range 0.3-0.7 cm^{2o}C/W. Honeywell claimed the thermal resistance of their PCM (PTM 6000 & PTM 5000) to be as low as 0.07 cm^{2o}C/W. Roy *et al*. [12,13] reported the thermal resistance of Laird Tech. Tpcm 585 and Tpcm 5810 to be about 0.10 cm^{2o}C/W and 0.16 cm^{2o}C/W, respectively, at 345 kPa (50 psi). In general, PCMs have lower thermal conductivity and higher thermal resistance compared to the greases. Besides, PCMs can form a strong bond with the mating substrates, which hinder them from being applied between sophisticated components.

2.1.3 Thermal gel

Typically, gels consist of silicone oil, a cross-linker, and thermally conductive particles [14]. Gels have similar properties to greases before being cured. However, gels are cured to a partially cross-linked structure, which keeps them from pump-out and migration from the interface like greases. Blazie [11] reported that the thermal resistance of gels falls in the range 0.4-0.8 $cm^{2o}C/W$. Roy *et al*. [12] reported the thermal resistance of Chomerics Gel 30 was about 0.3 $cm^{2o}C/W$. Samson *et al*. [15] reported the thermal resistance of an undisclosed gel to be as low as 0.1 $cm^{2o}C/W$. Since gels are cured, they do not flow like greases and thus cannot offer thermal resistance as low as the greases. In addition, delamination (due to the CTE mismatch of mating substrates) is a major concern with gels [14].

2.1.4 Thermal pad

Thermal pads are composed of silicone or other similar elastomers loaded with thermally conductive ceramic particles, and may include a woven fiberglass or dielectric film reinforcement to improve handling [11]. Pads are easy to apply and remove and can be reused. They don't suffer from "pump-out" or "dry-out' problem as the greases do [16]. However, their thermal performance are not as good as greases, PCMs, and gels. In addition, moderate to high pressure is required to conform to the mating surfaces. Thermal resistance ranges from 1-3 $cm^{2o}C/W$ [11]. Wasniewski *et al*. [7] and Roy *et al*. [8] reported the thermal resistance of a Bergquist Gap pad 5000S35 was in the range 0.82-0.90 $cm^{2o}C/W$ at 345 kPa, whereas, the reported thermal resistance of a Bergquist Sil pad A2000 was about 1.65 $cm^{2o}C/W$ at 345 kPa [12].

2.2 Emerging TIMs

In this section, thermal performance and practical concerns of developing TIMs such as carbon nanotube, graphene, low melt alloys, metallic nanospring are discussed.

2.2.1 Carbon-based TIMs

Carbon-based materials such as carbon nanotubes (CNTs), can be used directly [7,17-19] or as a filler in composites [20-23] and graphene [24,25] have been investigated by many researchers as TIMs due to the extremely high thermal conductivity these materials. The reported thermal conductivity values are as high as 6600 W/m^{o}C [26], 3000 W/m^{o}C [19], 2000 W/m^{o}C [24] for individual single-walled, multi-walled CNTs, and graphene respectively. The lowest reported thermal resistance of MWCNTs was about 0.01 cm^{2}°C/W [19]. Researchers found that the dry contact between the CNTs and the mating substrate produced higher overall thermal resistance. This problem was addressed by using a solder [19] or a commercial TIM (PCM) [17] at the free ends of CNTs. Xu and Fisher [17] found the thermal resistance of dry contact of CNT arrays (Cu-CNT-Si) to be about 0.198 cm^{2o}C/W at 0.445 MPa (65 psi). However, they found that the addition of a PCM attached to the free end of CNT array (Cu-PCM-CNT-Si) substantially reduced the thermal resistance. At 0.35 MPa, the lowest resistance recorded was 0.052 cm^{2o}C/W, while the lowest resistance recorded for the PCM compound without CNTs was 0.162 cm^{2o}C/W under the same pressure [17]. Tong *et al*. [19] reported the thermal resistance was about 0.01 cm^{2o}C/W when CNT free-end was welded to the substrate via a thin indium layer. Even though anomalous increase in thermal conductivity of the composite was observed when CNTs were mixed with oil [20, 21], Fabris *et al*. [22] did not report any notable improvement in thermal resistance after mixing CNTs with commercial grease (Arctic Silver 5) and silicone oil.

One of the issues concerning the use of CNT films as TIMs includes the extremely high temperature (>600^{o}C) [27] needed for CNT fabrication since those temperatures do not allow for direct synthesis onto electronic devices. Another concern is the weak adhesion between the CNTs and their original substrate [27]. Not only does the poor bond between the CNTs and growth substrate contribute significantly to the thermal resistance at that interface, but it also affects long-term functionality. Zhu *et al*. [27] focused on resolving those problems by developing a CNT transfer process in their study, which was dubbed "CNT transfer technology." With that CNT transfer technology, Zhu *et al*. [27] reported the thermal resistance of CNT arrays was 0.43 cm^{2}°C/W. Cross *et al*. [18] reported the thermal resistance of transferred and bonded CNT array as low as 0.1 cm^{2}°C/W. Barako *et al*. [28] reported the thermal resistance was in the range of 0.28-0.71 cm^{2}°C/W and 0.15-0.50 cm^{2}°C/W when CNTs were bonded with indium and nanofoil, respectively. Melissa *et al.* [29] found the thermal resistance of transferred vertically aligned CNT array as 0.42 cm^{2}°C/W at 345 kPa (50 psi). Comparing the results, it can be observed that even though CNT transfer technology can potentially solve the high-temperature growth issue, the interfacial resistance of transferred CNT arrays is comparatively higher compared to the direct-grown CNTs. The CNT transfer technology is further needed to be improved to achieve a low overall thermal resistance. In general, design complexity and higher costs are associated with CNT-based TIMs. CNT-based TIMs have yet to appear as commercially available products.

Investigators [24,25] found that the addition of graphene to a composite increases the thermal conductivity significantly. However, graphene-based composites have lower thermal conductivity (10 W/m^{o}C at 5vol. % graphene [25]) compared to vertically-aligned CNTs (>200 W/m^{o}C [30]). Furthermore, no data on thermal resistance of graphene-based composites have been reported up to this point.

2.2.2 Low melt alloys

Low melt alloys (LMAs) are usually alloys of gallium, indium, bismuth, & tin. The phase change temperate depends on the composition of the alloys. For application as TIMs, the alloys are chosen in such a way that they stay in liquid phase at the operating temperature of the component attached. As the LMAs melt, they flow into the surface irregularities and reduce the contact resistances. LMAs contain no organics, and thus no curing is required during application. LMAs have high degree of thermal conductivity and superior wetting, which make them promising TIM candidate materials. Mercury, lead and cadmium-based alloys are hazardous and usually avoided due to their toxicity and environmental issues [16].

Several researchers [4, 8, 31-37] have encouraged using LMAs as efficient TIMs. In 1984, Cook *et al.* [31] were the first to investigate the performance LMAs as TIMs. They tested the LMAs in three different forms. First, the alloy was applied on a porous metallic structure, which they referred as Porous Carrier. The porous structure facilitated the alloy containment. Second, the alloy applied on both sides of a thin substrate (copper or copper-plated aluminum), which was denoted as Solid Carrie and the third configuration was to apply the alloy as a thin sheet, which was referred as Alloy configuration. In their study, a eutectic alloy of bismuth, lead, tin, indium and cadmium, which had a melting temperature of 47 ^{o}C was used. The tests were conducted at 90 kPa (13 psi) and the lowest resistance achieved was 0.11 $cm^{2o}C/W$ with the Alloy configuration. The bare joint (without the LMA TIM) thermal resistance was 3.12 $cm^{2o}C/W$ under the same conditions. Results showed that LMA performance was an order of magnitude better than the bare joint.

In 2002, Webb and Gwinn [32] tested the performance of LMAs using an ASTM D 5470 standard tester. They tested the thermal resistance of the alloy in molten and solid state. The molten

state tests were performed at 2 K above the melting point and the solid state test was carried out below the melting point of the alloy. The reported thermal resistances of alloy 117 (44.7Bi/22.6Pb/19.1In/8.3Sn/5.3Cd) at 138 kPa (20 psi) were 0.058 cm^2°C/W in molten state and 0.077 cm^2°C/W. Results showed that solid state thermal resistance was about 33% higher than the molten state resistance. Tests were also carried out at different pressure from 34.5 to 138 kPa and results showed that thermal resistance variation was less than 5% in this pressure range, which indicates that high contact pressures are not necessary to achieve a lower thermal resistance for LMAs. Webb and Gwinn [32] also tested the reliability of LMAs in terms of thermal cycling. The cycling test were carried out with alloy 117 from room temperature (RT) to 80^{o}C at pressure of 59 kPa. Results showed that after 1000 cycles, the contact area was reduced by about 50% due to the extrusion of the alloy from the interface, which in turn, increased the thermal resistance. Thermal cycling test was also carried out by applying the alloy 117 on a nickel-coated copper substrate. The copper substrate was 50 µm thick and the nickel coating was 5 µm on each side. The alloy was tinned on the both sides of the nickel-coated copper substrate and thermally cycled from RT to 80^{o}C. In this case, significant performance degradation was observed. Back scatter electron imaging was conducted and revealed that the alloy diffused into the nickel and formed intermetallic compounds (IMCs). They concluded that alloy extrusion (due to the poor wetting) and IMCs formation were the primary causes for the performance degradation upon thermal cycling. However they did not attempt to improve the wetting of alloy and re-do the cycling test. They also repeated the thermal cycling test with In-Bi-Sn alloy (51In/32.5Bi/16.5Sn) at different temperatures, 7 K, 10 K, and 18 K above the melting point of the alloy (333 K). Their results showed that performance of alloy degraded as the cycling temperature increased. It was concluded

that severe degradation in thermal performance could occur if the cycling temperature increased 20 K above the melting point of the alloy.

Hill and Strader [34] in 2006 developed a copper-LMA TIM by coating In-Bi-Sn alloy on both sides of a 70 micron nickel plated copper disk. The total thickness of the LMA TIM was about 130 μm. Two alloys of In-Bi-Sn were used in their analysis. The melting point of the two alloys were 60°C and 81°C. They reported the initial thermal resistance of 60°C alloy was 0.017 cm^2°C/W at 69 kPa (10 psi) and 0.015 cm^2°C/W at 345 kPa (50 psi) and the thermal resistance of 81°C alloy was 0.03 cm^2°C/W at 69 kPa and 0.024 cm^2°C/W at 345 kPa. They tested the reliability of their LMA TIM by exposing the TIM into harsh environments, which included highly accelerated stress testing (HAST) at 85°C and 85% relative humidity (RH) and thermal cycling. They observed that when alloy melted, it came out of the interface. To prevent the alloy escaping, they increased the size (diameter) of the TIM by 20% compared to the size of the disks and found that the oversized TIM reduced alloy escaping and had improved performance upon HAST and thermal cycling from -40 to 130°C. It was also found that the LMA TIM performed better between the copper surfaces compared to the aluminum surfaces. They reasoned that the alloy had an improved wetting of copper compared to aluminum and the IMCs were formed between copper and indium. With 60°C alloy, they ran the thermal cycling test on a pc simulator from room temperature to 150°C at 138 kPa (20 psi). No degradation was observed after 1000 cycles. It should be noted that Web and Gwinn [32] found significant degradation after cycling 20 K above the melting point of the alloy. However, in their study, Hill and Strader [34] did not find any degradation after cycling 90 K above the melting point of the In-Bi-Sn alloy. Thus, a complete understanding of the performance of LMA TIM is missing from the literature. Hill and Strader [34] also observed that if the operating temperate remained below the melting point of the alloy, the thermal resistance of the alloy did

not change (within experimental uncertainty) significantly. To facilitate the molten alloy confinement and to prevent the oxidation of the alloy, they suggested to use a compliant gasket around the perimeter. The gasket prevents the intrusion of the air into the interfacial region and thus prevents oxidation of the alloy. The performance of the alloy was tested with and without the gasket assembly and was found that the performance of the alloy with the gasket assembly was far better than the alloy without the gasket.

Martin and Kessel [4] in 2007 reported the thermal resistance of an undisclosed liquid metal TIM to be as low as 0.02 cm^2°C/W with a thermal conductivity of 31 W/m°C. LMAs possess high thermal conductivity (an order of magnitude higher compared to the traditional TIMs [3,5]) and they offer extremely low thermal resistance at small contact pressures (~7 kPa) and at a thin bond line. With the application of wetting layers, no evidence of pump-out with LMA was observed. They presented several ways to mitigate the failure of LMAs. For example, the wetting of LMA was improved by providing direct metal to metal contact, oxidation/corrosion problem was reduced with a hermetic containment to maintain a moisture free environment. It was also found that the diffusion of LMA into the chip material (silicon) was too small to be an issue over the lifetime of the product. Their reliability tests included HAST (85°C & 85% RH), aging at 125°C, thermal cycling from 10°C to 110°C and low temperature storage at -40°C. They did not find any notable degradation with the LMA TIM upon any of the reliability testing. With LMA TIM, they were able to show 750 W/cm^2 of cooling using a heater chip coupled to a water cooled heat sink.

In 2008, Carlberg *et al.* [35] developed a polymer-metal composite using a low melting temperature alloy of In-Bi-Sn with a melting point of 60°C. The in-Bi-Sn alloy was infiltrated into a three dimensional porous network of polymer fibers. The fibers provided the physical support

for the low melting temperature alloy. The thermal performance of the constructed polymer-LMA composite TIM was tested using an ASTM D5470 standard apparatus. The tests were carried out at different pressure ranging from 200 to 800 kPa and at different interface temperatures from 51^{o}C to 68^{o}C. Results showed that the composite TIM had a thermal resistance of 0.085 cm^{2}°C/W 800 kPa (116 psi) and about 0.11 cm^{2}°C/W at 200 kPa and at an interface temperature of 51^{o}C.The thermal resistance was found to increase with interface temperature. For example, at 800 kPa, the thermal resistance was found to increase from 0.085 cm$^{2^{\circ}}$C/W to 0.105 cm$^{2^{\circ}}$C/W as the temperature increased from 51^{o}C to 68^{o}C. The increase in thermal resistance with interface temperature was attributed to the decrease in thermal conductivity of the alloy with temperature. It was also observed that the BLT the composite TIM reduced by about 13% as the pressure increased from 200 kPa to 800 kPa.

Hamdan *et al.* [36] investigated the performance of mercury microdroplets as TIMs. The microdroplets were fabricated by condensing mercury vapor on a gold-plated silicon die. One array of 40/40 droplets and two arrays of 20/20 droplets were tested. The average size of the microdroplets were 15μm (radius) for 40/40 array and 20 μm for one 20/20 array and 22 μm for another 20/20 array. The thermal resistance of the microdroplet arrays was tested as a function of applied load. Results showed that at a particular load, the thermal resistance of 40/40 array was the lowest compared to the two 20/20 arrays. This was because 40/40 array had bigger area of contact compared to the 20/20 arrays. It was also found that between two 20/20 arrays, array with larger droplet size (22 μm) had a lower resistance compared to the array with smaller droplet size (20 μm). Again, this was because of the larger contact area with the bigger droplet size. The thermal resistance was found to vary from 0.085 cm^{2}°C/W to 0.00253 cm^{2}°C/W as the pressure increased from 80 kPa to 2000 kPa. Even though an extremely low thermal resistance value is

reported with mercury droplets, however, because of the toxicity and health concerns, mercury should be avoided unless its use is absolutely required.

In 2014, Yang *et al.* [37] developed Cu/LMA/Cu time by sandwiching the LMA between two copper sheets of thickness 30 μm each. The alloys used in their analysis were 17Sn26In57Bi and 17Sn51In32Bi with melting temperatures 80.3^{o}C and 60^{o}C respectively. The thermal resistance was measure using transient laser flash method. Thermal aging tests at 100^{o}C showed that thermal resistance of 17Sn51In32Bi alloy did not change even after 800 hours of aging. However, for 17Sn26In57Bi alloy the resistance increased by about 51%. SEM cross-sectional analysis revealed the interfacial reaction between copper and LMAs. It was found that as a result of the interfacial reaction, indium and tin phase were lost from the alloys and bismuth phase remained. A thin layer of IMC ($Cu_6(SnIn)_5$) was found to form at the interface. This study also confirms the formation of IMCs at the copper-alloy interface. Interfacial crack was also observed with 17Sn51In32Bi alloy after heating at 150^{o}C for 400 hours.

Although the LMAs offer very low thermal resistances, there are several concerns such as oxidation/corrosion, intermetallic growth, dryout, dewetting, and migration. Several investigators provided different ways to mitigate those problems [8, 32-34]. For example, wetting can be improved by gently rubbing the LMAs onto the mating surfaces which in turn reduces the migration and improves the cycle life [8], oxidation/corrosion of LMAs can be mitigated by providing a hermetic seal, and the formation of IMCs can be prevented by applying a diffusion barrier coating [33]. Hill and Strader [34] found that the use of a gasket reduced oxidation significantly and facilitated alloy containment.

2.2.3 Other promising TIMs

Shaddock *et al*. [38] proposed metallic nanospring (copper /silver) as promising TIM. The nanospring was developed by glancing angle deposition (GLAD) process. The thermal resistance can be achieved lower than 0.01 $cm^2°C/W$. The idea of using nanospring is advantageous because the nanospring structure can accommodate the CTE mismatch between silicon die and copper heat sink. However, the fabrication of nanosprings requires precision control of deposition parameters. In addition, the copper nanosprings are prone to oxidation and form low thermal conductivity copper oxide, which can cause the performance degradation in actual application [38]. Luo *et al*. [39] developed boron nitride nanofiber-indium composite TIM. The nanofibers were fabricated by electrospinning process and nitridation treatment. The reported thermal resistance was <0.02 $cm^2°C/W$ at a thickness of about 25 μm.

2.3 Performance comparison

A performance comparison chart based on the previous research on a variety of TIMs is presented in Figure 2.1. It is evident from Figure 2.1 that LMAs offer lower thermal resistance compared to any class of material that was considered for the application as TIMs. For this reason, this study focuses on the reliability of LMAs as efficient TIMs.

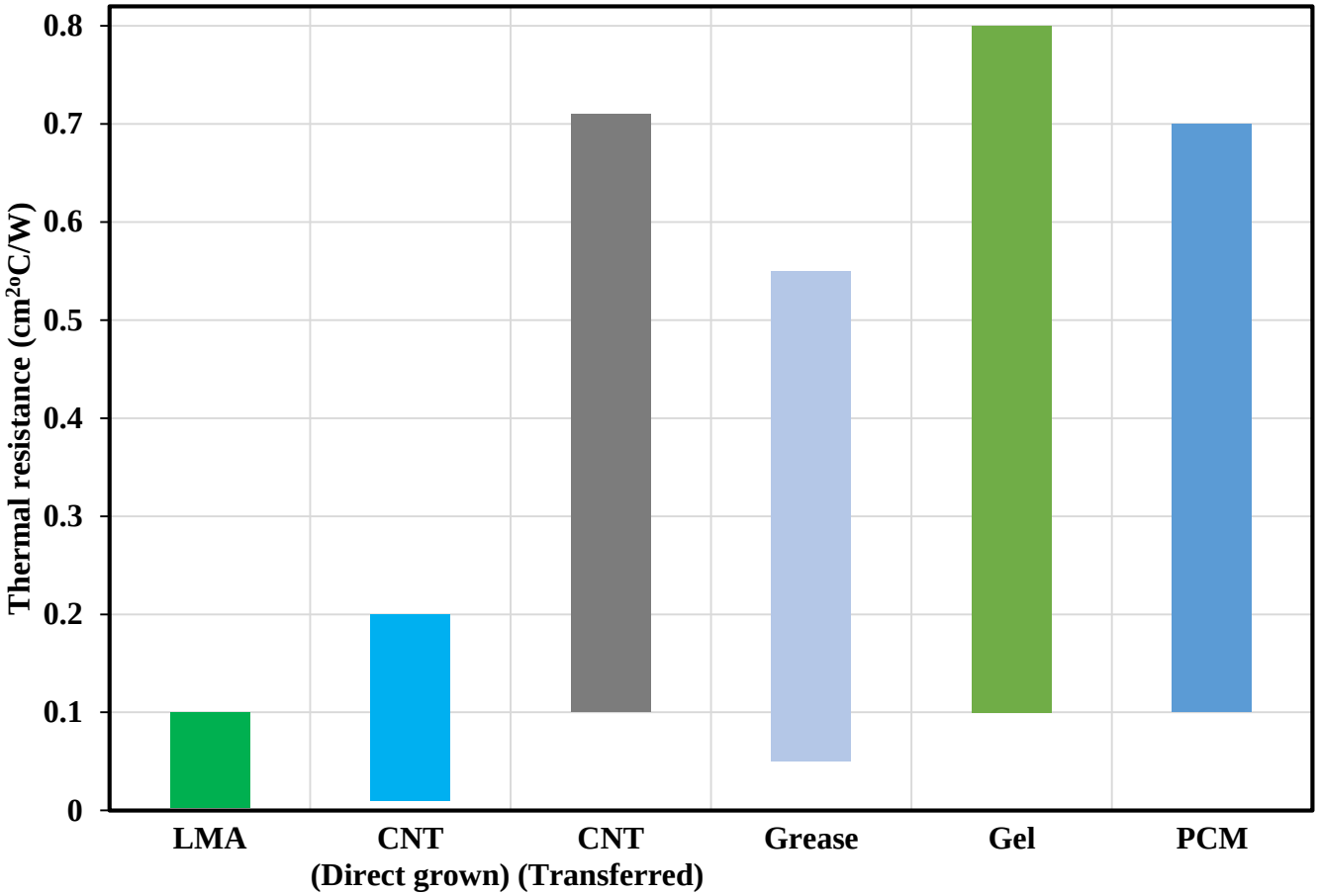

Figure 2.1: Thermal performance comparison of variety of commercial TIMs, Grease [2,4-6], PCM [2,8,11], Gel [11,12,14,15] and emerging TIMs such as CNT (direct grown [17-19] and transferred [18,27,28]) and LMA [4,32-34,36]

Chapter 3 : Experimental

3.1 Materials

In this work, the performance of commercial TIMs and LMAs has been investigated. Commercial TIMs include thermal grease, phase change materials, thermal pad and gels. For LMAs, three lead and cadmium free alloys were chosen to test the thermal performance. These alloys are primarily gallium and indium based alloys. The properties of these alloys are presented in Table 3.1. The reasons for choosing these three alloys are that they have wide range of melting temperatures (from 16^{o}C to 60^{o}C) spanning the range of interests for most application in today's markets and various compositions.

Table 3.1: Properties of the LMAs with melting temperature ranges from 16^{o}C to 60^{o}C

Alloy	Composition (% by mass)	Melting Point (^{o}C)	Density (gm/cm^3)	Specific Heat* (J/g^{o}C)
1	75.5 Ga, 24.5 In	16	6.35	0.34
2	100.0 Ga	30	5.90	0.37
3	51 In, 32.5 Bi, 16.5 Sn	60	7.88	0.20

***** The specific heats were calculated using Kopp-Neumann's law [40] and densities were obtained from the manufacturer data.

3.2 Thermal conductivity measurement

For testing the thermal conductivity of commercial TIMs as well as LMAs, a TCi Thermal Conductivity Analyzer (Figure 3.1) was used. A wide range of materials (solids, liquids, pastes, and powders) can be tested both easily and nondestructively with this device. It can test over a wide temperature range from -50°C to 200°C and can measure thermal conductivities from 0 to 120 W/m^{o}C. This device uses the modified transient plane source method to measure thermal conductivity. A known current is supplied to the sensor's spiral heating element, proving a small amount of heat. This heat will rise the temperature at the interface between the season and the sample, which results in a change in the voltage of the sensor element [41]. The rate of increase in the sensor voltage is used to determine the thermal properties of the sample.

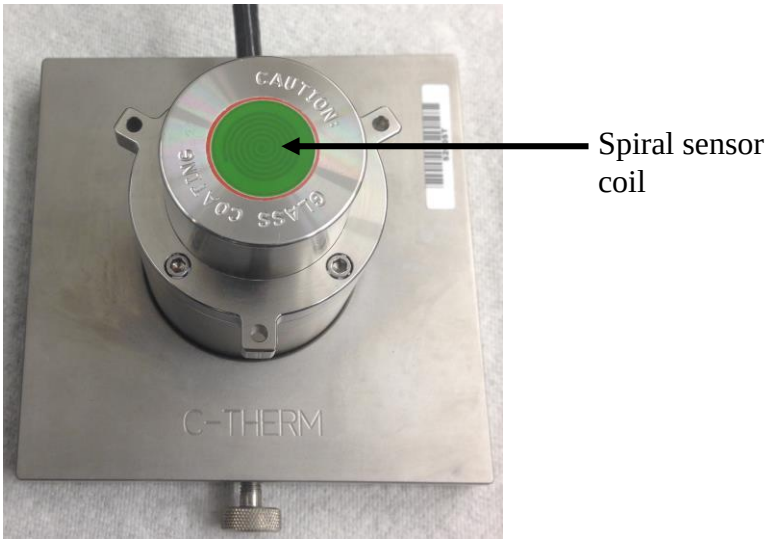

Figure 3.1: C-Therm Tci transient thermal conductivity analyzer

3.3 Thermal resistance measurement

In order to characterize the performance of the TIM, a standardized testing methodology was needed for the current investigation. The performance of any TIM is quantified by measuring the temperature jump across the joint (interface) per the level of heat flux travelling through the interface. Alternatively, this can also be described as the thermal resistance of the interface. The lower the temperature drop incurred across the thermal interface, the higher the performance of the TIM is regarded. Obviously, for high density computing applications, TIMs with the highest performance (lowest thermal resistance) are sought.

Several techniques such as steady state (ASTM D5470) [2,7,8,14], laser flash [37,38], thermoreflectance [19], transient plane source (TPS), synthesized dynamic models [42], photoacoustic [43], 3ω method [44], thermal test dies, and modified hot wire [45] are available to quantify the thermal performance of TIMs. The method chosen for measuring the performance of the TIMs investigated under this effort was ASTM D-5470, which is a standard, widely accepted method for testing the thermal performance of TIMs. According to the standard [46], the testing apparatus consists of two meter bars (hot & cold). Electrical heat is supplied through one bar as the other bar is cooled. The sample (TIM) is placed between the meter bars. Each meter bar is equipped with several temperature sensors to measure the drop across the sample. A typical ASTM D5470 standard setup is presented in Figure 3.2. Several assumptions are made such as the sample thickness being uniform at the interface and the resulting heat flow is uniform, perpendicular to the test surfaces and purely one dimensional with no lateral heat spreading [46].

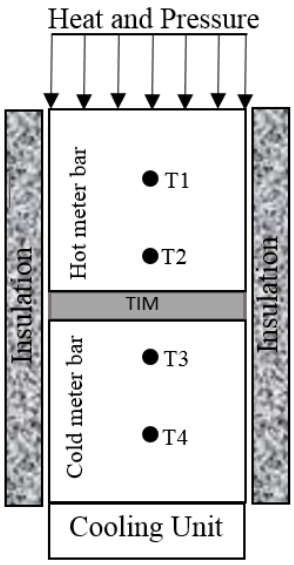

Figure 3.2: Schematic of a typical ASTM D5470 standard setup

Calculation of thermal resistance in ASTM D5470

The heat flow can be calculated in two ways, one way is to calculate from electrical power input, which is

$$q = V * I \tag{3-1}$$

Where: V is voltage supplied to heater and I is current flow through the heater.

A second way is to calculate from the Fourier's law using meter bars. The flow through the top meter bar is calculated as

$$q_{top} = k_1 * A * \frac{T_1 - T_2}{d} \tag{3-2}$$

Where: k_1 is the thermal conductivity of the upper (hot) meter bar material, A is the cross sectional area and d is the distance between temperature sensors. Similarly the heat flow in the lower meter bar is calculated by

$$q_{bottom} = k_2 * A * \frac{T_3 - T_4}{d} \tag{3-3}$$

Where: k_2 is the thermal conductivity of the lower meter bar material.

Then, the average heat flow is:

$$q_{avg} = \frac{q_{top} + q_{bottom}}{2} \tag{3-4}$$

The temperature of the hot and cold meter bar surfaces in contact with the TIM is calculated from

$$T_{top} = T_2 - d_2 * \frac{T_1 - T_2}{d} \tag{3-5}$$

$$T_{bottom} = T_3 + d_3 * \frac{T_3 - T_4}{d} \tag{3-6}$$

Where: d_2 is the distance between T_2 and top meter bar surface in contact with TIM and d_3 is the distance between T_3 and lower meter bar surface in contact with TIM. Then, the thermal resistance of the TIM is calculated from the equation below

$$R_{th} = \frac{(T_{top} - T_{bottom})}{(\frac{q}{A})} \tag{3-7}$$

This thermal resistance include both the conduction resistance of the TIM as well as the contact resistances at the top and bottom contact surfaces.

3.4 Description of the apparatus used

The thermal performances of LMA TIMs reported herein were generated using an ASTM D5470 standard TIM tester. The tester is commercially available through Analysis Tech. The detailed specifications of the apparatus used can be found in [47]. In this setup (Figure 3.3 a), heat flows through the upper meter bar and the lower meter bar is cooled with a chiller. This tester uses a linear variable differential transformer (LVDT) sensor to measure the *in situ* thickness of the TIM joint. An applied pressure can be controlled from 34.5 to 2600 kPa using several different

pressure kits. For the testing of LMAs, a pressure sensor in the range 34.5 to 655 kPa was used which was accurate to ±20 kPa. The electronic thickness measurement accuracy is ± 25 micron. The test surfaces of this testing device are a highly smooth, nickel polished finish with a flatness within 7-8 micron. The meter bars are thermally insulated to minimize the heat loss to the surroundings. This tester operates automatically through a software called WinTIM®. The software allows to vary the interfacial pressure and temperature of the tests.

3.5 Test rig modification

To avoid any contamination of the TIM tester surfaces and to improve the accuracy of the test results, the LMAs were tested by placing them between copper disks. The disks are made of alloy 110 of copper and mirror polished. The flatness of the disks was within 7-8 micron. The disks were 3.2 mm thick and 33 mm in diameter. The resulting disks' assembly was then placed under the tester, shown in Figure 3.3a and 3.3b. Silicone oil (Xiameter PMX-200, viscosity: 1000CS) was applied on the top and bottom surfaces to make a better and more reproducible contact between the test surfaces of the TIM tester and the copper disks. The temperature differential (ΔT) across the LMA TIM was measured by inserting two high precision thermistor probes (1 mm dia., accuracy 0.05^{o}C) in a 1.2 mm diameter hole (16.5 mm deep, radius of the disk) drilled in the middle of the copper disk. The holes were injected with thermal grease (Laird Tech. Tgrease 880) to reduce the contact resistance of the probe in the hole.

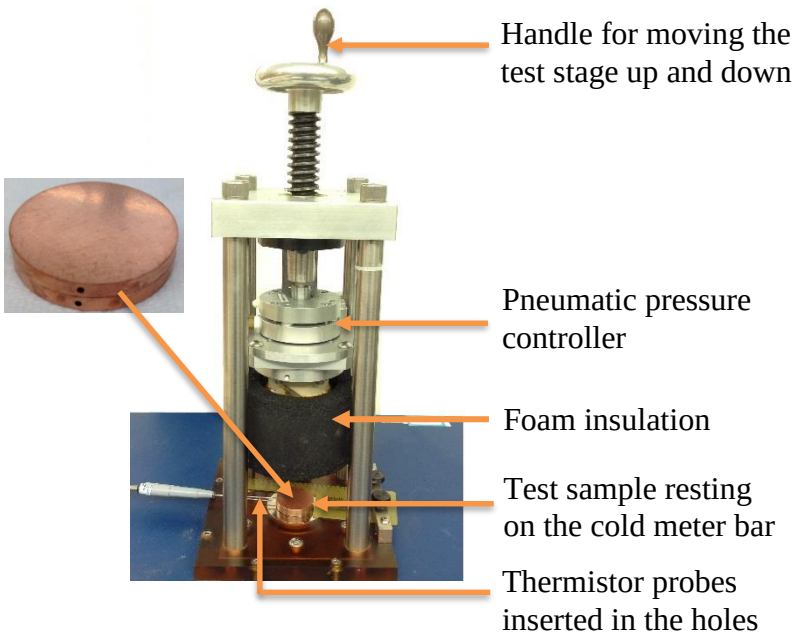

(a)

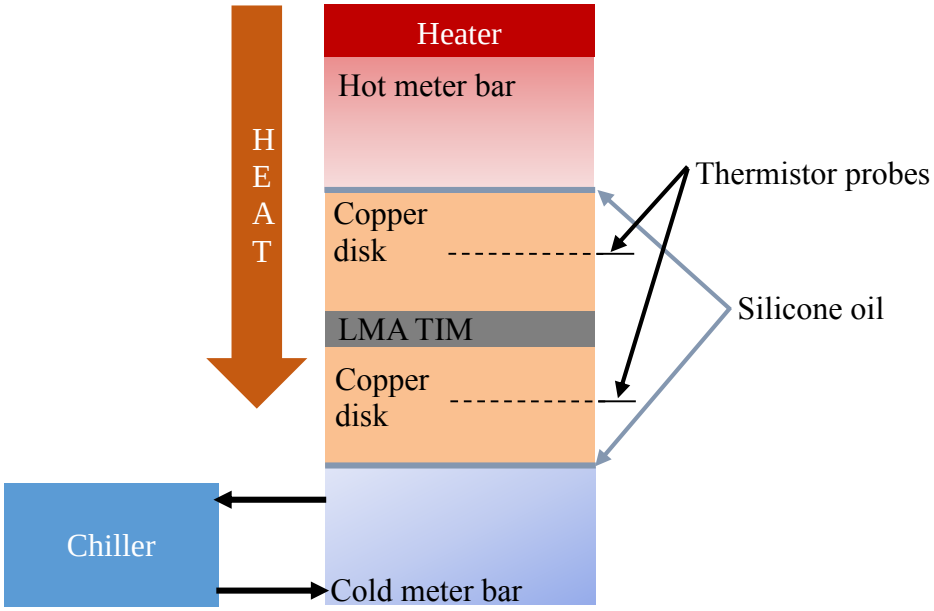

(b)

Figure 3.3: (a) Testing of LMA TIM using modified test rig; the cooper disks assembly with the TIM at the interface was placed between the TIM tester surfaces (b) Schematics of the modified test setup

3.6 Diffusion barrier layers

LMAs are known to diffuse and form IMCs with copper [32,34]. To retard the alloy diffusion and intermetallic formations, a thin metallic barrier layer was applied on the copper disk surfaces. As tungsten (W) provides superior protection against gallium (Ga) or gallium-based alloys, bare copper disks (Figure 3.4a) were coated with tungsten (Figure 3.4b) at two microns thickness (±10%.). For better adhesion of the tungsten, a 50 nm layer of titanium (Ti) was first applied. A thin layer of nickel (Ni) also provides some degree of diffusion barrier to LMAs. For this reason, nickel was also chosen to apply on the copper disk surfaces. The copper disks were plated with nickel (Figure 3.4c) at about five-micron thickness.

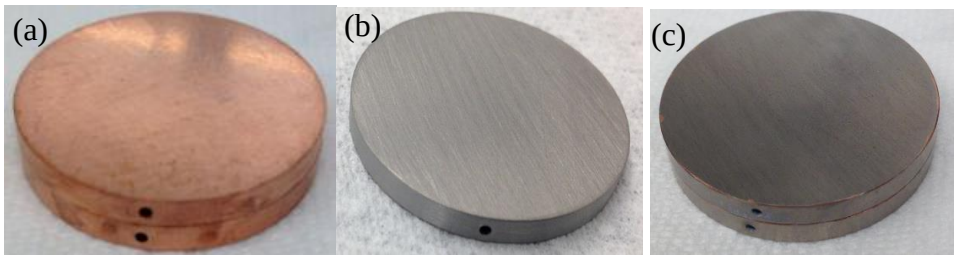

Figure 3.4: (a) Bare copper disks (b) Tungsten coated (2 micron) copper disk (c) Nickel coated (5 micron) copper disks.

3.7 Sample preparation

The disks were cleaned with methanol, acetone, and a hydrochloric acid solution (95% water & 5% HCl) and then rinsed in water. The LMAs were next applied onto the cleaned disks. To enhance the wetting, the disk surfaces were gently rubbed with the alloy using a cotton swab or a commercial brush. Figure 3.5 shows the application of Ga-In alloy on a copper surface. Liu *et al.* [48] described the reason for wetting of an alloy in an oxygen environment as the formation of

thin oxide layer onto which LMAs wet. In the case of pure Ga, both the alloy and the disks were heated on a hot plate above the melting point of the alloy after which the molten metal was applied onto the heated disk's surface by rubbing. In-Bi-Sn alloy was tested in three forms, as a four mil (102 micron) sheet, two mil sheet (51 micron) placed between two disks and in molten form (melted the alloy first and then applied on heated disk surfaces).

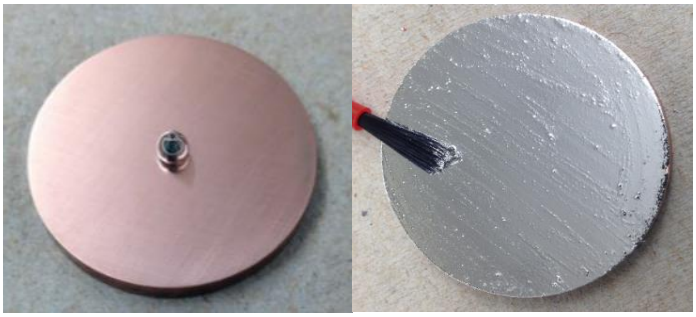

Figure 3.5: Wetting of Ga-In alloy on copper surface using a brush

3.8 Uncertainty analysis

The uncertainty in measuring thermal resistance is inversely related to the resistance value [32]. A lower resistance value results in a higher uncertainty. Since the thermal resistances of LMAs are expected to be relatively lower, the associated uncertainties would be higher. The calculated uncertainty in the measurement will be represented by the error bar in all foregoing figures representing the thermal resistance of LMAs. The details of the uncertainty analysis for the modified testing procedure (shown in Figure 3.6) using the copper disks is presented next.

The temperatures T_1 and T_2 were measured with thermistors, then the temperature drop across the TIM was calculated using the following equation:

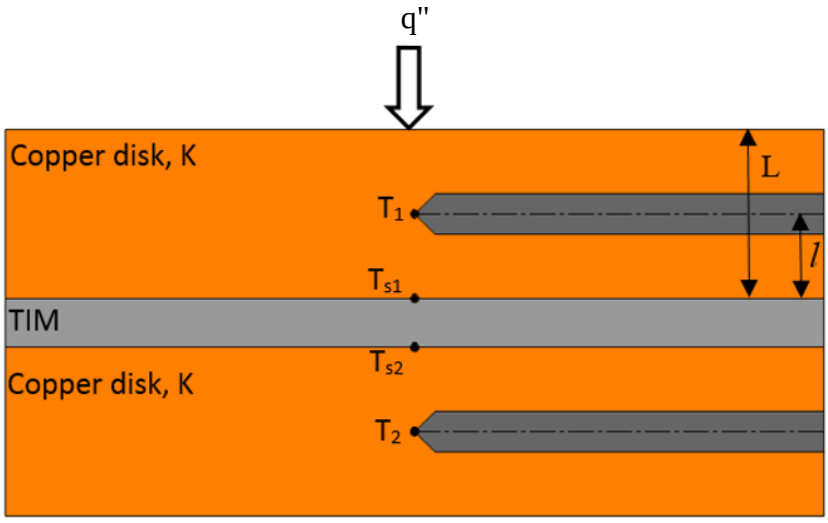

Figure 3.6: Copper disks assembly with probes inserted in the holes

$$\Delta T = T_{s1} - T_{s2} = T_1 - T_2 - \frac{2q''l}{k} \tag{3-8}$$

It is noticeable from the above equation (3-8) that the temperature drop (ΔT) across the TIM depends on two thermistors readings (T_1 and T_2), heat flux (q") through the sample, thermal conductivity (k) of the disk material, and location of the probe (l). In addition to the measurement uncertainties, the presence of the thermistor probes in the heat flow path might disturbed the assumed one-dimensional conduction heat flow. To quantify this disturbance, a numerical model simulation was pursued using ANSYS, Icepak. The probe disturbance is defined as the temperature deviation (due to presence of the probe) on the top surface of the TIM over the temperature drop across the TIM. Figure 3.7 represents the probe disturbance as a function of thermal resistance of the TIM placed between copper disks with stainless steel probe in the holes. Simulations were carried out at a specified heat flow (200 watts) on the top surface and constant temperature (20^{o}C) at the bottom surface. It is evident from Figure 3.7 that a low resistance value results in a high probe disturbance. Simulations were also carried out at different probe angles and it was found

that if the holes were perfectly aligned (designated as 0 degrees) then the disturbance was minimal as indicated in Figure 3.8, In the present case, the hole was drilled in the middle of disk, at *l* of 1.6 mm. The temperature distribution on the top surface of the TIM is presented in Figure 3.9. It can be observed that in absence of probes, the temperature on the TIM surface is uniform as indicated in Figure 3.9a whereas the presence of probes clearly affects the temperature distribution on the TIM surface.

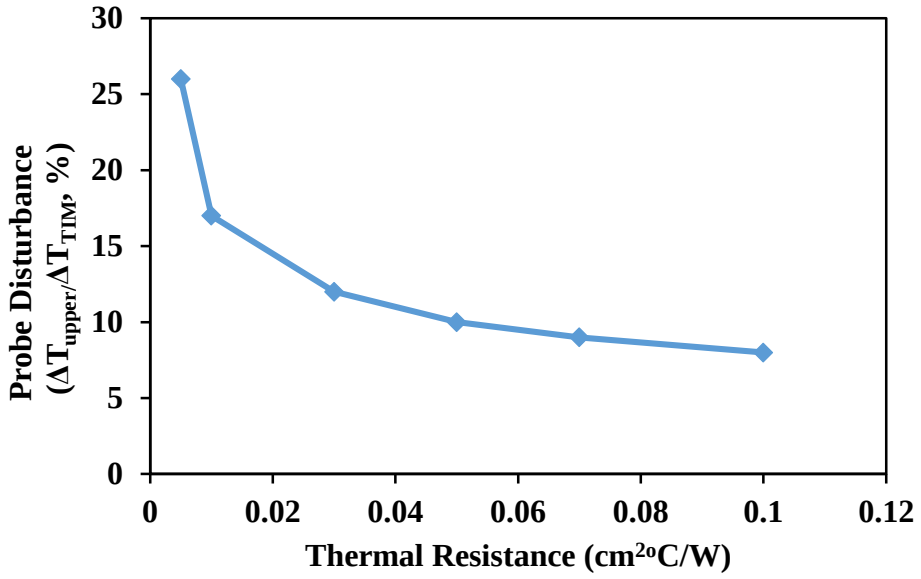

Figure 3.7: Probe disturbance as a function of thermal resistance of the TIM for perfectly aligned probes

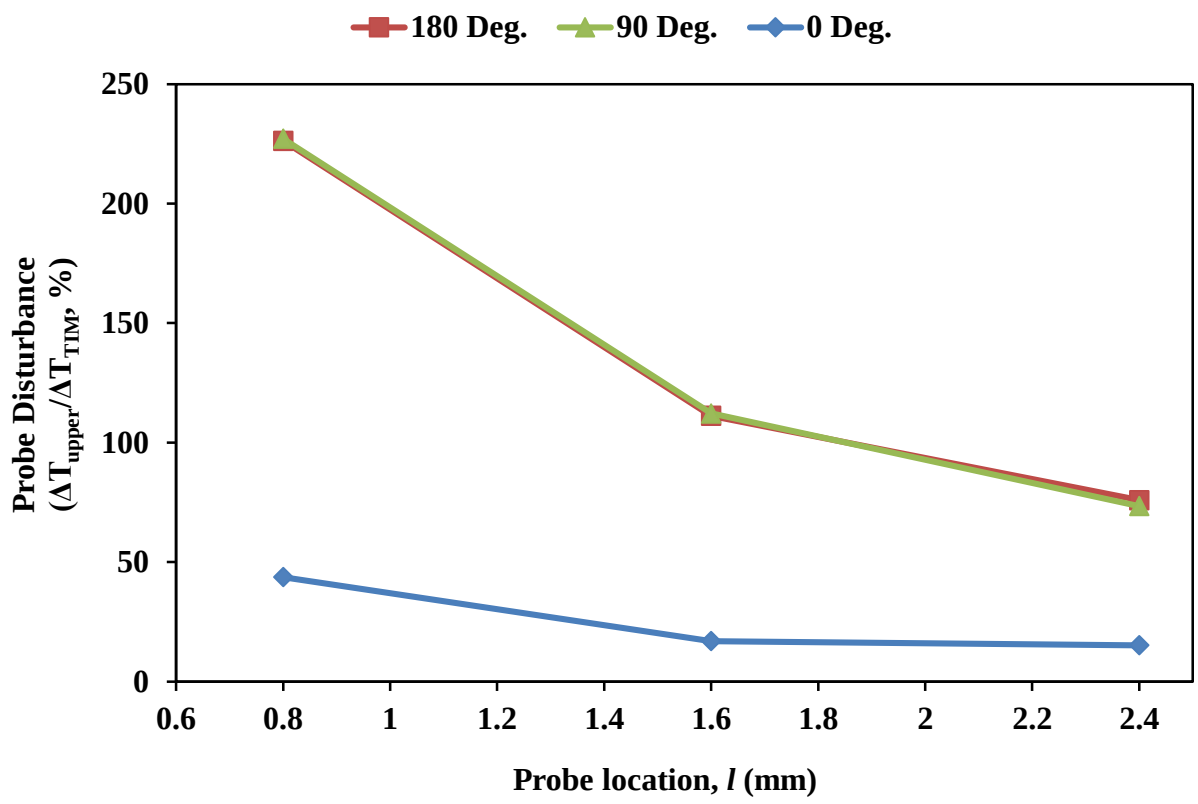

Figure 3.8: Probe disturbance as a function of probe location for a TIM of thermal resistance $0.01 cm^2 {}^oC/W$

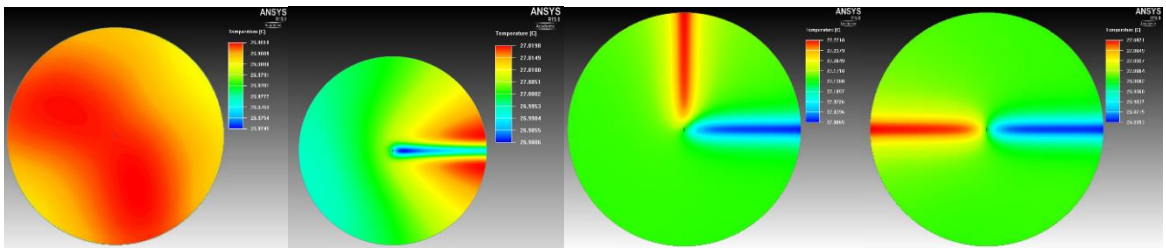

(a) (b) (c) (d)

Figure 3.9: Temperature distribution on the top surface of the TIM (a) without probes ($\Delta T=0.002^oC$) (b) probes are perfectly aligned ($\Delta T=0.04^oC$) (c) probes are at 90^o (bottom probe is rotated) ($\Delta T=0.26^oC$) (d) probes are at 180^o ($\Delta T=0.26^oC$)

Thus,

$$\Delta T = f\left(T_{1,}T_{2,}q^{"},l,k,Probe\ disturbance\right) \tag{3-9}$$

The uncertainty in measuring ΔT designated as $U_{\Delta T}$ was calculated by root-sum-square method [34].

$$U_{\Delta T} = \sqrt{\{\sum_{i=1}^{n}(\frac{\partial \Delta T}{\partial X_i}\partial X_i)^2\}} \tag{3-10}$$

The ultimate objective is to find uncertainty in thermal resistance measurement which is represented as:

$$R = \frac{\Delta T}{q^{"}} \tag{3-11}$$

Once $U_{\Delta T}$ is calculated then the uncertainty in thermal resistance can be calculated using the same root-sum-square method which is as follows:

$$\frac{U_R}{R} = \sqrt{(\frac{U_{\Delta T}}{\Delta T})^2 + (\frac{\mathrm{U}_{q^{"}}}{\mathrm{q}^{"}})^2} \tag{3-11}$$

In all uncertainty values presented hereafter with the reported measured results include: uncertainty in thermal conductivity U_k as ±1%, uncertainty in heat flux $U_{q"}$ as ±1% (manufacturer specifications), uncertainty in temperature measurement U_{T1} and U_{T2} as ±0.05ºC (thermistor accuracy), probe location uncertainty U_l as ±25 μm and the associated probe disturbance taken from Figure 3.7.

Chapter 4 : Commercial TIMs

4.1 Thermal conductivity measurement

Thermal conductivity is an important property of TIMs that directly affects the overall interfacial resistance. High thermal conductivity materials provide low conduction resistances. The thermal conductivity some commercial TIMs (thermal grease, pad) was measured using a modified transient plane source thermal conductivity analyzer by C-Therm (Figure 3.1). Results showed that modern greases have thermal conductivity >6 W/m^{o}C. The measured values were compared with the manufacturer data, shown in Table 4.1. Our results are in good agreement with the manufacturer data.

Table 4.1: Thermal conductivity of some commercial TIMs tested using a transient thermal conductivity analyzer

Material	Part Number	Thermal conductivity (W/m-K)	
		Measured	Manufacturer Spec.
Thermal grease	ShinEtusu X23-7921-5	6.24	>6
	Laird tech. Tgrease 880	3.64	3.1
Thermal pad	Gap pad	5.08	5
	Sil pad	2.7	3

4.2 Thermal resistance measurement

4.2.1 Thermal grease

The Figure 4.1 below presents the thermal resistance values measured as a function of applied pressure of several commercially available high performing thermal greases. All samples were tested at a fixed interface temperature (50^{o}C in the present case). It is noticeable from Figure 4.1 that for any particular grease the thermal resistance decreases with the applied pressure. This kind of behavior is expected because with any increase in pressure, more surface asperities and voids become filled by the grease, which reduces the contact resistances. In addition, the thickness decreases with increasing pressure, which in turn reduces the conduction resistance. However, the change in resistance with pressure is relatively lower in this case. This is due to the thin BLT of the greases. The thickness values measured did not vary significantly in the pressure ranges from 69 to 345 kPa. It was found that ShinEtsu X23-7921-5 thermal grease can provide a thermal resistance as low as 0.065 cm^{2}°C/W at 345 kPa with a bond-line of approximately 43 µm. The uncertainty in measuring a value as low as 0.065 cm^{2}°C/W is 10% with the test stand used. The highest measured thermal resistance was 0.46 cm^{2}°C/W found with Chomerics T670 grease at a thickness of about 96 µm.

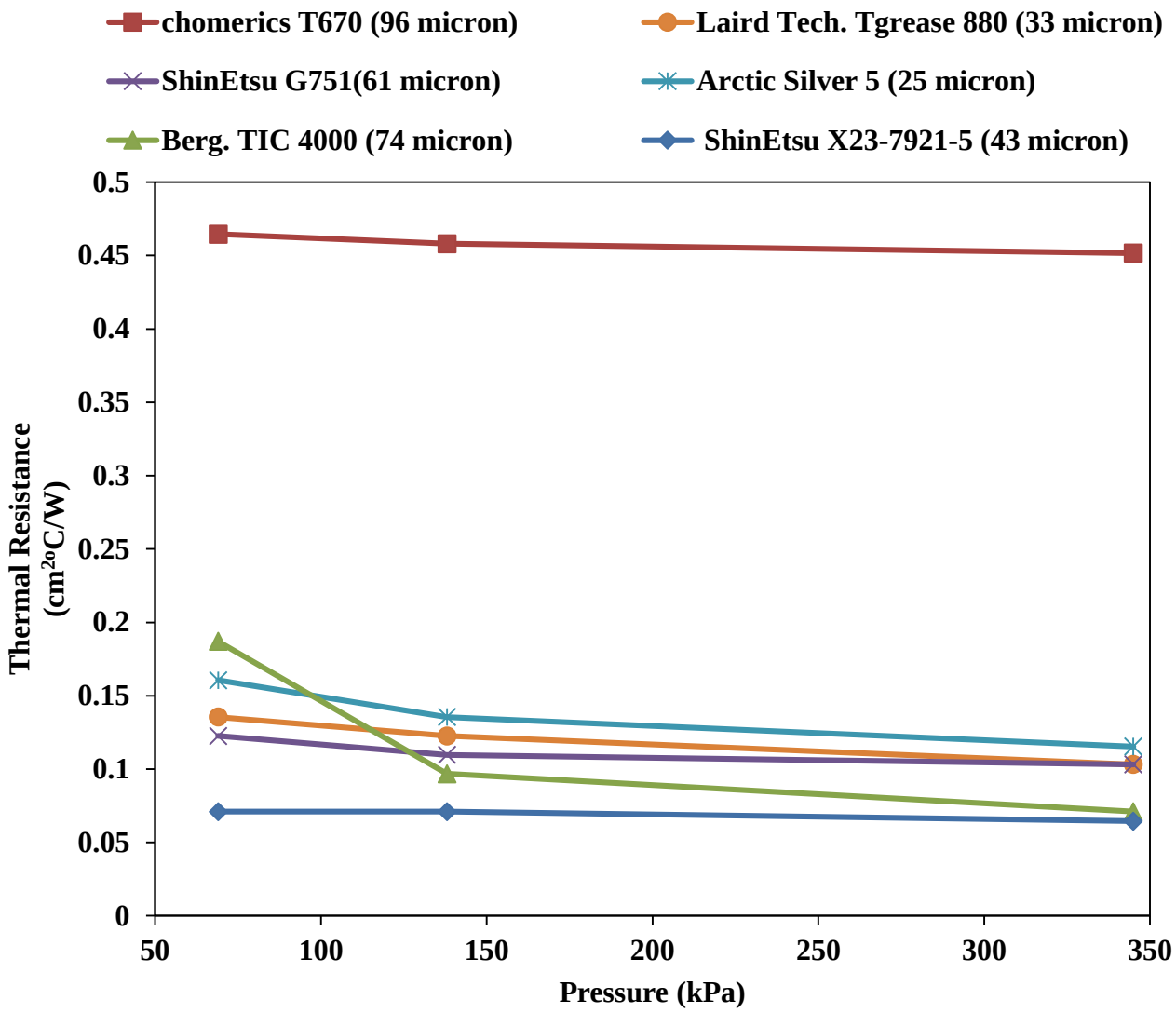

Figure 4.1: Thermal resistance as a function of applied pressure for different greases (note that bare junction resistance values are off scale: 2.5 to 1 $cm^2°C/W$)

The measured thermal resistances of Arctic Silver 5 at different pressures were compared with the data provided by Wasniewski *et al.* [7]. Our results are in good agreement with the data provided in [7] which is shown in Figure 4.2. Gwinn *et al.* [2] reported the thermal resistance of Arctic Silver as 0.018 $cm^2°C/W$ at 83 kPa (12 psi) which could not be reproduced using our test stand.

Finally, the comparison of our measurements of ShinEtsu grease X23-7921-5 with the manufacturer's published data is presented in Figure 4.3. Again, the test results are in good agreement with the manufacturer data.

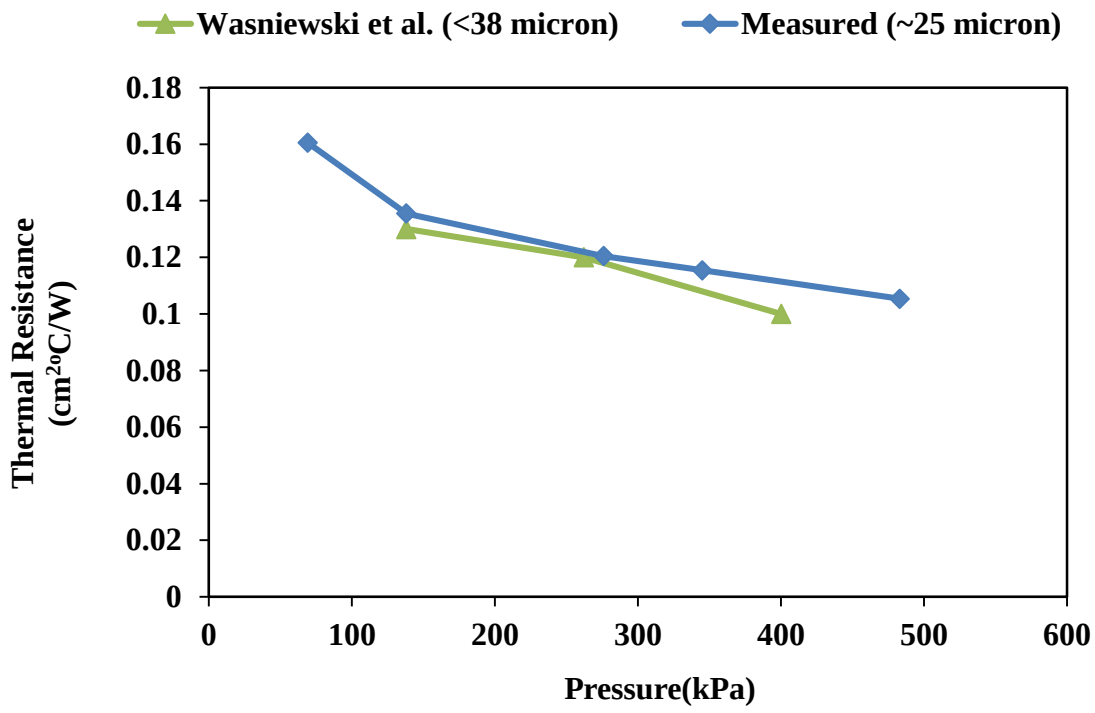

Figure 4.2: Thermal resistance comparison of Arctic Silver 5 grease with the data provided by Wasniewski *et al.* [7]

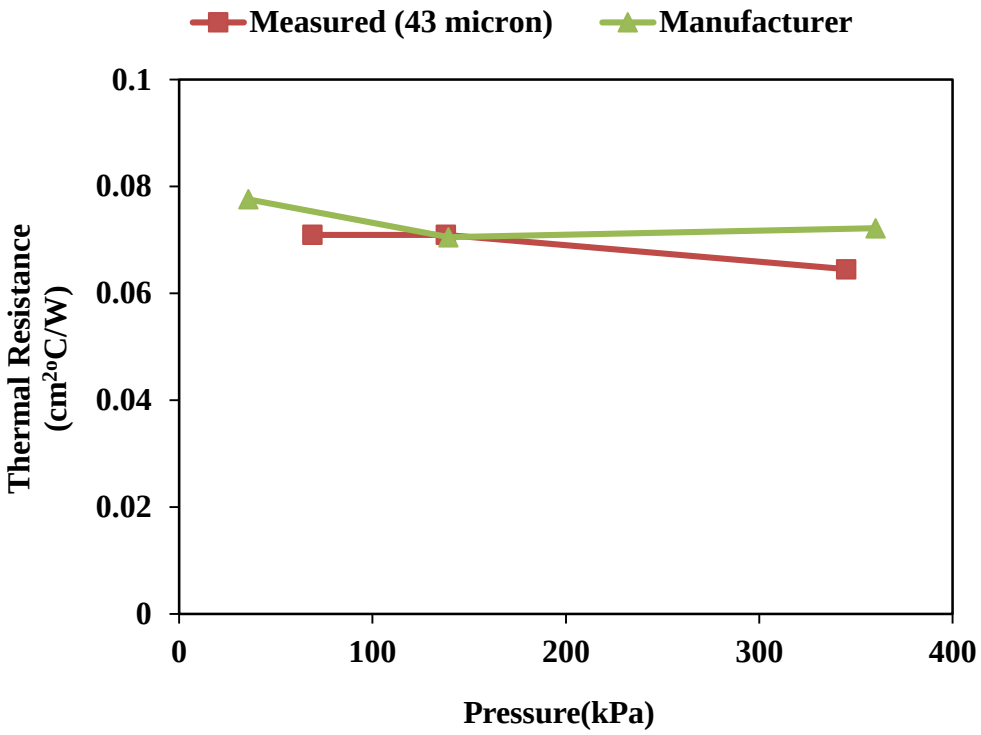

Figure 4.3: Comparison of measured thermal resistance of ShinEtsu X23-7921-5 grease with the manufacturer data

4.2.2 Phase change material

The thermal resistance of a variety of PCMs was tested as a function of varying applied pressure and the results are presented in Figure 4.4. The initial thickness was different for the PCMs since they come in various geometries and thicknesses. The phase change temperatures for the PCMs tested were 52°C and 50°C for the Bergquist and Laird Tech. PCMs, respectively according to the manufacture's specifications. The interface temperature was maintained at 60°C during all testing. All the PCMs were tested after an initial melting at 60°C for 5 minutes. The initial melting allows the PCM to be seated at the interface, filling all the air gaps and microscopic irregularities of test surfaces. From the figure below, the thermal resistance decreases for all PCMs

with increasing pressure, as it is expected. Note that PCMs show a much stronger pressure dependence when compared to the thermal greases. For example, resistance of Tpcm 585 decreases from 0.28 cm^2°C/W to 0.1 cm^2°C/W (a 64 % reduction) as pressure increases from 69 to 345 kPa. The thickness of Tpcm 585 was found to decrease from 127 µm to 64 µm (a 50% decrease) in the same pressure range. The change in thickness of Bergquist 565U was negligible in the same pressure range, which is why the resistance of 565U is almost invariant with pressure.

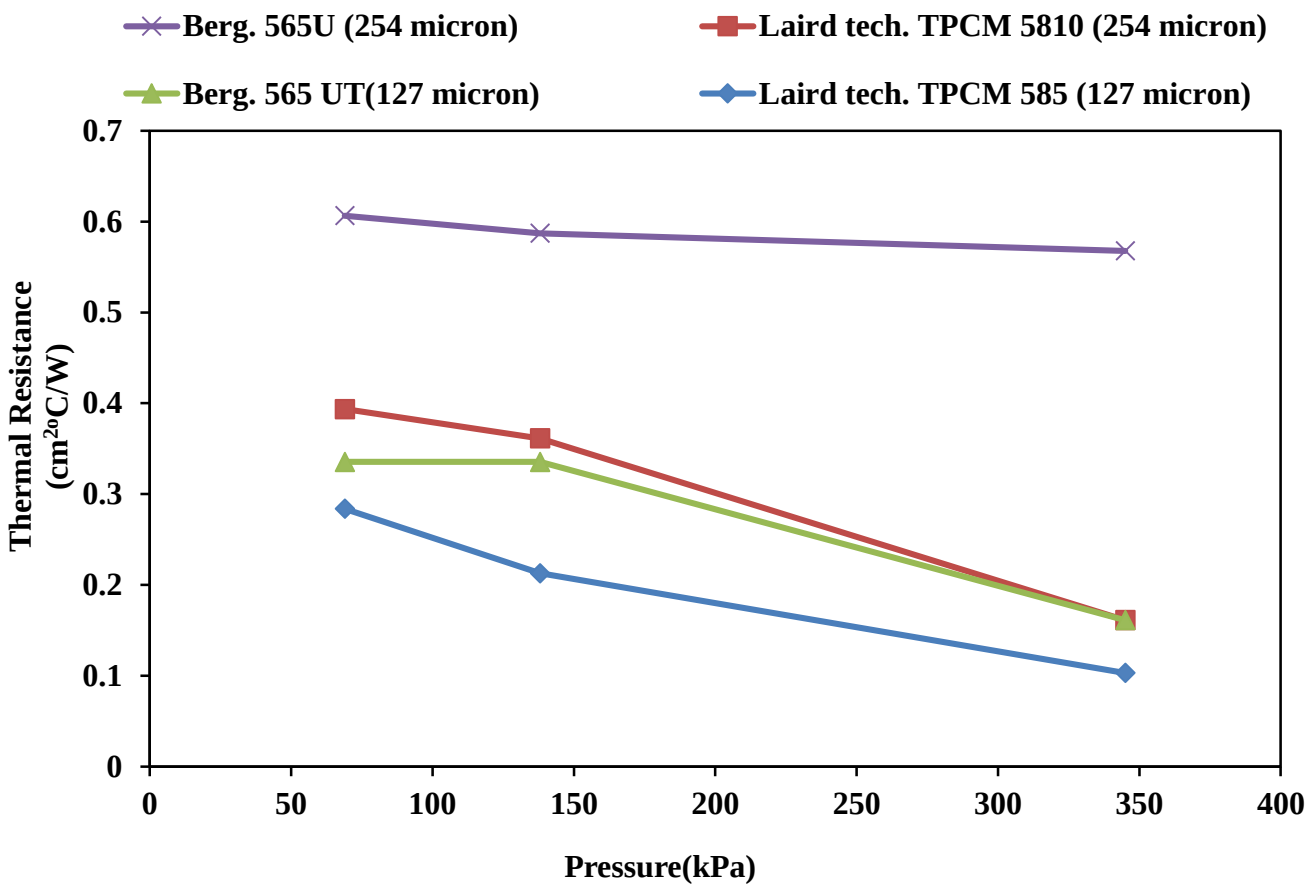

Figure 4.4: Thermal resistance as a function of applied pressure for different PCMs

Effect of initial melting

Figure 4.5 shows the thermal resistance as a function of the interface temperature for Laird Tech. PCM 588 and 5810. The test pressure applied at the joint was 138 kPa. The thermal

resistance was found to decrease with increasing temperature if the PCM was not pre-melted before starting the test. It was observed that after an initial melting at soak 60°C (10°C above the softening temperature) for five minutes that the interface temperature did not affect the thermal resistance as significantly as was observed when no initial melt soak was performed. The thermal resistance without initial melting is higher because the PCM does not fill the microscopic voids and surface irregularities at the interface which causes significant contact resistance. Whereas, an initial melting above the phase change temperature ensures the PCM seats at the interface filling all air gaps and thereby, reduces the contact resistance and also displays less variation in thermal resistance with interface temperature.

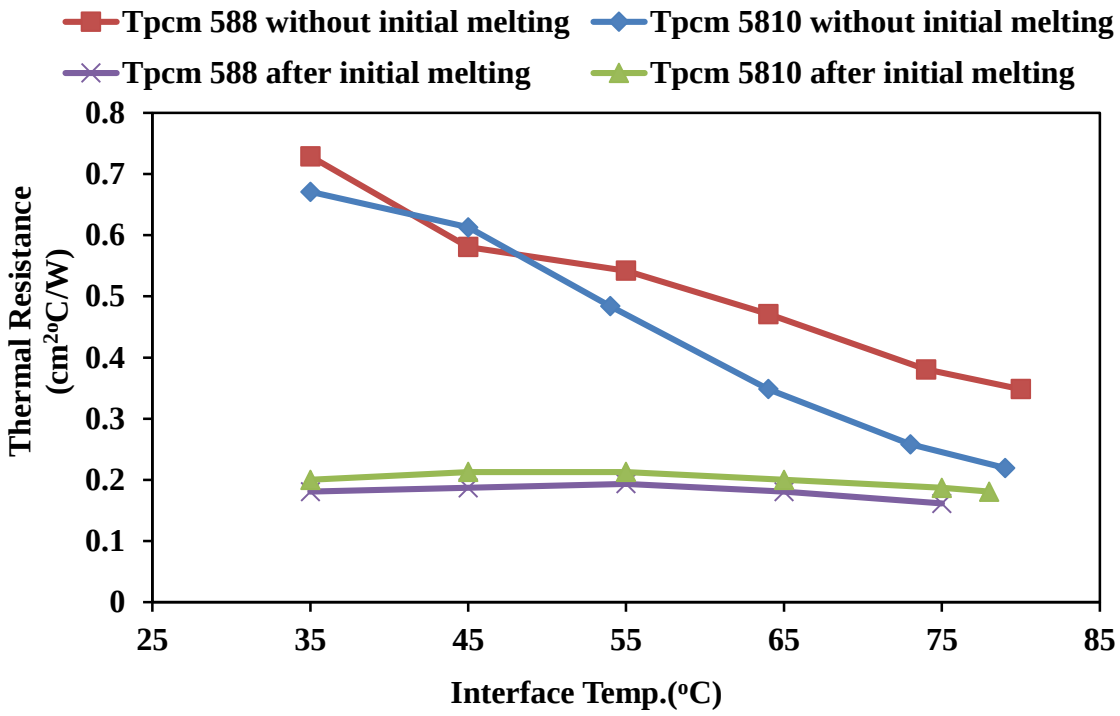

Figure 4.5: Thermal resistance as a function of interface temperature for Laird tech. Tpcm 588 and Tpcm 5810 with and without initial melting

The same experiments that were carried out on Tpcm materials, were also done using Bergquist 565U. Figure 4.6 shows the effect of initial melting for Bergquist high flow 565U (thickness 254 µm (10 mil) and phase change temperature 52^{o}C). Different behavior was observed with the 565 U material than that seen with the Tpcm 588 and 5810 materials. The thermal resistance decreased until the phase change temperature was reached and then it started to increase slightly with temperature for both cases (with and without initial melting). The thermal resistance is higher without initial melting at every temperature. The reason could be, as explained before, the PCM does not fill the microscopic voids and surface irregularities at the interface when no initial melting was accomplished prior to testing.

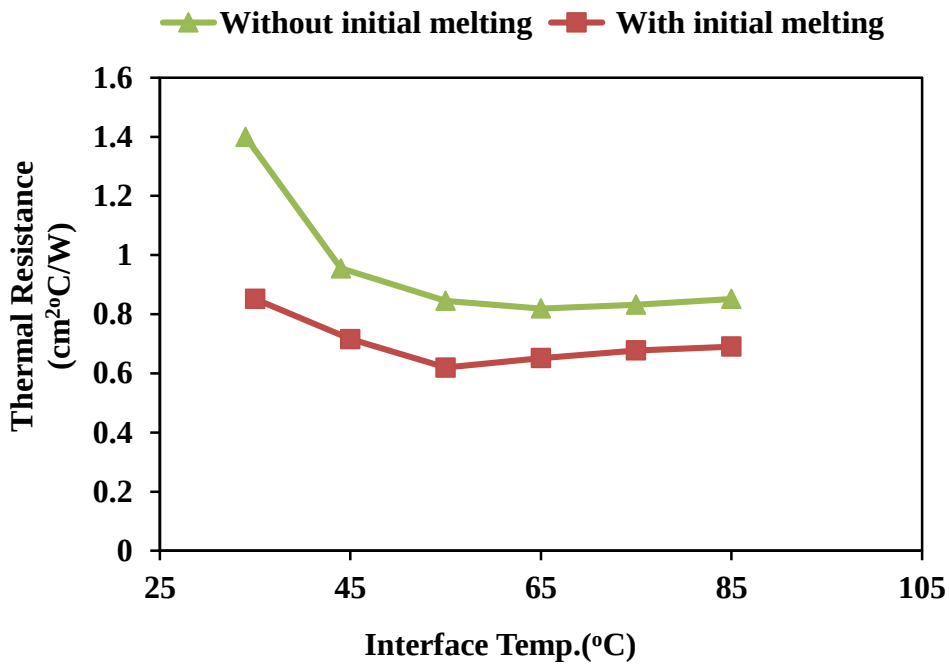

Figure 4.6: Thermal resistance as a function of interface temperature for Berg. 565U

Effect of interface temperature

In actual high density computing applications the interface temperature is typically not constant. For this reason, it is important to investigate the response of a TIM at various interface temperatures. Figure 4.7 shows the thermal resistance of Bergquist 565U as a function of pressure at different interface temperatures. The experiments were carried out after an initial melting at 60°C for 5 minutes. It is obvious from the plot that the thermal resistance decreases with pressure at any interface temperature. Also, the thermal resistance increases with interface temperature at all pressures tested. For example, at 345 kPa, the thermal resistance increases from 0.48 cm^2°C/W to 0.61 cm^2°C/W as the interface temperature increases from 40°C to 80°C.

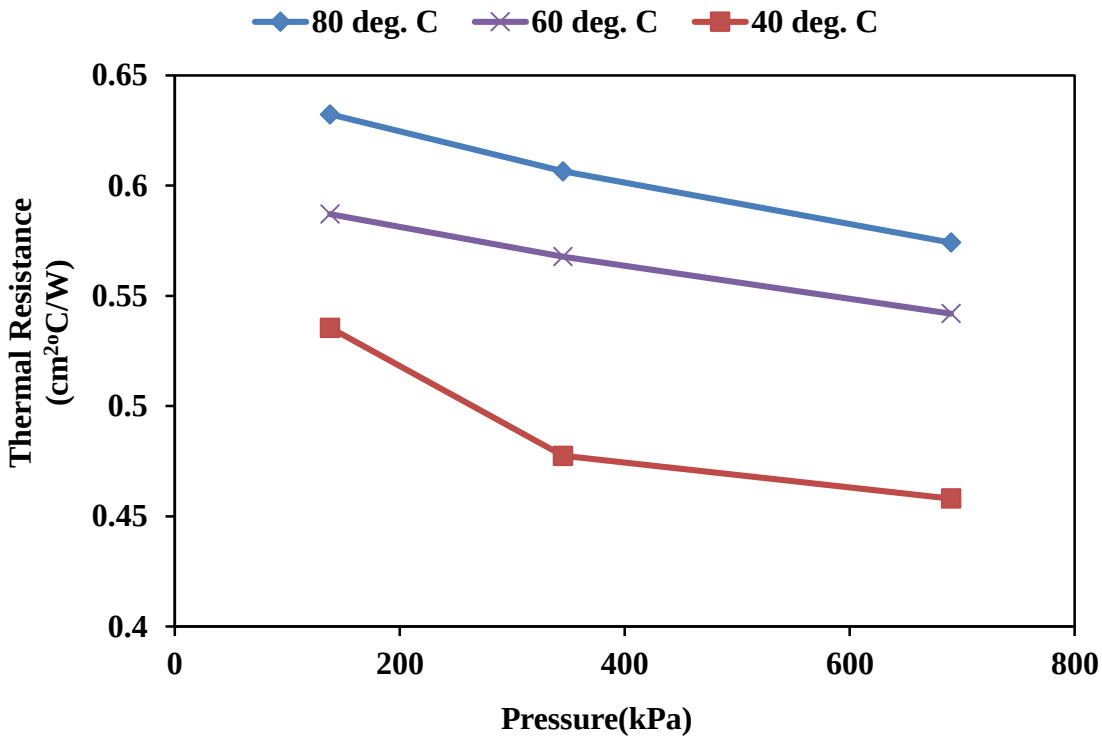

Figure 4.7: Thermal resistance as a function of pressure at different interface temperatures for Bergquist 565U

4.2.3 Thermal pad

Testing of sil pad

Bergquist A2000 sil pad is a high thermal conductivity (~3 W/m°C) silicone elastomer. The thermal resistance of Bergquist sil pad (A2000) with initial uncompressed thickness of 381 µm (15 mil) was measured as a function of applied pressure and the results were compared with the manufacturer as presented in Figure 4.8. The interface temperature was set at 50°C. The thermal resistance was found to decrease from 2.10 cm^2°C/W to 1.59 cm^2°C/W as the pressure was increased from 69 kPa to 690 kPa. The reason for showing this kind of behavior with increasing pressures is as explained earlier. The change in thickness in the pressure ranges from 69-690 kPa was found negligible (within the instrumental accuracy limit ±25 µm). The comparison shows that in the low pressure range, the test data are not in good agreement with the manufacturer data. However, at higher pressures agreement between measurements and manufacture's published data improves.

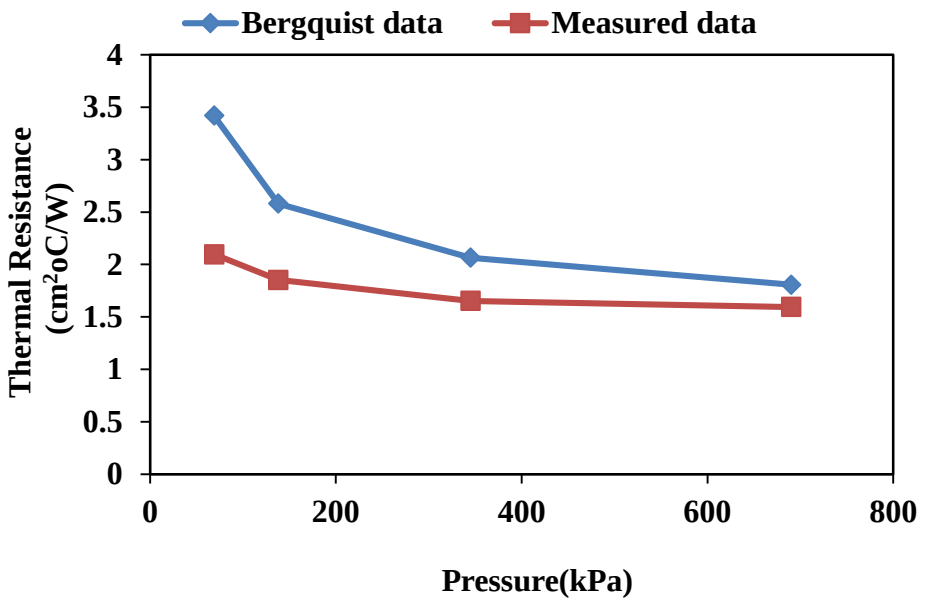

Figure 4.8: Thermal resistance of Bergquist sil pad A2000 as a function of pressure

Multiple samples testing

The pressure dependent tests of Bergquist sil pad were repeated with five different samples to investigate the reproducibility of the test results reported. The results of the repeated tests are shown in Figure 4.9. The maximum variation from the mean was found to be 0.15 $cm^2°C/W$ (8 %) at 138 kPa. The test instrument's output is adequately consistent.

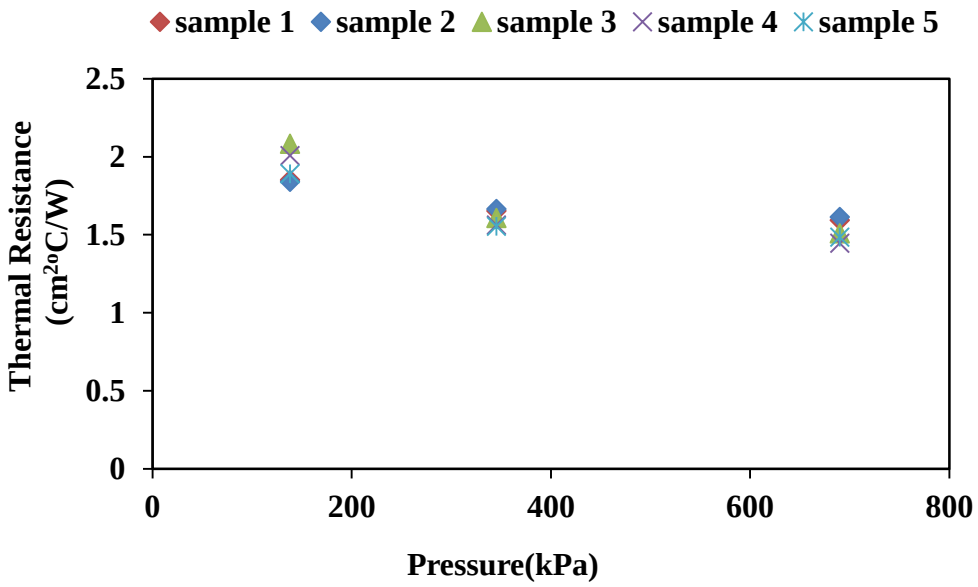

Figure 4.9: Thermal resistance of Bergquist sil pad (A2000) as a function of pressure for five samples

Effect of interface temperature

The tests were carried out at a particular pressure (345 kPa in this case) varying the interface temperature to observe the temperature dependent characteristics of Bergquist Sil pad A2000. Results are shown in Figure 4.10. It was found that the thermal resistance increased from 1.587 to 1.755 $cm^2°C/W$ (~11% increase) as the interface temperature increased from 35 to 85°C.

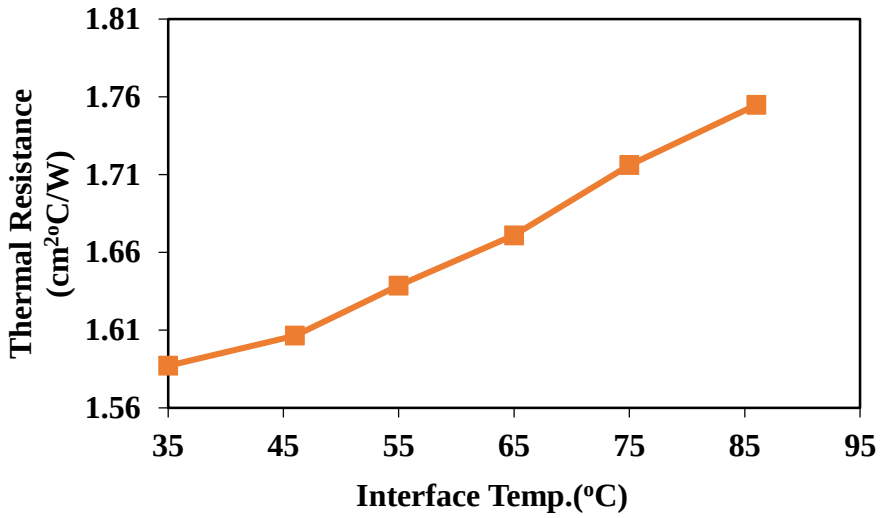

Figure 4.10: Thermal resistance as a function of interface temperature for sil pad A2000

Repeating test of sil pad

Figure 4.11 below shows the repeated test result for sil pad A2000 at 345 kPa. In the repeating test mode, the same sample was tested recurrently. After each test, the sample was cooled down for 15 minutes, and then started the test again. After thirty five repeated measurements, the interface resistance was found to decrease from 1.66 cm^2°C/W to 1.50 cm^2°C/W (~10 % change). The change in thickness was less than the instrumental accuracy (± 25 micron). According to the manufacturer data, the thermal resistance of 15 mil A2000 sil pad at 345 kPa (50 psi) is 2.06 cm^2°C/W.

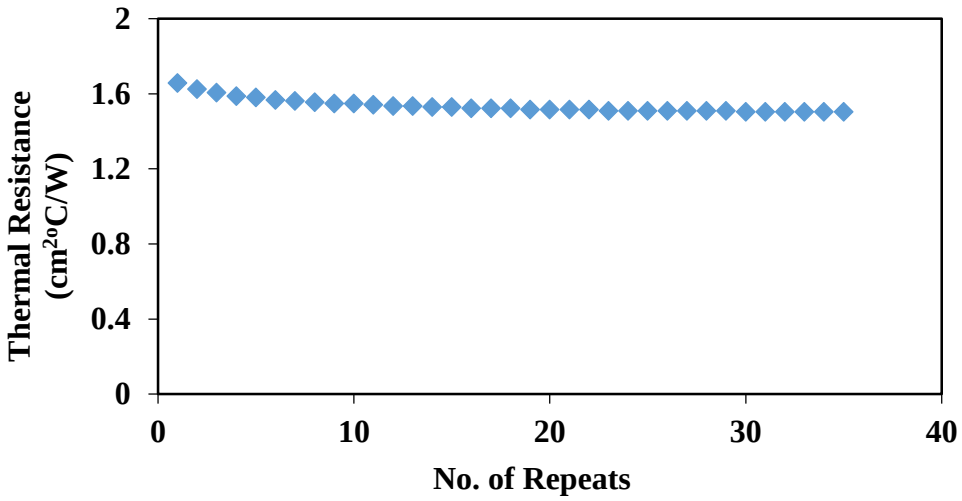

Figure 4.11: Repeated test of Bergquist Sil Pad A2000

Testing of gap pad

Bergquist 5000S35 gap pad is a soft, fiberglass reinforced highly conductive (~5 W/m°C) thermal pad. Its' soft consistency allows the pad to conforms to the mating surfaces. The thermal resistance of the Bergquist 5000S35 gap pad with an initial uncompressed thickness of 508 µm (20 mil) was measured at different pressures and the results are compared with the work of Wasniewski *et al.* [7] and manufacturer's data, and is shown in Figure 4.12. The thermal resistance decreased from 1.02 cm^2°C/W to 0.81 cm^2°C/W as the pressure was increased from 69 kPa to 690 kPa. The reason is explained before. Due to the softness of this gap pad, the thickness was found to decrease from 483 µm to 406 µm as the pressure increased from 69 kPa to 690 kPa. Comparing the thermal resistances with the Bergquist sil pad A2000 (Figure 4.8), it can be concluded that the performance of gap pad is superior.

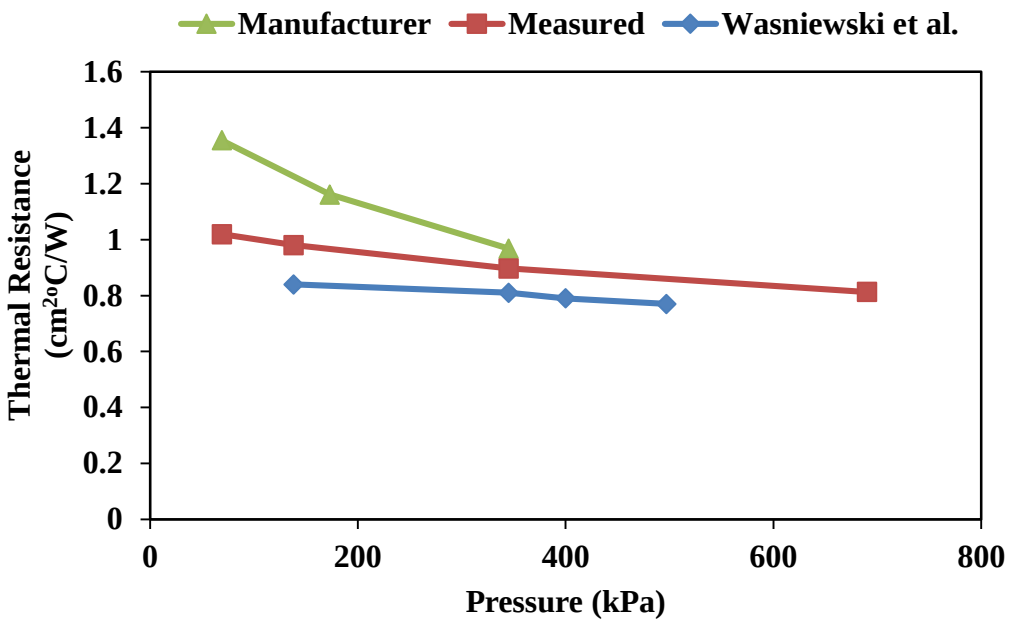

Figure 4.12: Thermal resistance of gap pad 5000S35 as a function of pressure, compared with manufacturer data and Wasniewski *et al.* [7]

Multiple samples testing

The pressure dependent tests were repeated with multiple samples of the gap pad material similar to the Sil pad tests (Figure 4.9). The maximum variation from the mean was found to be 0.065 $cm^2°C/W$ (6%) at 69 kPa.

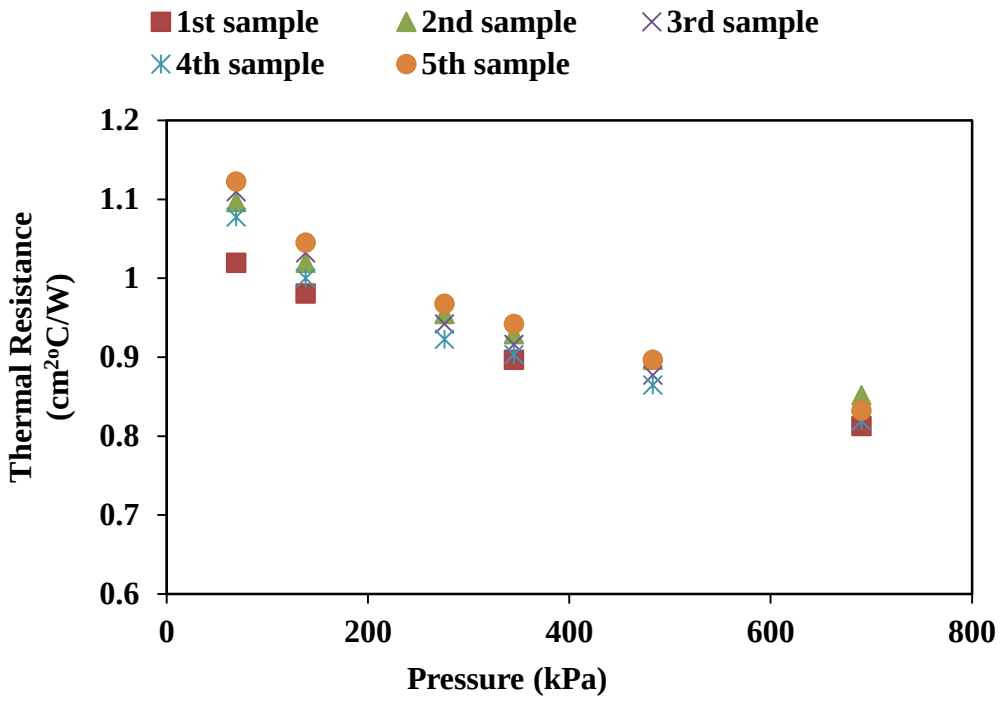

Figure 4.13: Thermal resistance as a function of pressure for five samples of gap pad

Repeating tests of gap pad

This test was similar to what was conducted for the Sil pad (Figure 4.11). After thirty one repeated measurements at 345 kPa with the same sample, the interface resistance was found to decrease from 0.87 cm^2°C/W to 0.74 cm^2°C/W (15% change). Due to the softness of the gap pad, the in-situ thickness decreased from 429 µm to 366 µm (about 15%) at 345 kPa. Thus, a 15% decrease in thickness resulted in a 15% decrease in thermal resistance. The decrease in thermal resistance is due to the effect of time (more air displaced), aided with the reduction in conduction resistance (due to decrease in thickness).

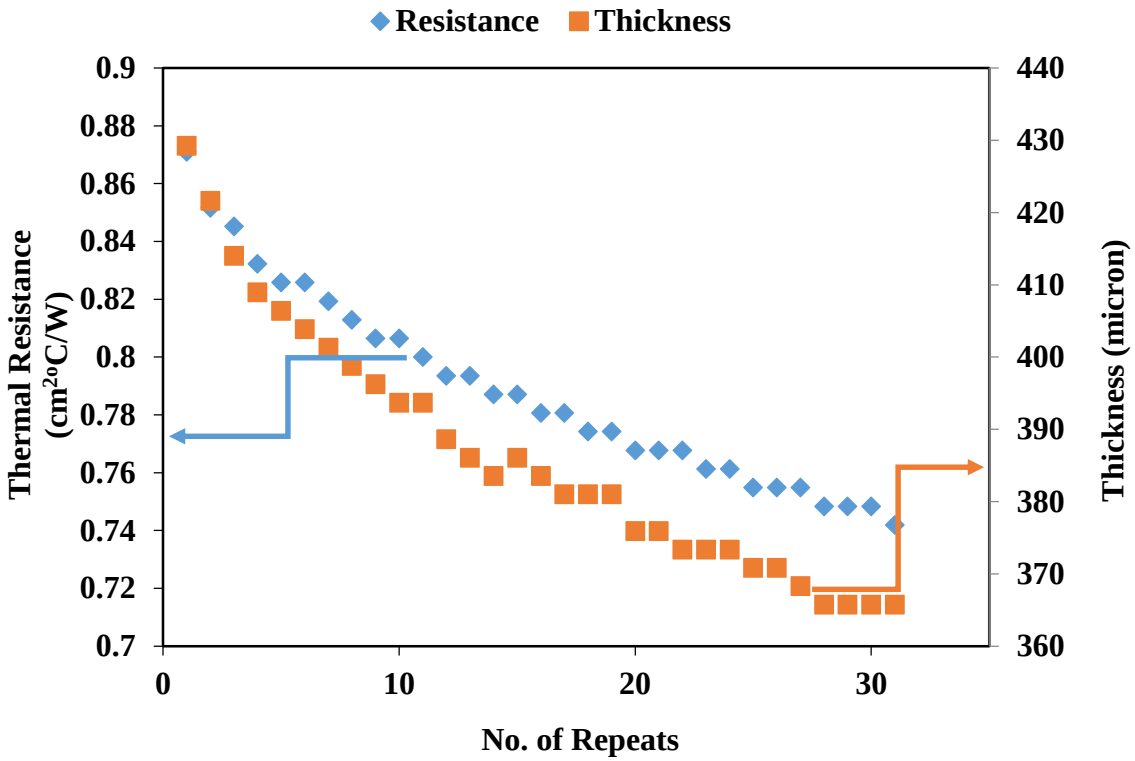

Figure 4.14: Repeated test of Bergquist gap pad 5000S35

Effect of interface temperature

Figure 4.15 shows the response of the gap pad at various interfacial temperatures. It can be concluded that the thermal performance of gap pad is not significantly affected by interface temperature. It was found that the thermal resistance changes only by only 2% (increased from 0.92 to 0.94 cm^2°C/W) as the interface temperature increased from 35 to 85°C. In the same temperature range the sil pads' resistance also increased by 11% (Figure 4.10).

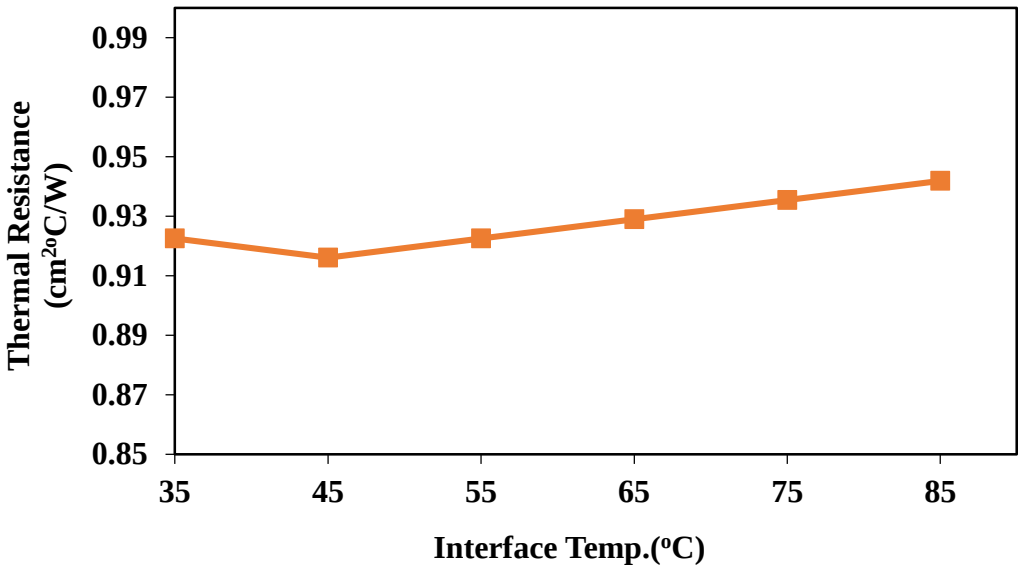

Figure 4.15: Effect of interface temperature for gap pad 5000S35

4.2.4 Testing of indium heat spring

Heat springs are a compressible soft metal alloy TIM (SMA-TIM) offered by Indium Corporation of America. Indium Corporation recommended using this TIM above 241 kPa (35 psi) in order to get an acceptable thermal performance. The thermal resistance of the 102 µm (4 mil) thick indium heat spring was measured at different pressures and the results were compared with the data provided by Indium Corporation. This comparison is shown in Figure 4.16. Again, the thermal resistance was seen to decrease from 0.56 cm^2°C/W to 0.16 cm^2°C/W as the pressure increased from 138 kPa to 690 kPa. Repeated test at 345 kPa revealed (Figure 4.17) that the thermal resistance was reduced by around 56% (0.25 cm^2°C/W to 0.11 cm^2°C/W) after 31 measurements. Again, the time under pressure is shown to be a significant factor in determining the thermal resistance.

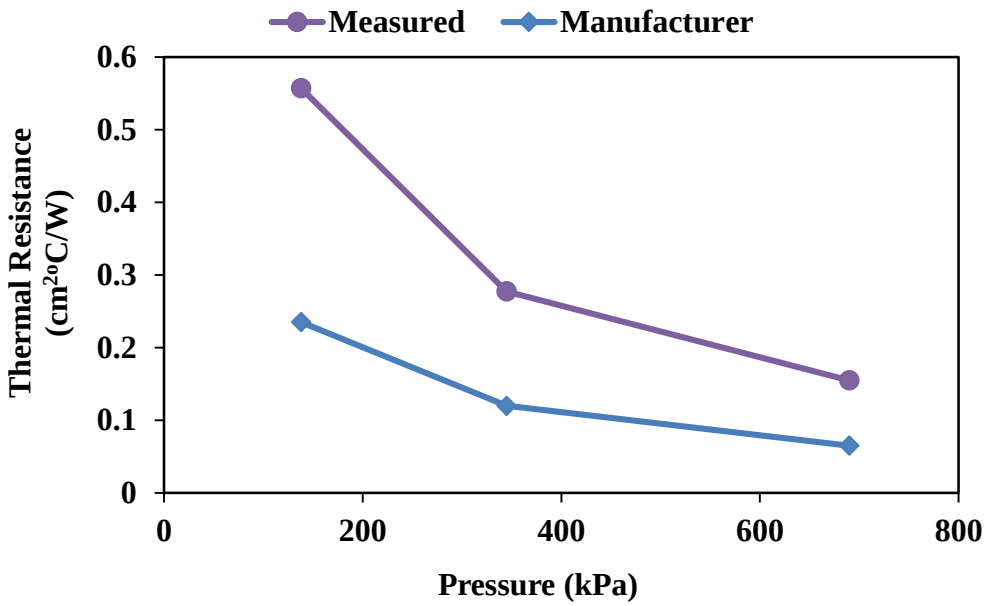

Figure 4.16: Thermal resistance of Indium 4(100In) heat spring

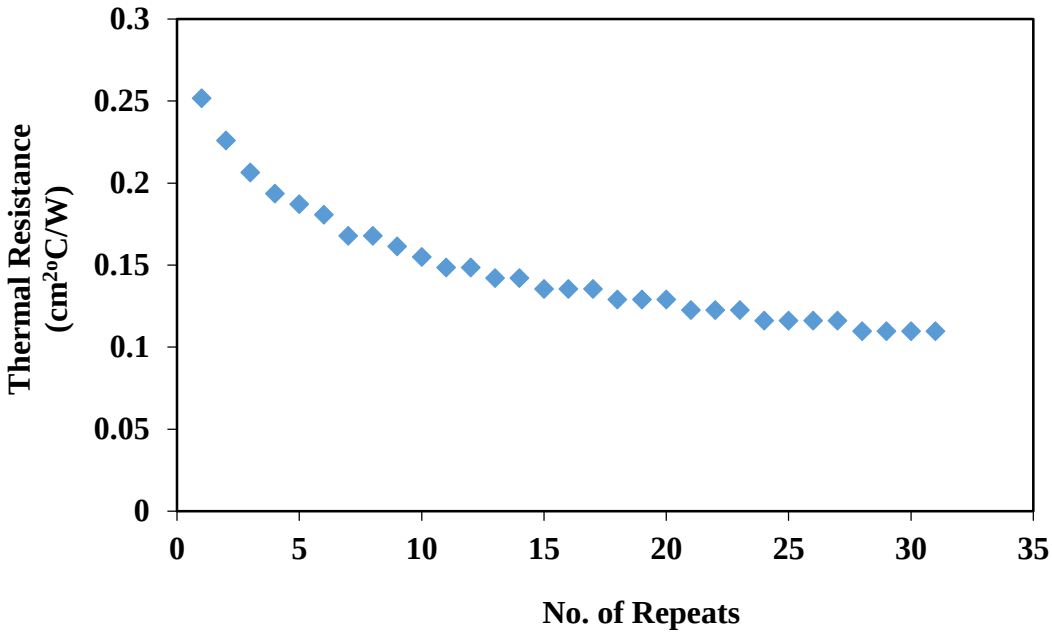

Figure 4.17: Repeated test of Indium 4 (100 In) heat spring

4.3 Overall performance comparison

Figure 4.18 provides an overall comparison of all the commercial TIMs tested using the same apparatus. The bare contact (without any TIM) thermal resistances are also presented for comparison. The best performing TIM was found as the ShinEtsu X-23-7921 thermal grease. The lowest measured thermal resistances of this grease were 0.071 $cm^2°C/W$ and 0.065 $cm^2°C/W$ at 69 and 345 kPa respectively with a thickness of 43 µm. PCMs were found as the second best performing commercial TIM technology. They displayed a lower resistance when compared to other TIMs except the ShinEtsu grease. The Bergquist sil pad A2000 had the highest thermal resistance as compared to all other TIMs tested under this investigation. The gap pad showed better performance compared to the sil pad even though the initial uncompressed thickness of the gap pad was higher (508 µm) as compared to sil pad (381 µm).

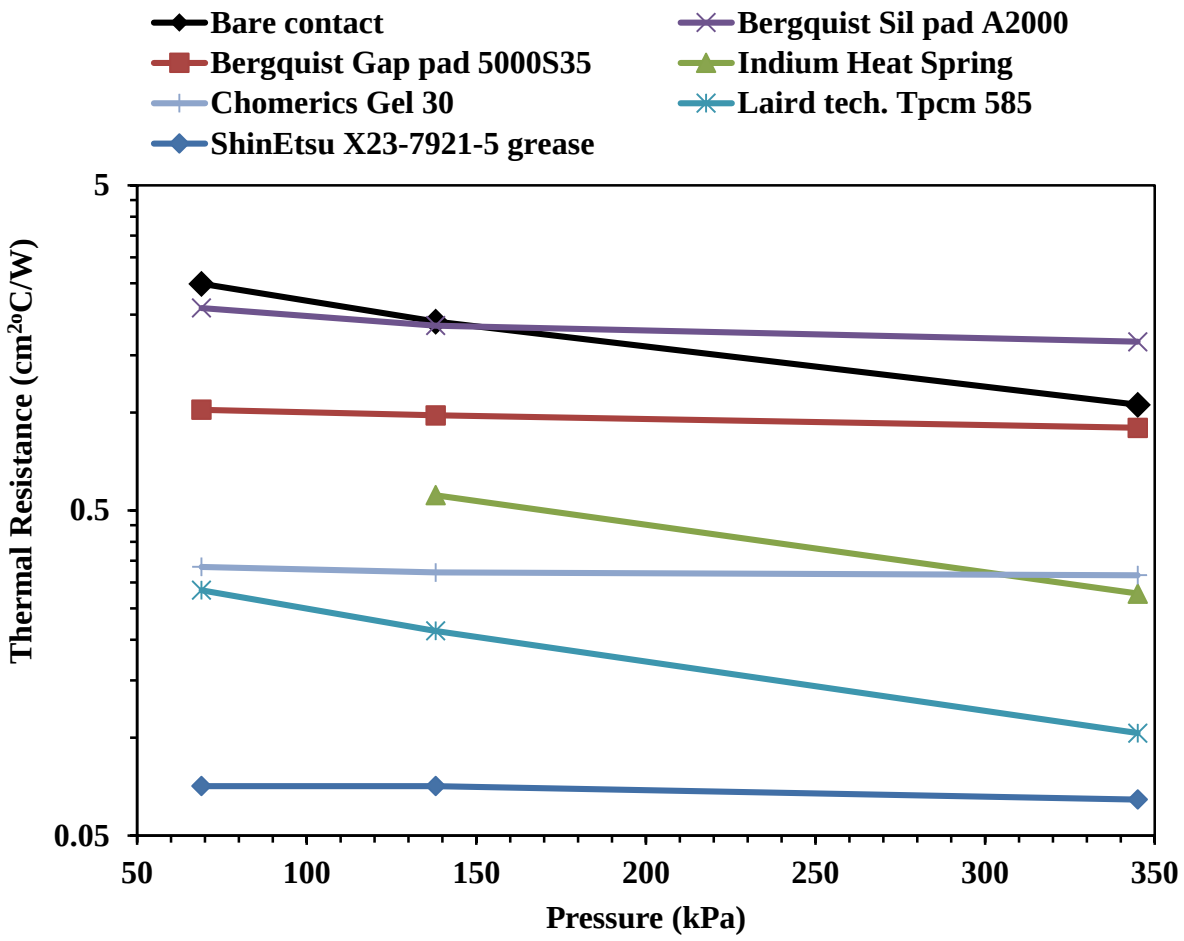

Figure 4.18: Performance comparison of various commercial TIMs

4.4 Summary of commercial TIMs testing

Several conclusions can be drawn from the testing of variety of commercially available TIMs

- Thermal pads (sil pad, gap pad) have higher thermal resistances compared to other commercial TIMs. The performance of Bergquist's gap pad 5000S35 is superior compared to their sil pad A2000 even though the initial thickness of the gap pad is 33% higher compared to the Sil pad. Sil pad A2000 is hard, so the change in thickness in the pressure ranges from 69 to 690 kPa was found negligible. However, gap pads are soft and the

thickness reduces by around 15% in the same pressure range. Thermal pads are easy to apply and remove from the interface.

- Heat springs (100% In) shows better performance in the high pressure range. They are also easy to apply and remove from the interface like thermal pads.
- Repeated test results reveals that the duration that a TIM kept under pressure is a significant factor in determining thermal resistance. For example, thermal resistance of the Indium heat spring reduces by as much as 56% after thirty one repeated measurements at 345 kPa.
- PCMs provide lower resistance compared to thermal pads and gels. But they form a strong bond with the test surfaces upon melting which make it difficult to remove from the interface after testing. There will be rework concerns with PCMs.
- ShinEtsu X-23-7921-5 thermal grease has the lowest thermal resistance and a thinner BLT. However, due to high the viscosity of greases, they are messy and difficult to apply and remove from the interface. Greases do not form any chemical bonding with the test surfaces like PCMs. Excess grease was found to extrude out from interface with the application of higher pressure, must be cleaned to avoid any electrical shorts in actual CPU-heat sink application.

Chapter 5 : Performance of LMAs

5.1 Thermal conductivity measurement

One of the crucial reasons for using an LMA as TIM is due to their extremely high thermal conductivity, which is an order of magnitude high compared to conventional TIMs [4]. The thermal conductivity of Ga-In alloy (liquid at room temperature) was measured using a transient thermal conductivity analyzer by C-Therm (Figure 3.1) and was found to be 25 W/m°C as presented in Table 5.1 , which is more than four times higher than the best thermal grease (6 W/m°C for ShinEtsu X23-7921-5, Table 4.1).

Table 5.1: Thermal conductivity of Ga-In alloy at room temperature

Material	Test	Thermal conductivity (W/m°C)	Average	Standard deviation	%RSD
Ga-In Alloy	1	25.66	25.00	0.36	1.43
	2	24.98			
	3	25.02			
	4	24.94			
	5	24.58			
	6	24.84			

5.2 Thermal resistance measurements

The thermal resistances of nine different substrate-alloy combinations (three alloys between three different surfaces) tested using the modified test-rig (i.e. using the copper disks previously described) is presented in Figure 5.1. For example, a total of five samples were tested with In-Bi-Sn alloy between bare copper disks, designated as Cu/In-Bi-Sn/Cu. The lowest resistance measured was 0.014 $cm^2°C/W$, whereas the resistance also measured as high as 0.065 $cm^2°C/W$ on a separate test sample. The calculated uncertainties are represented by the error bars in Figure 5.1. Each resistance value presented here is the average of three repeated measurements. The measured lowest resistance was as low as 0.005 $cm^2°C/W$ with W/In-Bi-Sn/W and as high as 0.065 $cm^2°C/W$ with Cu/In-Bi-Sn/Cu. The variation in thermal resistance for the same substrate-alloy combination results from the unique nature of each sample and points to workmanship issues. Since LMAs are highly conductive and the joints are relatively thin, the contact resistances (mostly due to surface irregularities such as surface roughness and flatness) dominate the interfacial resistance. Even a small change in surface properties would result in observable changes in the overall thermal resistance. It was assumed that all the disks had the same degree of surface roughness and flatness, but this is not valid in reality. It should be noted that it was not possible to maintain the exact amount of LMAs at the interface for each pair of disks during testing. Another source of variation might appear from the manual scrubbing (wetting) of LMAs onto the disk surfaces. During the wetting process, it was found that some samples were more easily wetted while others required hard scrubbing to induce wetting. If the LMAs do not wet the entire surface properly, small air pockets might be present at the interface, which in turn increases the thermal resistance. Considering all these factors, each disks pair was different and it was a challenge to reproduce the result even with similar substrate-alloy combination. Other properties of the alloys

such as viscosity, surface tension, and oxidation state during application might cause the variation in thermal performance for different substrate-alloy combinations.

5.3 Repeatability

Table 5.2 represents the results of ten separate tests of thermal resistances on a single sample of In-Bi-Sn alloy between bare copper disks at 138 kPa. After each test, the sample was taken out, the silicone oil was cleaned from the surfaces, and then the sample was set back to start another test. The measurements showed that the average thermal resistance was 0.030 $cm^2°C/W$ with a relative standard deviation (RSD) of 5.42%. The results indicate an excellent repeatability of the setup.

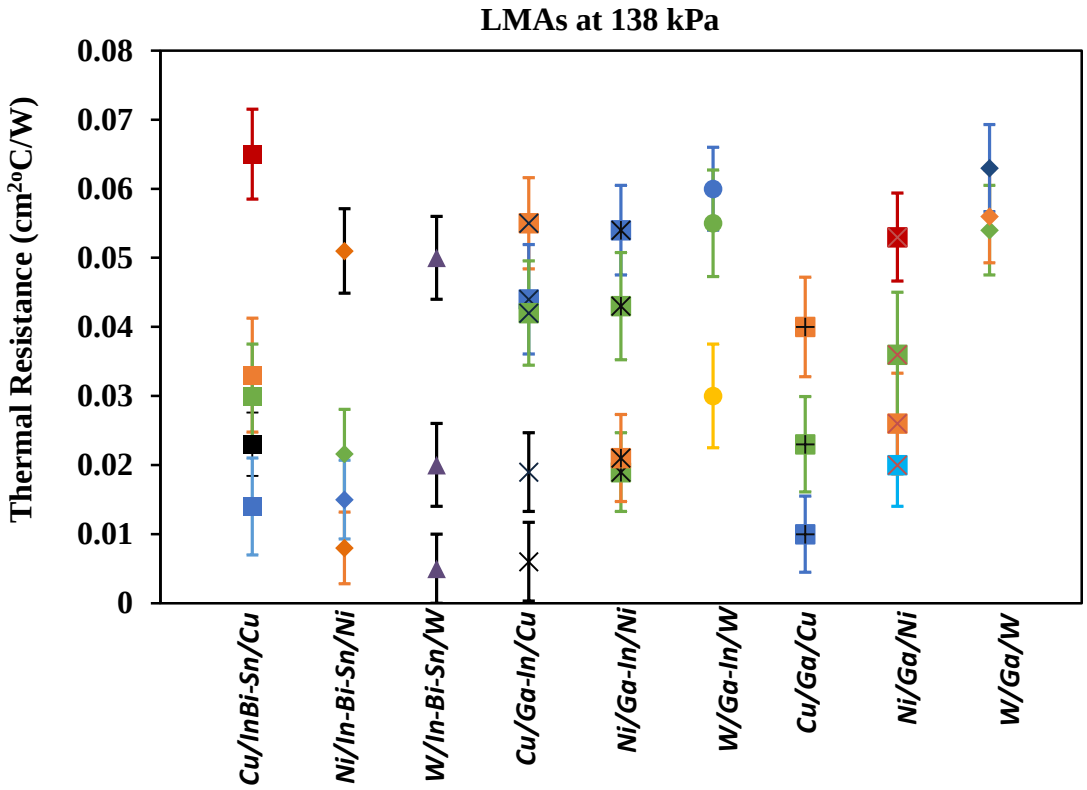

Figure 5.1: *In situ* thermal resistances of different substrate-alloy combinations

Table 5.2: Repeatability of the thermal resistance measurement at 138 kPa

Material	Test	Thermal resistance ($cm^2{}^oC/W$)	Average	%RSD
Cu/In-Bi-Sn/Cu	1	0.030	0.030	5.42
	2	0.028		
	3	0.028		
	4	0.030		
	5	0.030		
	6	0.032		
	7	0.030		
	8	0.029		
	9	0.033		
	10	0.031		

5.4 Effect of interfacial pressure

The thermal resistances of Ga-In, Ga, and In-Bi-Sn (102 micron sheet and molten) as a function of applied pressure are presented in Figure 5.2. For all the alloys, the thermal resistance was found to be almost independent (within the experimental uncertainty) of the applied pressure in the range 34.5-345 kPa as shown in Figure 5.2. Since the LMAs are non-viscous liquid in molten form, high pressure is not required to fill the mating surface irregularities. This observation agrees well with the results of Web and Gwinn [32] where they found only 5% variation of thermal resistance in the pressure range 34.5-138 kPa. Based on the results, it can be concluded that LMAs offer excellent thermal bond even at a small pressure.

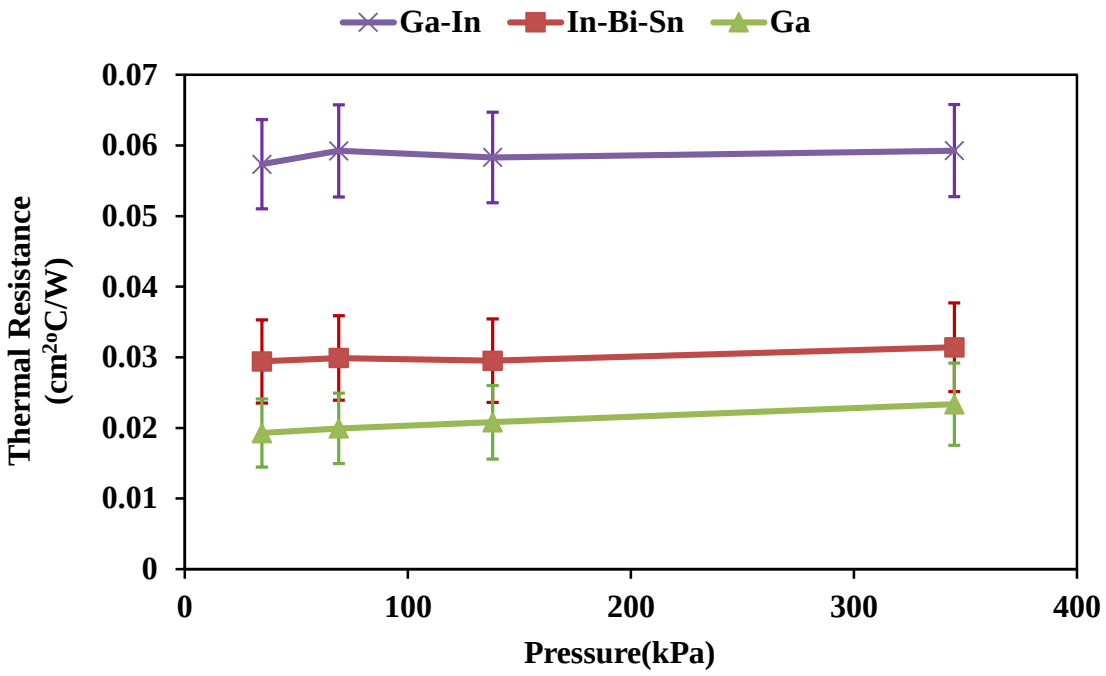

Figure 5.2: Thermal resistances of Ga-In, Ga, and In-Bi-Sn alloy as a function of applied pressure

5.5 Effect of interface temperature

A series of tests were conducted to observe the effect of interfacial temperature on the thermal resistance of In-Bi-Sn alloy (102 µm sheet and molten). The tests were conducted at different interfacial temperatures in the range 35-85^{o}C keeping the pressure constant at 69 kPa. The results are presented in Table 5.3. The thermal resistance was found to be insensitive to the interface temperatures tested. This study concludes that once the alloy melts and seats at the interface, the interface temperature does not affect the performance significantly.

Table 5.3: Thermal resistances of In-Bi-Sn alloy (sheet and molten) at different interface temperatures

Interfacial temperature (^oC)	In-Bi-Sn Alloy (102 µm sheet) Thermal Resistance ($cm^2{}^oC/W$)	In-Bi-Sn (molten) Thermal Resistance ($cm^2{}^oC/W$)
35	0.033±23%	0.037±20%
55	0.031±25%	0.039±18%
75	0.033±23%	0.039±18%
85	0.033±23%	0.037±20%

5.6 Reliability testing (phase 1)

Phase 1 reliability testing includes high temperature aging at 130^{o}C and thermal cycling from -40^{o}C to +80^{o}C. The alloys were placed between bare copper (Cu/alloy/Cu), nickel-coated copper (Ni/alloy/Ni) and tungsten-coated copper substrates (W/alloy/W) to investigate different substrate-alloy interactions upon thermal aging and cycling.

5.6.1 Accelerated thermal aging

Accelerated aging was carried out by exposing the disks assembly with alloys at the interface at an elevated temperature of 130^{o}C (followed reliability conditions of [49]) in an atmospheric furnace (Cress electric furnace, model: C136) for extended periods of time.

5.6.1.1 Thermal aging of In-Bi-Sn alloy

Figure 5.3 shows the accelerated thermal aging behavior of In-Bi-Sn alloy in molten form applied between bare copper, nickel-coated copper, and tungsten-coated copper surfaces. The tests were carried out at 138 kPa and an interface temperature 10^{o}C above the melting point of the alloy. The thermal resistances are plotted as a function of aging time and the associated uncertainty is represented by the error bars. It was found that after 1,900 hours of aging with In-Bi-Sn alloy between bare copper surfaces (designated as Cu/In-Bi-Sn/Cu), the thermal resistance did not change significantly (remained within the experimental uncertainty) compared to the initial resistance. The results indicate an excellent thermal performance of In-Bi-Sn alloy between bare copper surfaces. Yang *et al.* [37] did not find any degradation of the same In-Bi-Sn alloy placed between bare copper foil after heating at 100^{o}C for 800 hours. However, they found an interfacial crack after heating at 150^{o}C for 400 hours, which concludes that degradation may occur anywhere between 130^{o}C and 150^{o}C. With In-Bi-Sn alloy between nickel surfaces, the resistance increased by about 133% (from 0.024 cm^{2}°C/W to 0.056 cm^{2}°C/W) after 1,900 hours of aging. Even though this seems a large percentage increase, the thermal resistance is still lower (0.056 cm^{2}°C/W) compared to the performance of commercial TIMs presented in chapter 4. The thermal resistance of In-Bi-Sn alloy between tungsten-coated surfaces started to increase steadily after 576 hours (24 days). The resistance increased from 0.011 cm^{2}°C/W to 0.032cm^{2}°C/W after 1,900 hours of aging.

The superior aging performance of In-Bi-Sn alloy is believed to be due to the enhanced wetting of the alloy with the substrate surface. If the alloy wets the mating surfaces properly, the thermal performance will degrade very slowly. Since In-Bi-Sn alloy contains 51% In, it is most likely to form IMCs with copper and nickel [32, 34, 37, 50]. Most common IMCs of In with copper and nickel at a temperature below 130^{o}C are $Cu_{11}In_{9}$ and $In_{27}Ni_{10}$ [50]. In addition, the growth of

In-Ni intermetallic is slower compared to the growth of Cu-In intermetallic (the growth rate of $Cu_{11}In_9$ at 393K is $31.024*10^{-14}$ cm^2/s, while the growth rate of $In_{27}Ni_{10}$ at the same temperature is $14.976*10^{-14}$ cm^2/s) [50]. Perhaps, for this reason, the thermal resistance of In-Bi-Sn alloy between nickel surfaces increases comparatively faster than between copper surfaces upon aging. However, due to the growth of IMCs in the interfacial region, a mechanical bond between two disks was formed. The disks were hard to separate. Therefore, rework concerns would have to be addressed for the combination of this alloy between bare copper.

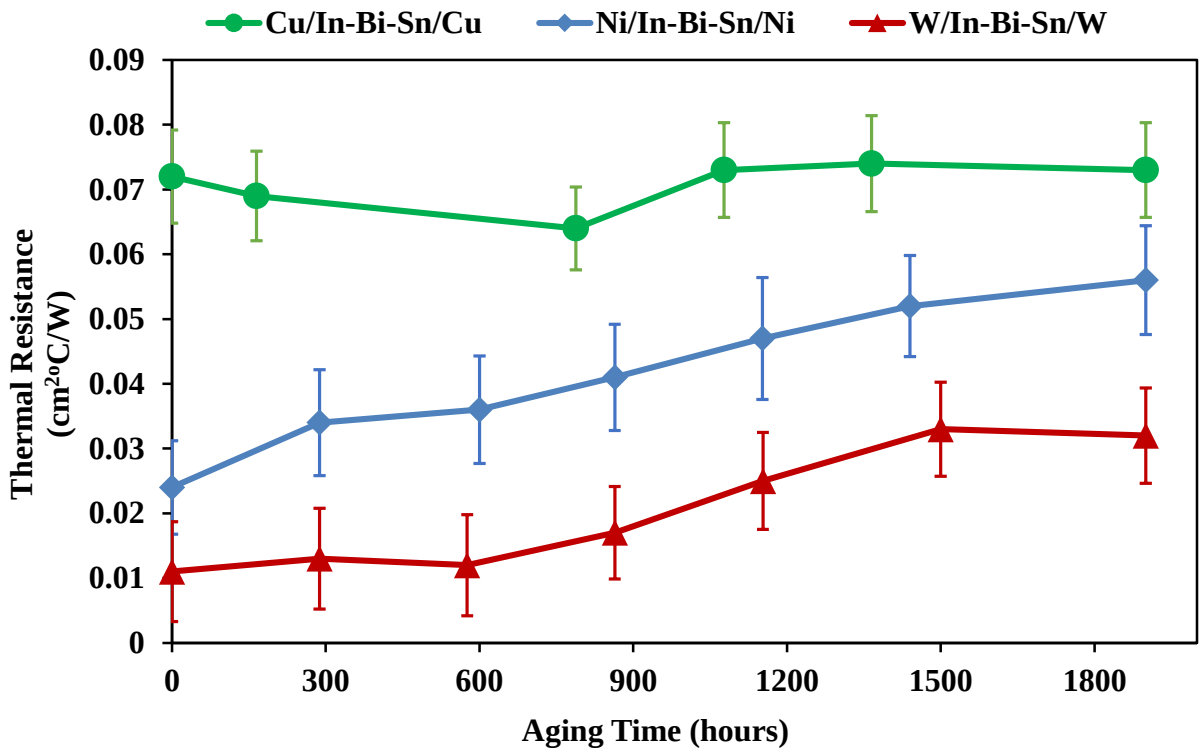

Figure 5.3: Thermal resistances of In-Bi-Sn alloy between different substrate surfaces in response to isothermal aging at 130°C [51]

5.6.1.2 Thermal aging of Ga

The thermal aging test results of Ga between different substrate surfaces are presented in Figure 5.4. It was found that thermal resistance of Ga between bare copper remained almost constant (increased by about 7%, the uncertainty in measurement was about 18%) after 2,277 hours of aging compared to the initial resistance of 0.042 $cm^2°C/W$. With Ga between nickel surfaces, the thermal resistance did not change significantly after 2,300 hours of aging. Ga between tungsten surfaces also showed a negligible change in thermal resistance up to 576 hours of aging. However, the resistance started to increase rapidly thereafter. The thermal resistance increased from 0.057 $cm^2°C/W$ to 0.18 $cm^2°C/W$ after 1,152 hours of aging.

Gallium is most likely to diffuse into copper and nickel and form IMCs [33,52,53]. One common IMC between copper and Ga is $CuGa_2$ [52]. Also, there are several IMCs possible between nickel and Ga at a temperature below 130^oC [53]. Our results suggest that any diffusion and formation of these IMCs that may have occurred did not negatively impact the thermal performance over time. As the thin layer of tungsten resisted the diffusion of Ga into copper, the alloy could not interact with the underlying copper substrate, and therefore, could not form a mechanical bond between the substrates. The tungsten disks were easy to separate due to the absence of intermetallic growth at the interface.

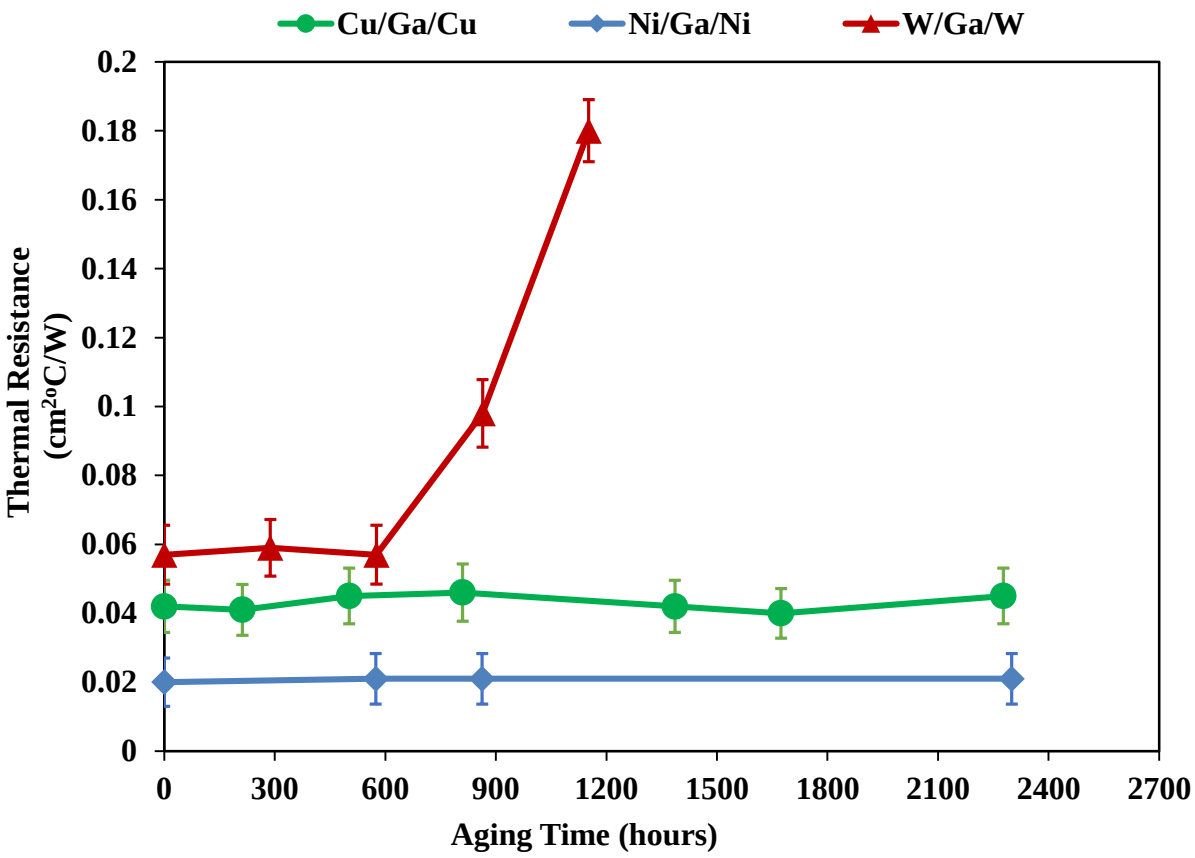

Figure 5.4: Thermal resistances of Ga between different substrate surfaces in response to isothermal aging at 130°C [51]

5.6.1.3 Thermal aging of Ga-In alloy

The thermal aging test results of Ga-In between different substrate surfaces are presented in Figure 5.5. Again, Ga-In alloy (contains 74.5%Ga and 24.5%In) between copper and nickel surfaces exhibited a superior aging behavior. With Ga-In alloy between bare copper and nickel surfaces, the thermal resistance remained unchanged (within experimental uncertainty) after a long aging time (2,000 hours between bare copper and 2,030 hours between nickel-coated copper). However, the thermal resistance of Ga-In alloy between tungsten surfaces was found to increase by about three times after 2,019 hours of aging, which indicates a non-reliable thermal joint.

It can be observed that the aging behavior of Ga-In alloy (Figure 5.5) is similar to the response of Ga (Figure 5.4). This is because both alloys have similarity in their composition, pure gallium contains 100% Ga and Ga-In alloy contains 74.5 % Ga. Therefore, it was expected for both alloys to behave in a similar manner. All these results suggest that interactions between the alloy and the substrates make the joint more thermally reliable.

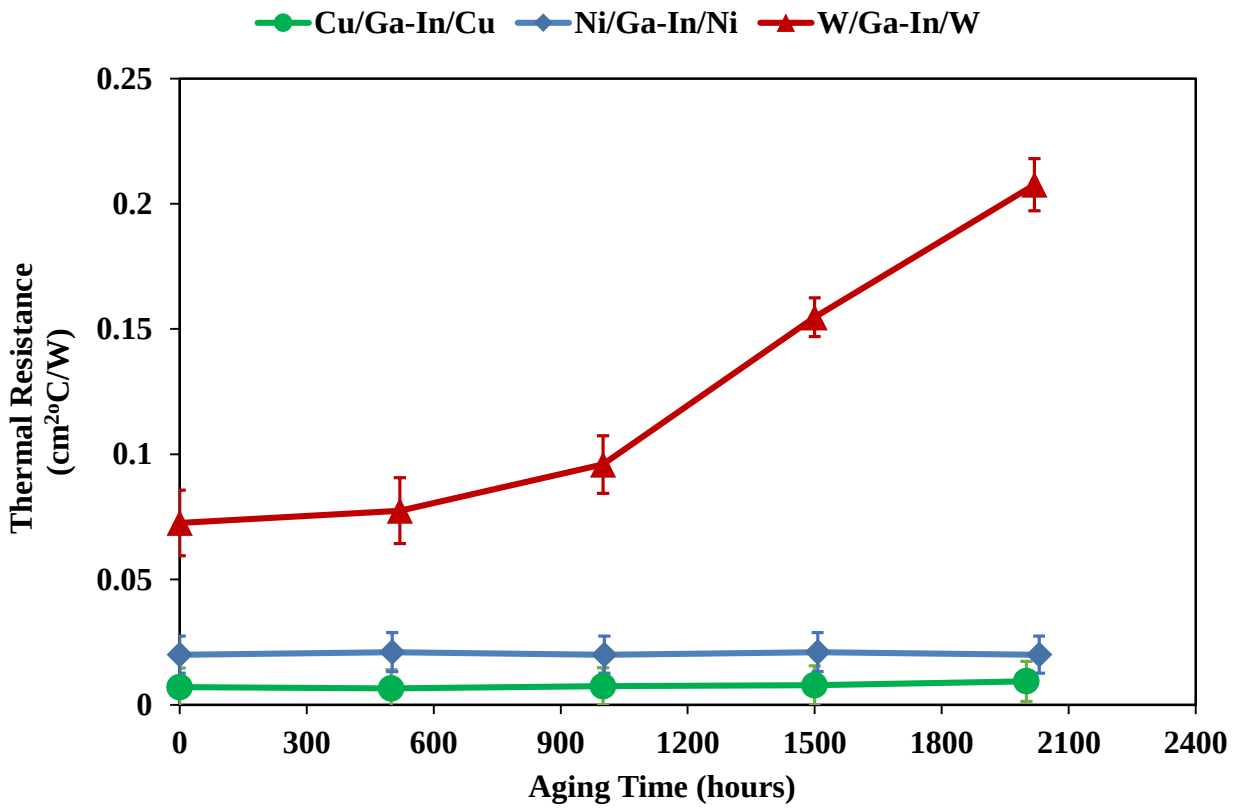

Figure 5.5: Thermal resistances of Ga-In alloy between different substrate surfaces in response to isothermal aging at 130°C

5.6.1.4 Commercial TIMs

To compare the performance of different alloys, a commercially available liquid metal, Liquid Ultra and thermal grease, ShinEtsu X23-7921-5, were also aged similar to the method used to age LMAs. With the Liquid Ultra between bare copper surfaces, the thermal resistance did not increase significantly (within experimental uncertainty) after 1000 hours of aging, as shown in Figure 5.6. With the ShinEtsu grease, the resistance was found to increase by about 75% (from 0.08 cm^2°C/W to 0.14 cm^2°C/W) after 1000 hours of aging. It is well-known that the greases dry out over time [2], which results in increased joint thermal resistances upon aging.

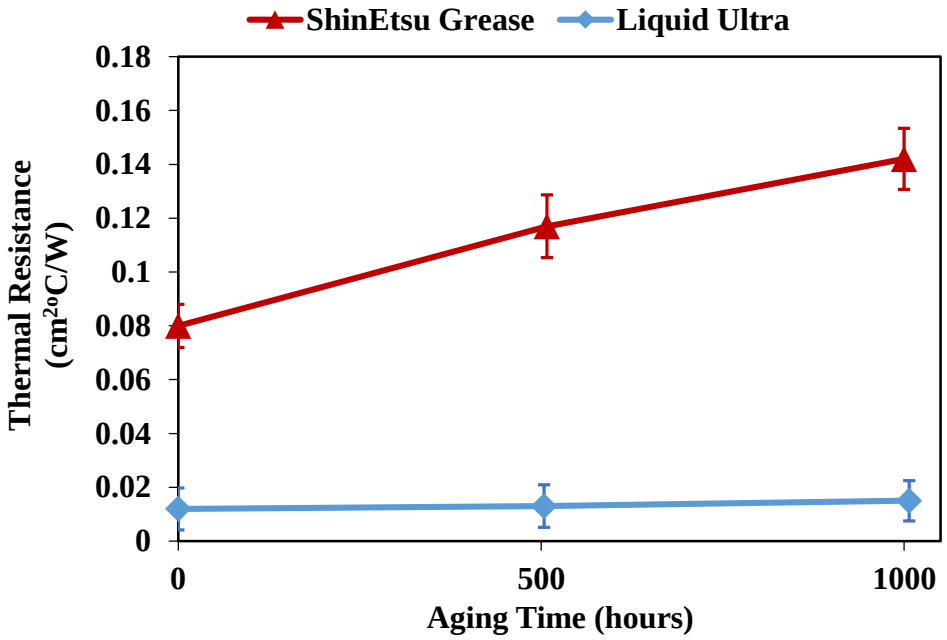

Figure 5.6: Thermal resistances of commercial TIMs in response to isothermal aging at 130°C

5.6.1.5 Summary of accelerated aging results

The normalized thermal resistance (found after dividing by the initial thermal resistance) of three alloys between copper, nickel and tungsten surfaces are presented in Figure 5.7, 5.8, and 5.9 respectively. The isothermal aging results showed that the alloys between copper surfaces

survived extended periods of aging without significant performance degradation (Figure 5.7). Ga and Ga-In alloy between nickel surfaces did not show any degradation in thermal resistance (Figure 5.8). However, the thermal resistance of In-Bi-Sn alloy between nickel surfaces increased by about 133% after 1,900 hours of aging. Alloys between tungsten-coated surfaces could not endure longer aging times. The thermal resistance increased significantly for all three alloys (Figure 5.9). This can be attributed to the poor alloy-tungsten interaction which is primarily due to the lack of alloy diffusion and interfacial reaction. LMAs can perform remarkably well compared to the commercial TIMs when proper substrate-alloy combinations are chosen.

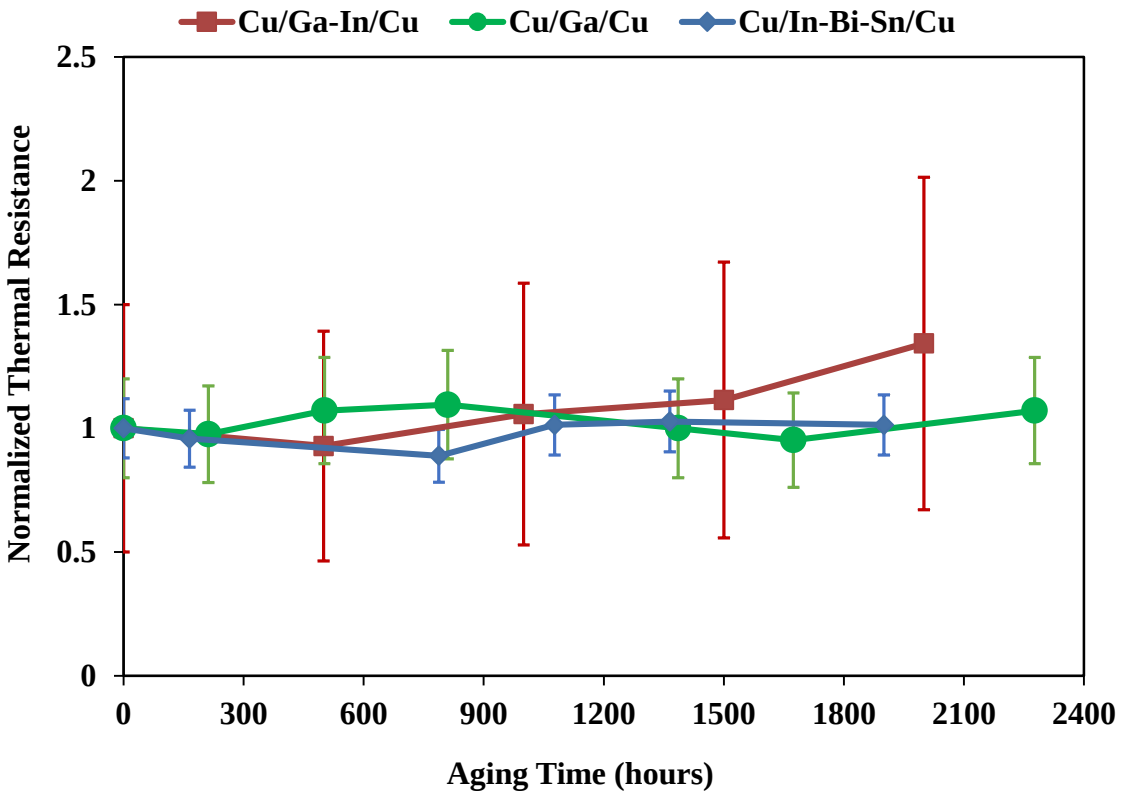

Figure 5.7: Normalized thermal resistance of three alloys placed between bare copper surfaces in response to thermal aging at 130^{o}C [54]

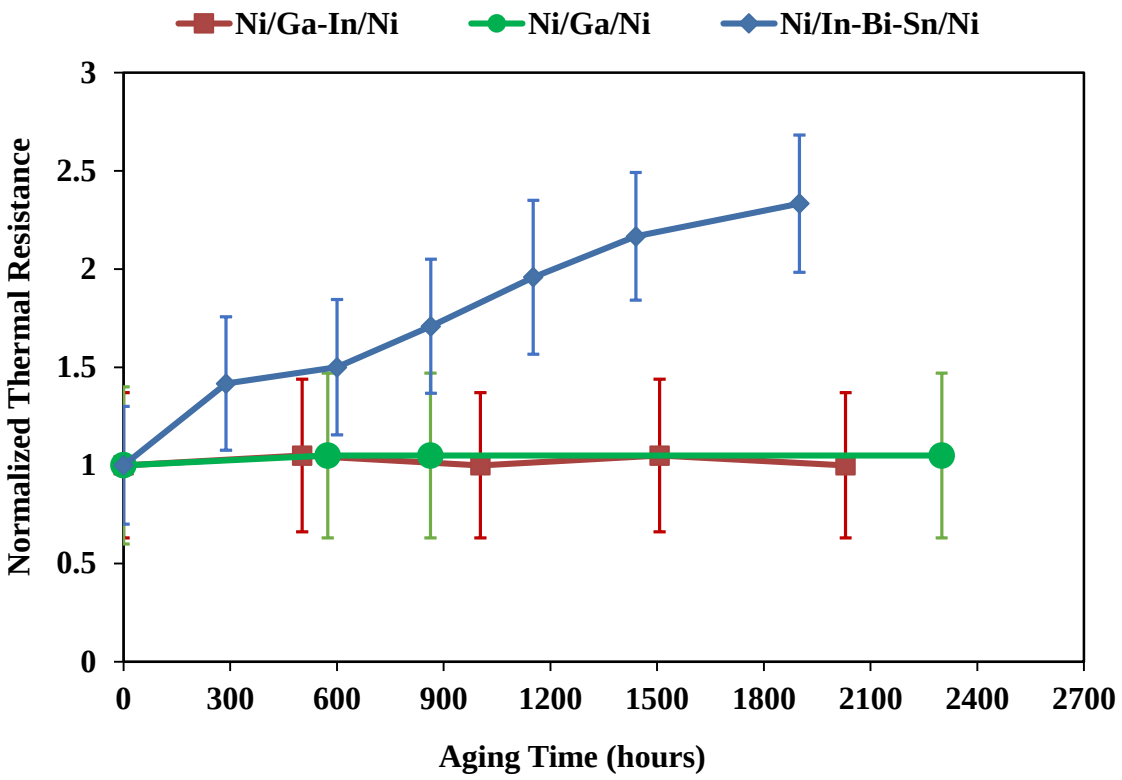

Figure 5.8: Normalized thermal resistance of three alloys placed between nickel surfaces in response to thermal aging at 130^{o}C

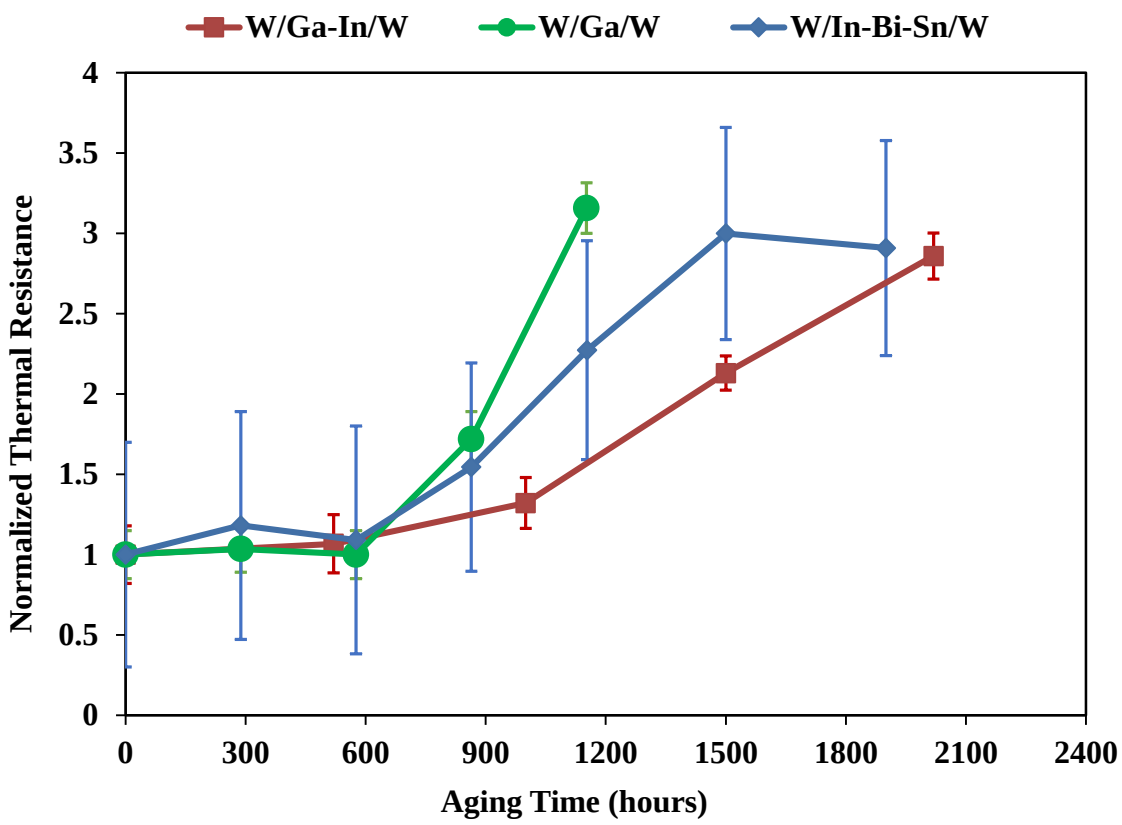

Figure 5.9: Normalized thermal resistance of three alloys placed between tungsten surfaces in response to thermal aging at 130^{o}C

5.6.2 Thermal cycling

The purpose of these tests is to cycle each sample above and below the melting point of the interfacial alloy. The disks assembly with alloys at the interface was placed in a thermal cycling chamber to cycle from -40^{o}C to 80^{o}C [49]. The heating and cooling were performed at ramp rates of 3^{o}C/minute for both the heating and cooling transitions. The samples were soaked for 20 minutes at the two extreme temperatures, ensuring that the interface reached the chamber temperature. The time needed to complete a thermal cycle was 2 hours.

5.6.2.1 Interface response

Figure 5.10 shows how the interface of a copper disk pair responded with the chamber temperature. The interface temperature was measured by taking the average of two thermocouples readings, which were inserted into the holes of two copper disks while the chamber temperature was measured using a four wire RTD placed inside the chamber. For two cycles (240 minutes), the temperature was recorded using an Agilent 34972A data acquisition system. The response is presented in Figure 5.10. The graph shows that 20 minutes of soak time is sufficient for the interface to reach the chamber air temperature. Also, it can be noticed that the interface takes about 10 minutes to reach the chamber temperature.

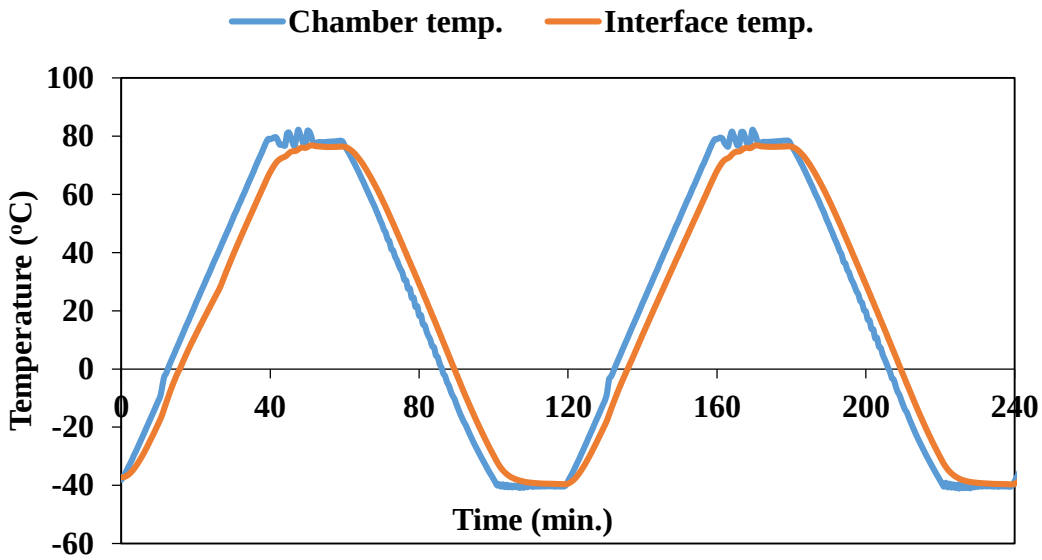

Figure 5.10: Interface temperature of the copper disks assembly and chamber air temperature for 2 cycles (240 minutes)

5.6.2.2 Thermal cycling of In-Bi-Sn alloy

Thermal cycling of In-Bi-Sn alloy in different forms (molten and 102 micron sheet) on different surfaces is presented in Figure 5.11 below. It is apparent from the figure that In-Bi-Sn alloy in its molten form (melted the alloy first and then applied on the heated disks) has an improved thermal cycle performance when compared to its sheet application. After 1,400 cycles (2800 hours) of In-Bi-Sn alloy between bare copper surfaces, the thermal resistance increased only by about 22% from its initial value of 0.023 $cm^2°C/W$ (the measurement uncertainty was about 32%), while the thermal resistance of In-Bi-Sn alloy as a 102 micron (4 mil) sheet increased significantly (by about 5.5 times) after 1,400 cycles. Roy *et al.* [8] discussed this reason as the enhanced wetting of the alloy in molten form. When applied as a solid sheet, most of the alloy came out of the interface upon melting. After the test, upon separation of the disks, it was found that the alloy did not wet the interface properly. As a result, the alloy extruded out of the interface due to expansion and contraction occurred upon thermal cycling, which resulted in the loss of the contact area. For this reason, the thermal resistance increased significantly upon thermal cycling. On the other hand, when applied in molten form, the disks were mechanically scrubbed with the molten alloy to induce wetting. Hence, the alloys remained within the interface, no extrusion was observed upon thermal cycling, and thereby voids could not be formed at the interface. Therefore, the thermal resistance did not change significantly upon thermal cycling. This result agrees well with the work of Hill and Strader [34], where no degradation of this alloy was found after running 1,000 cycles between room temperature and 150^oC.

In-Bi-Sn alloy between nickel-coated surfaces was also found to perform well; after 1,400 cycles, the thermal resistance remained within the experimental uncertainty. The thermal cycling test of In-Bi-Sn alloy between nickel surfaces was repeated with a second sample to ensure the

repeatability of the test results. A second sample of In-Bi-Sn alloy between nickel surfaces also responded well to thermal cycling as shown in Figure 5.11.

Along with the alloy-substrate interaction, another factor that affects the thermal performance of the TIM is the CTE mismatch between different substrates. Due to the CTE mismatch, the TIM gradually extrudes out of the interface because of the expansion and contraction occurring during thermal cycling. This phenomenon is known as the pump-out of the TIM. Voids can be created at the interface because of this pump-out effect, which in turn increases the thermal resistance. The CTE mismatch between copper and nickel is smaller (about 4 $\mu m/m^oC$). In addition to that, the diffusion of In into nickel produces a good thermal joint, improving the performance under thermal cycling.

With In-Bi-Sn alloy between tungsten surfaces, the resistance was found to increase significantly upon thermal cycling, which indicates the failure of the thermal joint. It is shown in isothermal aging of In-Bi-Sn alloy between tungsten surfaces (Figure 5.3) that the thermal resistance started to increase after certain hours (576 hours), however, during cycling, the resistance increased significantly just after 200 cycles (400 hours). This can be attributed to the poor alloy-tungsten interaction as well as the large CTE mismatch between copper and tungsten (about 13 $\mu m/m^oC$). During the wetting process, it was found that the tungsten-coated disks required hard scrubbing to induce wetting because the tungsten layer resisted the formation of an oxide layer on the surface. The large CTE mismatch along with the improper wetting of the alloy on tungsten resulted in an extrusion of the alloy from the interface upon thermal cycling, causing the thermal resistance to increase significantly.

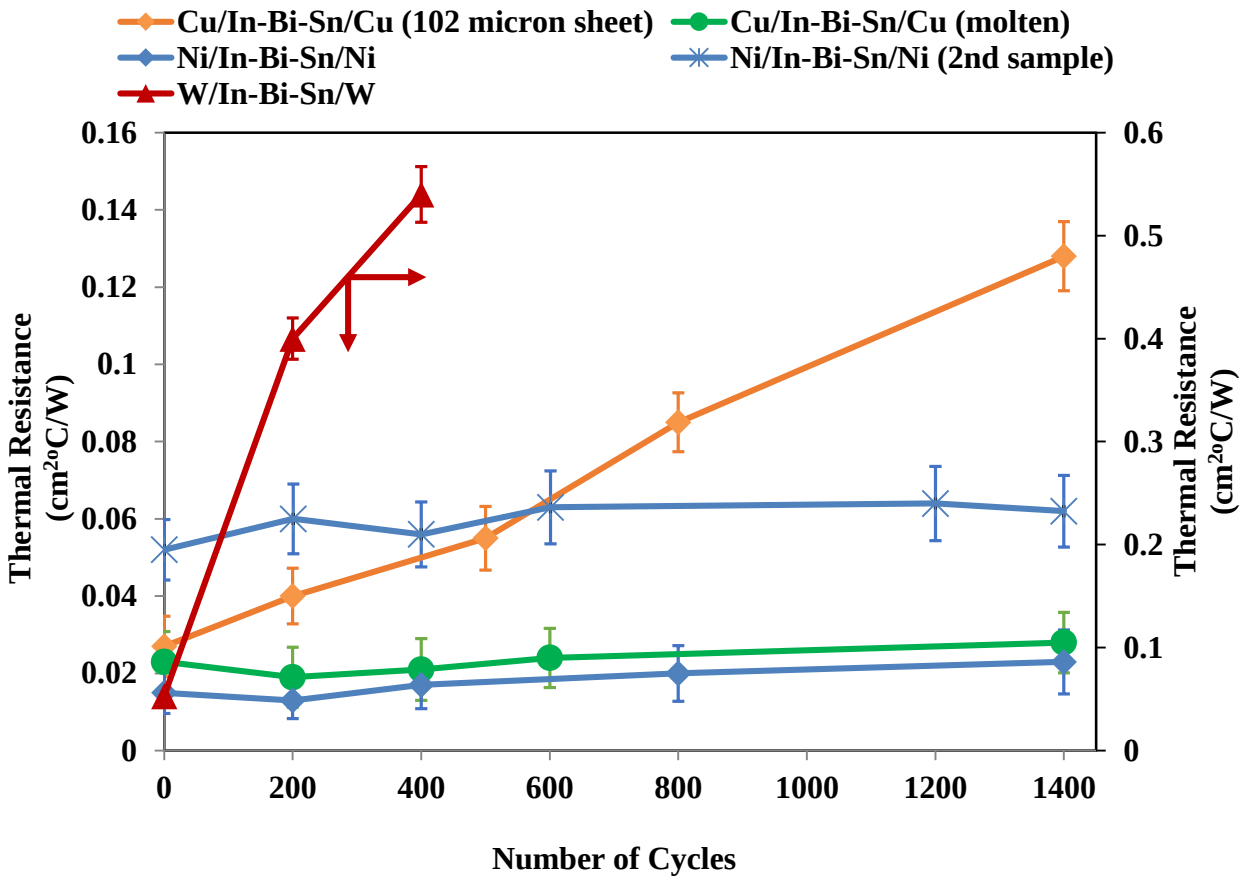

Figure 5.11: Thermal cycling (-40°C to +80°C) of In-Bi-Sn alloy between different substrate surfaces [51]

5.6.2.3 Thermal cycling of Ga

Figure 5.12 shows thermal cycling of Ga between different substrate surfaces. The results showed that the thermal resistance of Ga between bare copper surfaces did not change significantly even after 1,400 cycles. However, the thermal resistance of Ga between nickel surfaces increased by about four times (300% increase) after 1,000 cycles. With Ga between tungsten surfaces, the thermal resistance increased significantly upon thermal cycling; it doubled for the first sample and increased by about 4.5 times for the second sample as shown in the Figure 5.12 below. Although Ga between nickel surfaces survived a long aging time (Figure 5.4), it failed to endure thermal

cycling. This is because, during aging, the sample was kept at a constant temperature; there was no pump-out due to expansion and contraction of the thermal joint as in thermal cycling. The interaction between the bare copper substrate and Ga makes the thermal joint more durable. It was found that the disks were bonded together like a solder joint. However, due to this diffusion and bonding, the disks were hard to separate after the test.

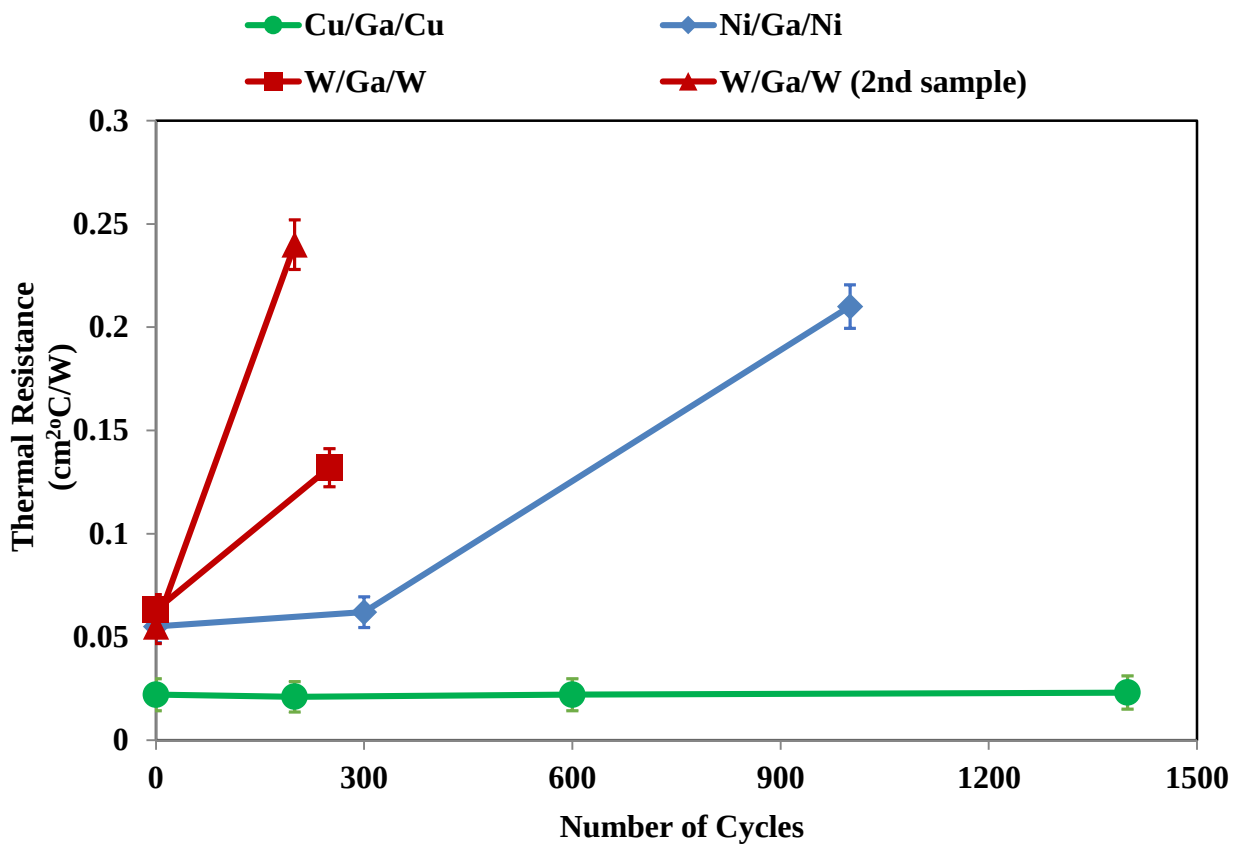

Figure 5.12: Thermal cycling(-40°C to +80°C) of Ga between different substrate surfaces

5.6.2.4 Thermal cycling of Ga-In alloy

The thermal cycling response of Ga-In alloy between different surfaces is presented in Figure 5.13. The tests were repeated with multiple samples to observe the repeatability of the

results. Similar to Ga, Ga-In alloy between bare copper surfaces performed very well with thermal cycling. The thermal resistance did not change significantly for both samples even after 1,400 cycles, which indicates an excellent thermal joint. Again, this can be attributed to the interaction (diffusion and interfacial reaction) of the Ga-In alloy (which contains 75% Ga and 25% In) with bare copper substrate, which makes the thermal joint highly reliable. Thermal resistances of Ga-In alloy between nickel and tungsten surfaces increased significantly after a small numbers of cycles. The tests were repeated with multiple samples and both samples displayed the same trend, which ensured the repeatability of the test results. It can be noticed that similar to aging, the thermal cycling response of Ga-In alloy (Figure 5.13) is very similar to Ga (Figure 5.12). Both alloys between bare copper survived large number of cycles (1,400). However, between nickel and tungsten surfaces, the resistances increased significantly for both alloys.

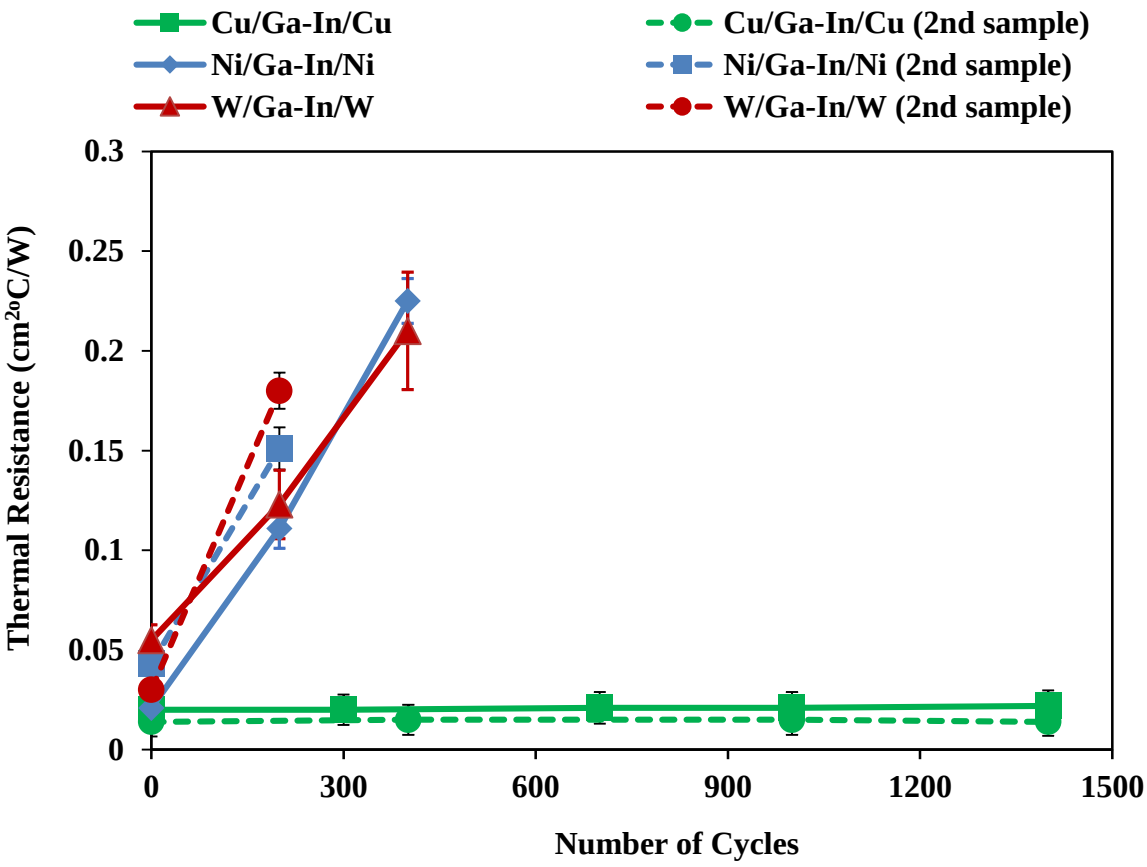

Figure 5.13: Thermal cycling (-40°C to +80°C) of Ga-In alloy between different substrate surfaces

5.6.2.5 Thermal cycling of commercial TIMs

Similar to aging, to compare the thermal cycling performance of the proposed alloys, commercial ShinEtsu X23-7921-5 grease and Liquid Ultra were also thermally cycled by placing between bare copper disks and the results are shown in Figure 5.14. The thermal resistance was found to increase by about 175% after 800 cycles for ShinEtsu Grease and after 1,400 cycles for Liquid Ultra. Comparing the performance of commercial TIMs with all three alloys, it can be concluded that the suggested alloys performed remarkably well when placed between bare copper disks.

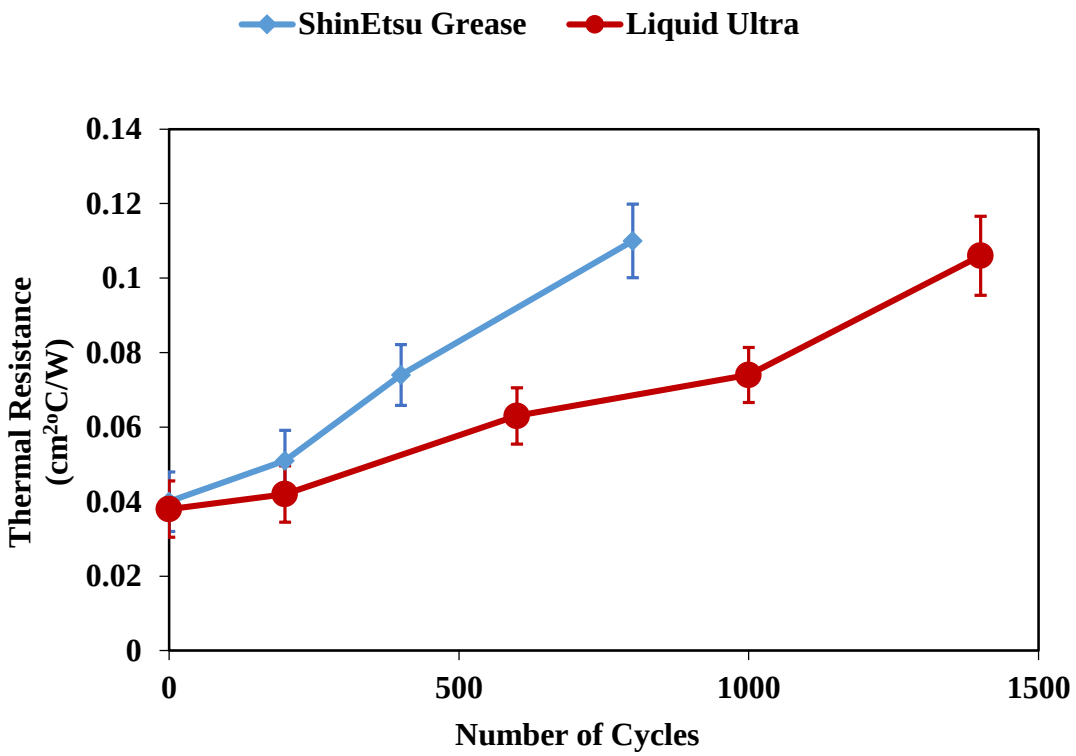

Figure 5.14: Thermal cycling (-40°C to +80°C) of Liquid Ultra and ShinEtsu grease between bare copper surfaces [51]

5.6.2.6 Summary of thermal cycling

The normalized thermal resistances (found after dividing by the initial thermal resistance) of three alloys between copper, nickel, and tungsten surfaces are presented in Figure 5.15, 5.16, 5.17 respectively. The thermal cycling results showed that the alloys between bare copper surfaces survived 1,400 cycles without significant performance degradation (Figure 5.15). In-Bi-Sn alloy between nickel surfaces did not show any degradation in thermal resistance upon thermal cycling. However, the thermal resistance of Ga and Ga-In alloy between nickel surfaces increased significantly after few cycles, which indicates the failure of the thermal joint (Figure 5.16). All the alloys between tungsten-coated surfaces did not survive thermal cycling (Figure 5.17). Again, as

discussed earlier, this might be due to the poor alloy-tungsten interaction. LMAs can perform remarkably well compared to the commercial TIMs (Figure 5.14) when proper substrate-alloy combinations are chosen.

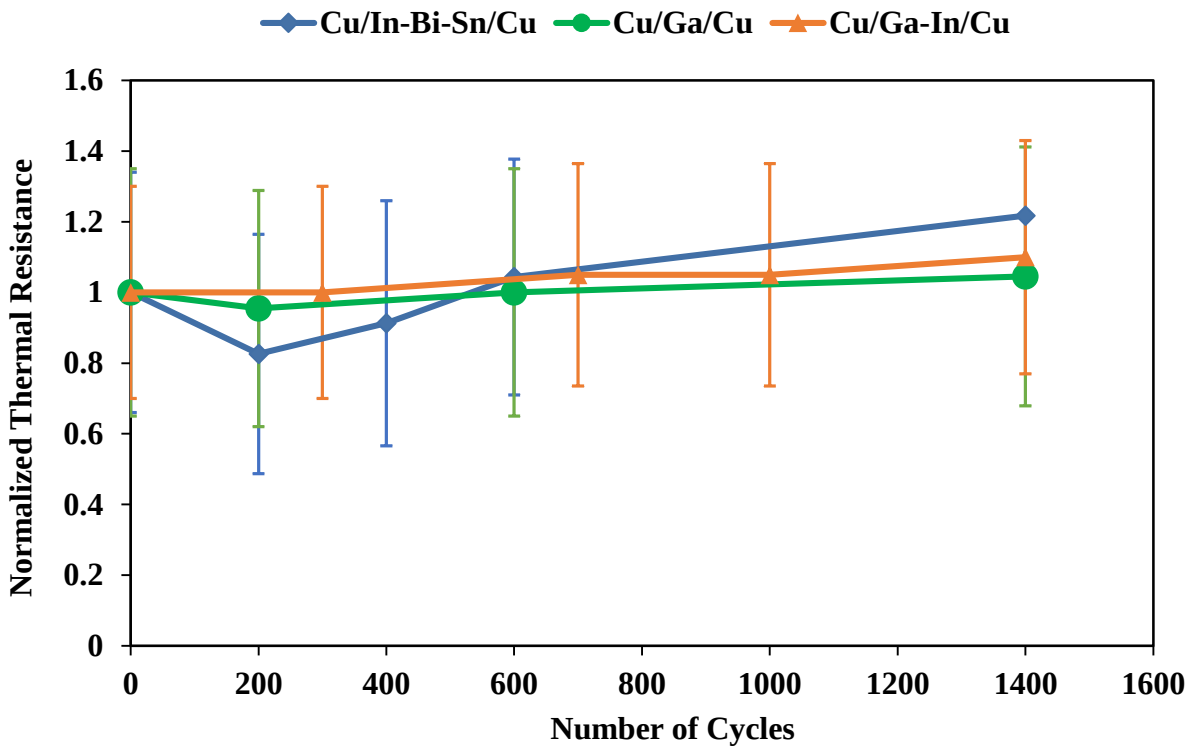

Figure 5.15: Normalized thermal resistance of three alloys placed between bare copper surfaces in response to thermal cycling (-40^{o}C to +80^{o}C)

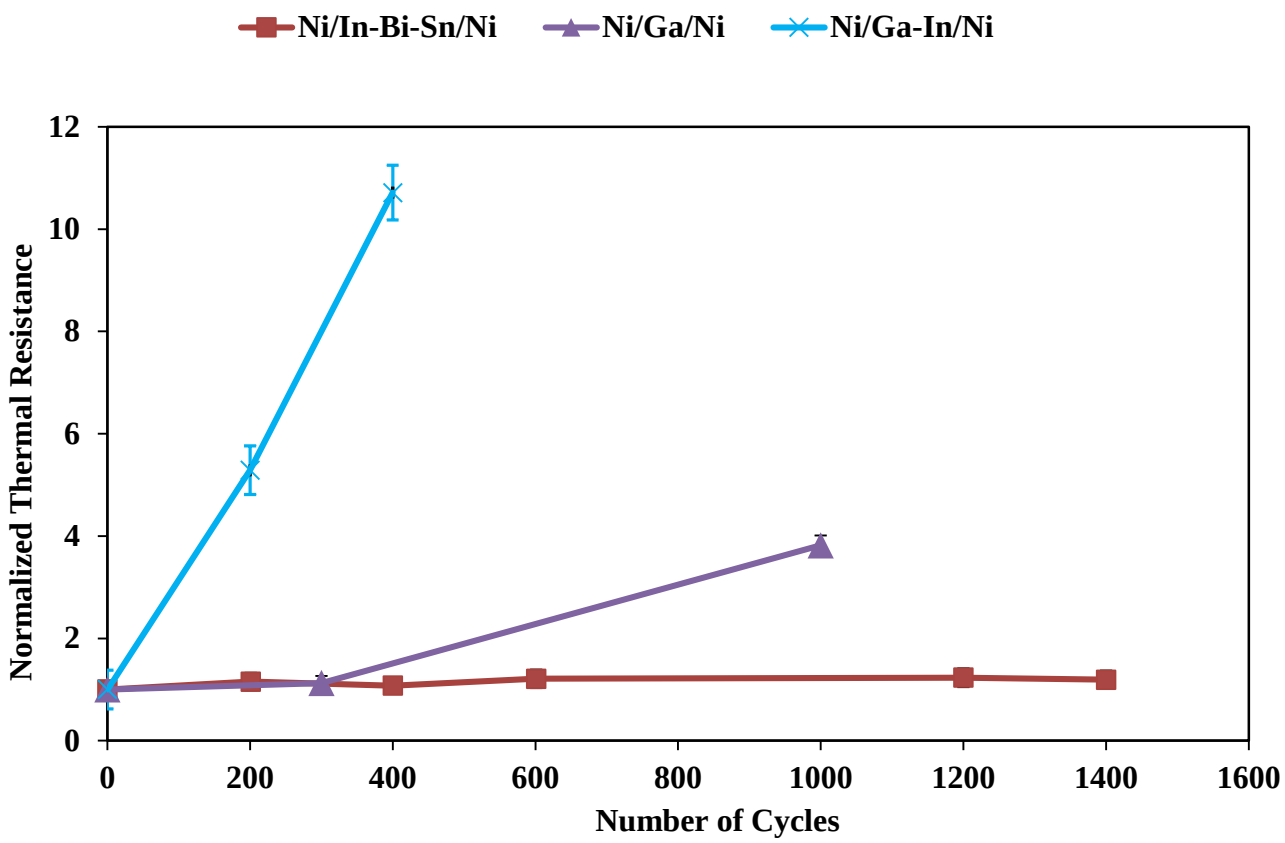

Figure 5.16: Normalized thermal resistance of three alloys placed between nickel surfaces in response to thermal cycling (-40^{o}C to +80^{o}C)

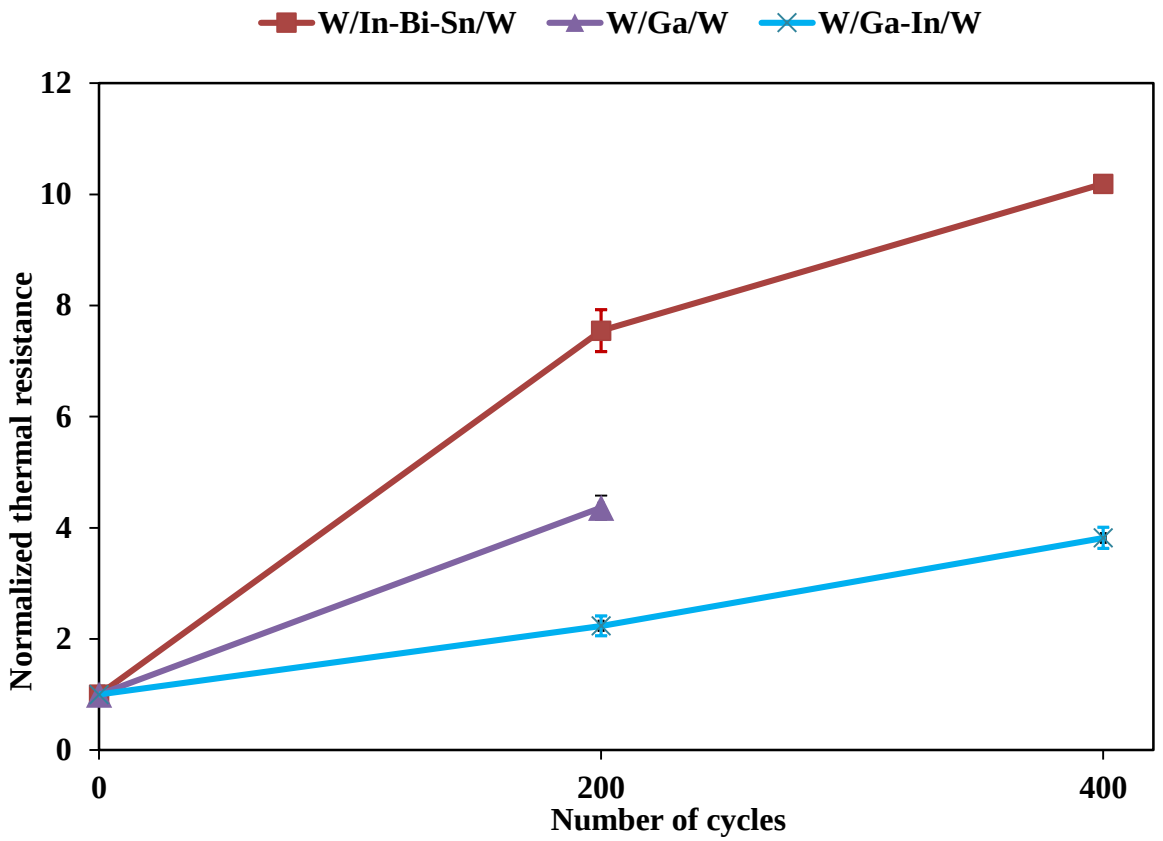

Figure 5.17: Normalized thermal resistance of three alloys placed between tungsten surfaces in response to thermal cycling (-40^{o}C to +80^{o}C)

5.7 Reliability testing (phase 2)

In phase 1 reliability testing described above, the alloys were placed between similar materials (Cu-alloy-Cu, Ni-alloy-Ni and W-alloy-W). In phase 2 testing, the alloys were placed between copper and nickel surfaces (Cu-alloy-Ni) to investigate the reliability of alloys at the interface between dissimilar materials. Then, the alloys were exposed to high temperature aging and thermal cycling as before.

5.7.1 Accelerated thermal aging

Figure 5.18 shows the accelerated thermal aging (at 130^{o}C) behavior of three alloys (Ga-In, Ga, and In-Bi-Sn) placed between copper and nickel surfaces. All tests were carried out at 138 kPa (20 psi) and at a temperature above the melting point of the alloy. The thermal resistances are plotted as a function of aging time and the associated uncertainty is represented by the error bars. It can be noticed from Figure 5.18 that all three alloys offer very low initial thermal resistance and survived as long as 3,000 hours of aging at 130^{o}C without significant performance degradation. The results indicate that the proposed alloys are remarkably reliable at the interface between copper and nickel in terms of high temperature aging. For the Ga-In alloy, a jump in thermal resistance was observed between 1,000-1,500 hours. However, the resistance did not change thereafter (remained within the experimental uncertainty), between 1,500-3,000 hours. The thermal resistance is still lower compared to the performance of any existing commercial TIMs [7,8,12] after such a prolonged exposure to high temperature.

As described above, the superior aging performance of all three alloys is believed to be due to the enhanced wetting of the alloy with the substrate surface and the alloy-substrate interactions. These results suggest that any diffusion and formation of IMCs that may have occurred did not negatively impact the thermal performance over time. However, it was difficult to separate the disks due to the growth of IMCs in the interfacial region. Therefore, rework concerns need to be addressed.

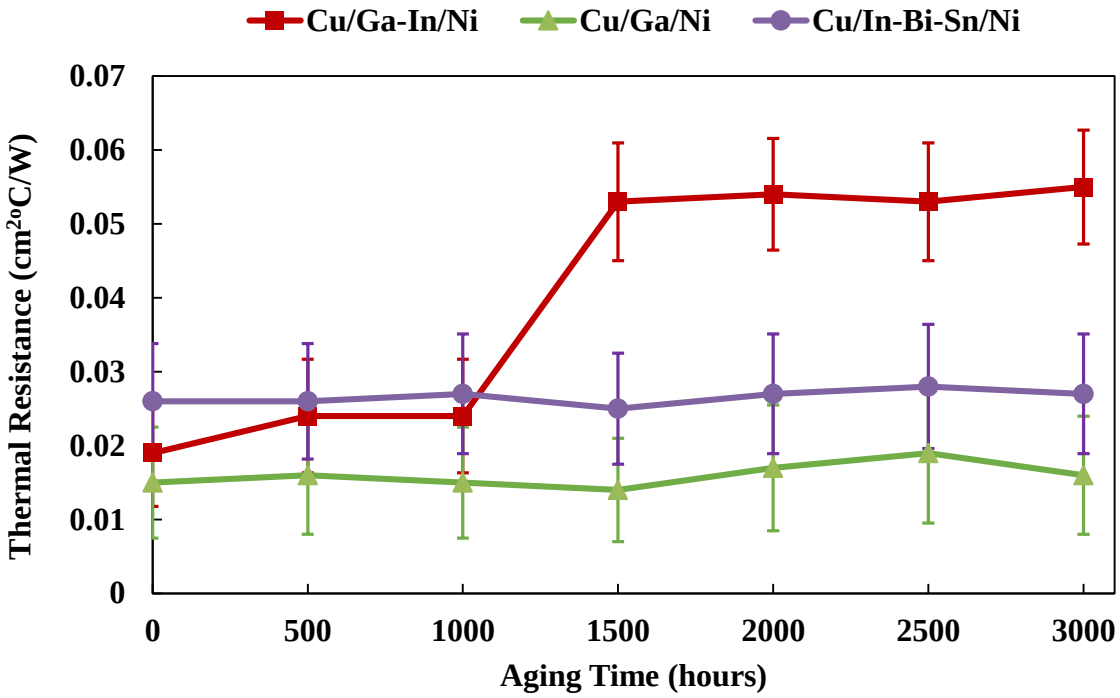

Figure 5.18: Isothermal aging (130°C) performance of Ga-In, Ga, and In-Bi-Sn alloys between copper and nickel surfaces [55]

5.7.2 Thermal cycling

The thermal cycling tests of three alloys between copper and nickel surfaces were carried out in the same manner as before, from -40°C to +80°C. The time needed to complete a thermal cycle was 2 hours.

The results of thermal cycling of three alloys between copper and nickel surfaces are shown in Figure 5.19 below. It is apparent from the figure that Ga and In-Bi-Sn alloys were able to withstand 1,500 cycles (3,000 hours) without significant performance degradation, which indicates an excellent thermal joint. However, for the Ga-In alloy, a jump in thermal resistance (similar to that seen in aging, Figure 5.18) was observed in early cycles between 0-300 cycles. The resistance remains unchanged thereafter. It can be noticed that for the Ga-In alloy, during aging, a jump in

thermal resistance was observed between 1000-1500 hours; however, in cycling, the jump occurred within 600 hours (300 cycles). The expedited jump during cycling can be attributed to the expansion and contraction of the thermal joint in cycling, which causes the degradation to start earlier compared to aging, where the sample kept at constant temperature. Even with the jump in thermal resistance for Ga-In alloy, the performance is still superior to the existing commercial TIMs [7,8,12].

It can be noticed from phase 1 reliability testing that the thermal resistance of Ga and Ga-In alloys when cycled between two nickel surfaces increased significantly (Figure 5.16). However, no degradation was observed for those alloys when cycled between two bare copper surfaces (Figure 5.15). In phase 2 testing, no significant degradation was observed with Ga and Ga-In alloys after cycling between copper and nickel surfaces (Figure 5.19). These results indicate that the alloys interact well with copper, which is primarily due to the diffusion and interfacial reaction. For this reason, when the alloys are in contact with copper at the interface, a more durable thermal joint is formed.

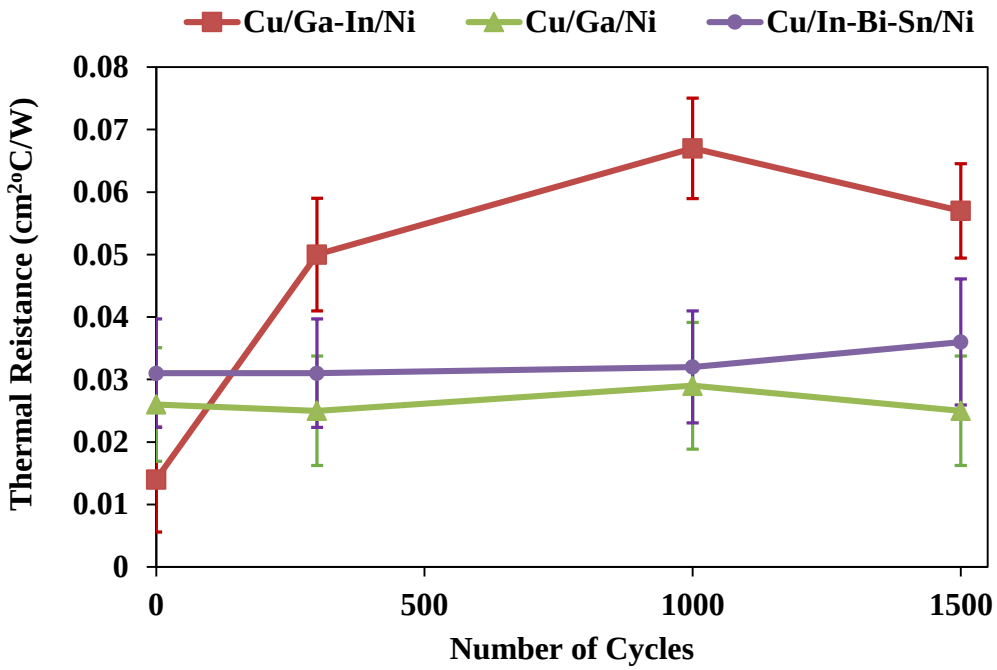

Figure 5.19: Thermal cycling (-40 to +80°C, 2 hours/cycle) of Ga-In, Ga and In-Bi-Sn alloys between copper and nickel surfaces [55]

5.8 Reliability testing (phase 3)

Phase 3 reliability testing includes highly accelerated stress testing at 85°C and 85% relative humidity and thermal cycling from -40°C to +125°C. The alloys were placed between bare copper (Cu/alloy/Cu) surfaces and then carried out the reliability testing.

5.8.1 HAST (highly accelerated stress test)

HAST was carried out by exposing the disks assembly with alloys at the interface at 85°C and 85% relative humidity (RH) for extended periods of time.

Figure 5.20 shows the HAST test results of three alloys (Ga-In, Ga, and In-Bi-Sn) applied between bare copper disk surfaces. All tests were carried out at a temperature above the melting

point of the alloy. The thermal resistances are reported as a function of exposure time and the associated uncertainty is represented by the error bars. In-Bi-Sn alloy was tested in two forms, as a 51 micron (2 mil) sheet and molten (melted first then applied on the heated disk surfaces). It was found that all three alloys (Ga-In, Ga, and In-Bi-Sn) survived as long as 2,016 hours (84 days) of HAST condition without significant thermal performance degradation (remained within the experimental uncertainty). In phase 1 reliability testing, it was shown that that all three alloys between Cu surfaces were able to survive extended exposure at 130°C in absence of humidity (Figure 5.7). This HAST test shows are the alloys also perform well in the presence of humidity, which makes the LMA TIM very promising.

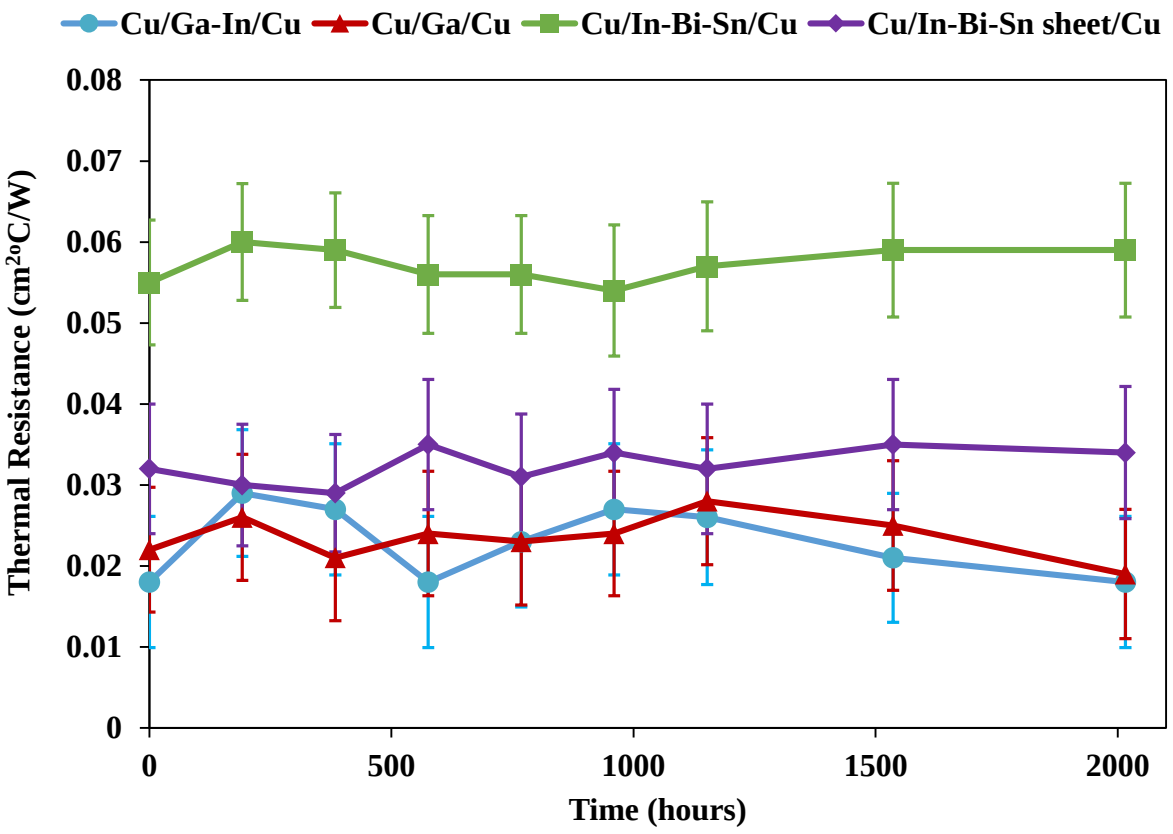

Figure 5.20: HAST results of three alloys between copper surfaces at 85°C and 85% RH

5.8.2 Thermal cycling (-40°C to +125°C)

The third phase thermal cycling test was carried out from -40°C to 125°C. The samples were heated and cooled at the rate of 3.67°C/min and soaked for 15 minutes at the two extreme temperatures, ensuring that the interface reached the chamber temperature. The time needed to complete a thermal cycle was 2 hours.

Thermal cycling results of Ga-In, Ga, and In-Bi-Sn (two forms, molten and 51micron sheet) alloys between copper surfaces are presented in Figure 5.21 below. It is apparent from the figure that Ga-In and Ga alloys survived 500 cycles (1000 hours) without significant increase in thermal resistance. However, for In-Bi-Sn alloy, the thermal resistance increased by about 190 % when applied as 51 micron sheet. In phase one testing (Figure 5.11), it was found that the thermal resistance of 102 micron (4 mil) sheet of In-Bi-Sn alloy increased by about 103% after 500 cycles from -40°C to +80°C. However, due to increase in cycling range (+80°C to +125°C), the degradation is higher (190%) in the current study after the same number of cycles (500). It can be noticed that In-Bi-Sn alloy (in both forms) performed well in response to HAST (Figure 5.20), however, in cycling, performance is degrading with the number of cycles. This is because during cycling the sample experiences expansion and contraction due to heating and cooling of the joint in contrast to HAST where the sample is kept at constant temperature. The expansion and contraction may cause the extrusion of alloy from the interface and thereby create voids at the interface, which in turn increases the thermal resistance.

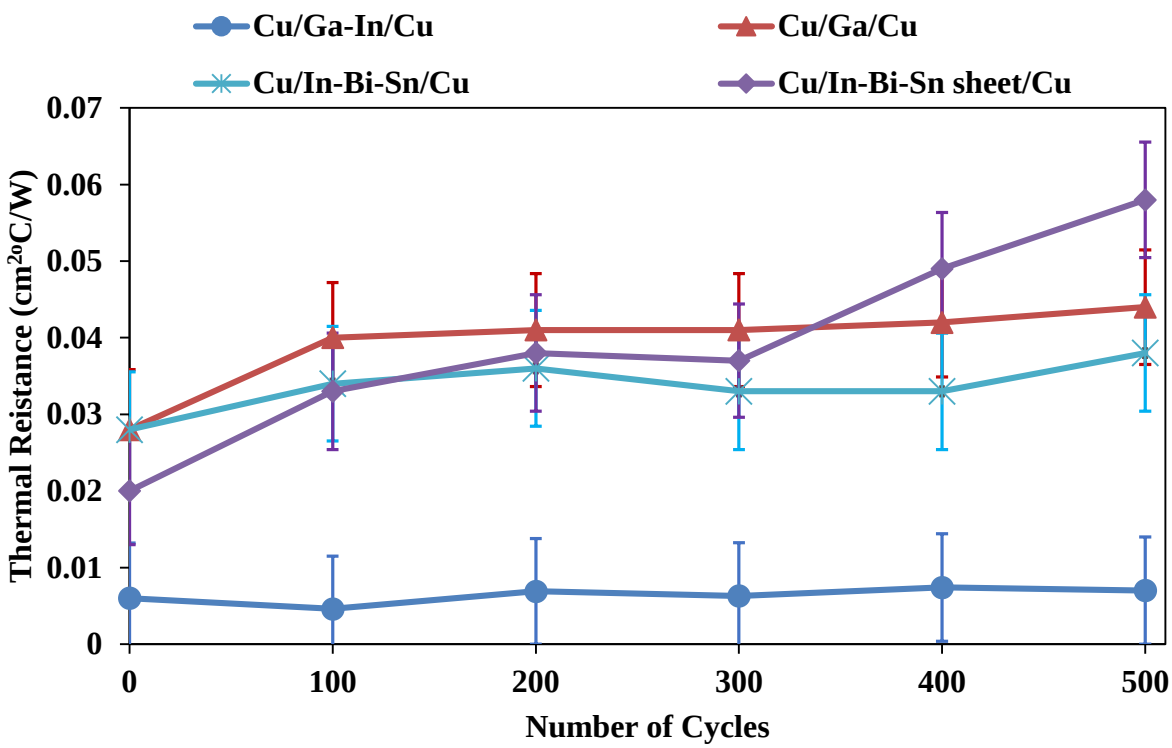

Figure 5.21: Thermal cycling (-40°C to +125°C) of three alloys placed between bare copper disks

5.9 Bond line thickness

LMAs were placed between disks surfaces without any shims or thickness controller. To measure the interfacial thickness, a cross-sectional analysis was carried out using scanning electron microscopy. It was found that the interfacial thickness was about 37 µm with Ga-In alloy placed between bare copper disks as shown in Figure 5.22. As LMAs are thin liquids (viscosity being very low) in molten form, it was expected for them to have a thin BLT and the result confirms this proposition.

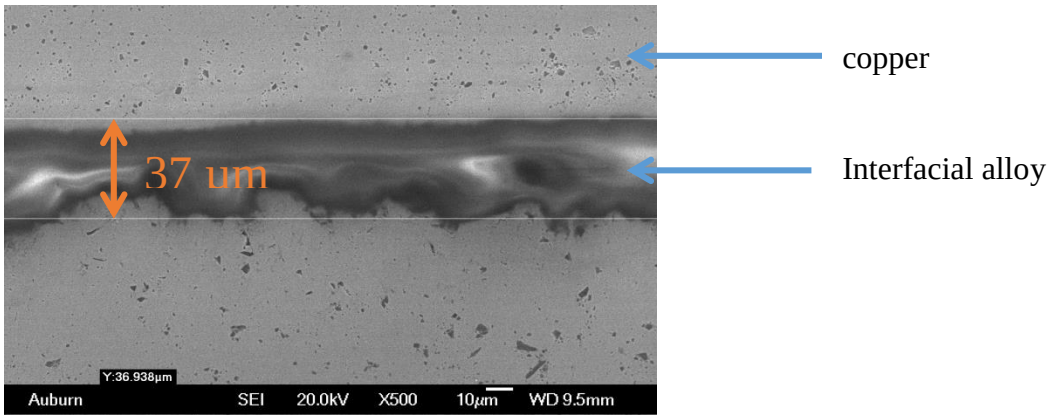

Figure 5.22: SEM cross-sectional image of Ga-In alloy placed between bare copper disks without any shims or thickness controller [54]

5.10 Issues with LMAs

5.10.1 LMA Containment

Confinement is a significant challenge when working with LMAs as TIMs. Since LMAs are a thin (non-viscous) liquid in molten form, it was found that the excess material extruded out from the interface after melting even at the slightest pressure (<0.5 psi). For example, when a 102 micron thick sheet of In-Bi-Sn alloy was placed between copper disks, it was found that upon melting almost 70-80% of the alloy came out of the interface as shown in Figure 5.23a below. This kind of escaping of molten metal from the interface is unwanted and might be detrimental to the system due to the fact that the electrically conductive molten metal can cause short circuits in actual electronics cooling application. The alloy extrusion can be greatly reduced by improving the wetting of the alloy with the mating surfaces which is simply achieved by gently rubbing the molten alloy on the surfaces. For example, when In-Bi-Sn alloy was placed in its molten form

(melted and applied a small amount on the heated disks by scrubbing), it was found that the amount of the alloy extrusion was very little or none in some samples. Since the alloy extrusion is very small in molten state application, it is presumed that only surface tension will hold the alloy in position which would significantly solve the alloy escaping problem. This result is displayed in Figure 5.23b. However, it cannot be understated that containment of the molten LMA is a significant system design concern.

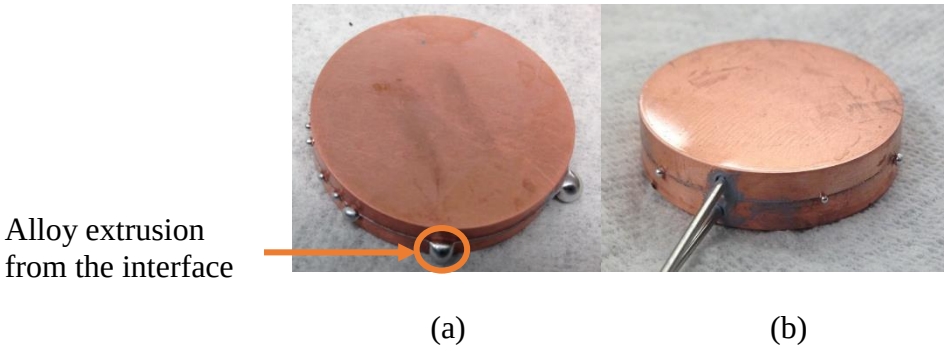

(a) (b)

Figure 5.23: In-B-Sn alloy (a) 102 µm thick sheet after melting (b) molten state application

5.10.2 LMA De-wetting

Another consideration of LMAs as TIMs is dewetting of the alloy over the lifespan of the device. It was found that for In-Bi-Sn alloy (102 micron sheet) between bare copper surfaces, after 500 cycles of thermal cycling from -40^{o}C to +80^{o}C, the thermal resistance increased significantly, up about 115% from the initial value of 0.059 cm^{2o}C/W to 0.127 cm^{2o}C/W. It was observed that the alloy came out of the interface during thermal cycling. Upon separation of the disks after 500 cycles, visual inspection of the interface showed that the alloy did not wet the interface properly (Figure 5.24a). Due to the improper wetting, the alloy extrudes out of the interface upon thermal cycling which is primarily because of the pump-out effect during expansion and contraction of the

substrate and the alloy. The alloy escaping results in the creation of voids at the interface which in turn increases the thermal resistance. After this observation, to enhance the wetting, In-Bi-Sn alloy was first melted and then applied the molten metal onto the heated copper surface by scrubbing (Figure 5.18b). The superior wetting by rubbing is due to the oxidation of the alloy itself. Liu *et al.* [48] while working on a galinstan (68.5Ga, 21.5In & 10Sn) alloy, observed that the alloy did not wet anything in an oxygen free environment (<1 parts per million), however, once the alloy oxidizes, a very thin oxidation layer is formed and that sticks to the surface, gives the illusion that the alloy wets. Gentle rubbing of surfaces with molten alloys using a cotton swab or small brush was found to be effective to induce wetting. The rubbing allows the alloy to oxidize and thus sticks to the surface. Thermal cycling of In-Bi-Sn alloy after this attachment technique was tried and showed a negligible (<%5 from an initial resistance of 0.023 $cm^{2o}C/W$) change in thermal resistance after 500 cycles. Thus, it can be concluded that the improved cycle life of In-Bi-Sn alloy in molten form is due to enhance wetting of the alloy with the disks' surface. Also, this molten state application reduced the amount of material extrusion significantly as discussed above.

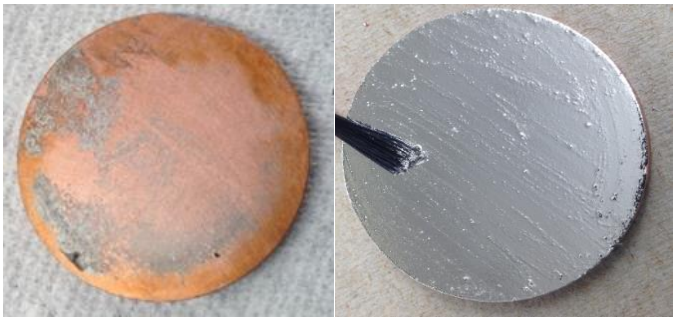

(a) (b)

Figure 5.24: In-Bi-Sn alloy (a) After 500 cycles, poorly wetted (b) A completely wetted surface

One side wetting

To avoid the extrusion of the molten alloy, the LAMs were applied as little as required to wet the surfaces. It was found that by wetting only one copper disk surface with pure Ga resulted in a significant increase in the thermal resistance upon thermal cycling. After 200 cycles from -40^{o}C to +80^{o}C, the thermal resistance was found to increase by about five times. Upon separation, it was observed that the alloy did not wet one disk surface as shown in Figure 5.25. This non-wetting results in a rapid increase in thermal resistance whereas it was shown (Figure 5.12) that wetting both surfaces with Ga between copper surfaces survived a large number of cycles. Thus, it is recommended to apply the alloys on both the mating surfaces, otherwise they won't form a good thermal joint.

Figure 5.25: Pure Ga between bare copper after 200 cycles, one side wetting

5.11 Cost consideration

From an economical point of view, LMAs are very promising. As LMAs are thin (low viscosity) liquids in molten form, only a very small amount (6-9 mg/cm^2) is required to wet the mating surfaces. For example, one gram of pure Ga costs only about $7 and with that it was possible to prepare at least seven samples (two copper disk of 8.55 cm^2 each), which means that

the LMA interface costs about $1 in the present case. This makes LMAs very cost competitive compared to many commercial TIMs.

Chapter 6 : Summary and Conclusions

Performance of TIMs play a crucial role in the thermal management of microelectronics. This study investigates the performance of commercial TIMs such as thermal grease, phase change material, thermal gel and thermal pad as well as low melt alloy as an emerging TIM. Three lead and cadmium free alloys (In-Bi-Sn, Ga, and Ga-In) with different melting points and various compositions were chosen to test the thermal performance. The thermal resistance was measured using the ASTM D5470 standard methodology with a small modification to avoid surface contamination and to facilitate reliability testing. The bare copper substrates were coated with nickel and tungsten to investigate different substrate-alloy interactions. To examine the long-term stability of LMA TIMs, reliability tests were carried out. Reliability tests include isothermal aging at 130^{o}C and thermal cycling from -40^{o}C to +80^{o}C and -40^{o}C to +125^{o}C and HAST (85^{o}C and 85% RH).

In-situ thermal resistance measurement at 138 kPa showed that the thermal resistance of LMAs can be as low as 0.005 cm^{2}°C/W and as high as 0.065 cm^{2}°C/W depending on the specimen preparation. In-situ test was carried out at different pressures from 34.5-345 kPa and results showed that the thermal resistance of LMAs was invariant with applied pressure in this range, which indicates an excellent thermal joint even at a lower pressure. Tests were also carried out at different interface temperatures keeping the pressure constant at 69 kPa (10 psi).

Results showed that the thermal resistances of the LMA joints tested were not sensitive to the interfacial temperature. From this measurements, it can be concluded that once the alloy melts and seats at the interface, the temperature will not affect the thermal performance. Phase 1 reliability tests showed that all three the alloys between bare copper surface were able to endure as long as 2,300 hours of aging at 130^{o}C and 2,800 hours of cycling (1,400 cycles) without deteriorating the thermal performance considerably. Ga and Ga-In alloy between nickel surfaces survived high temperature aging for longer duration (Figure 5.8), however, failed in thermal cycling (Figure 5.16). All three alloys between tungsten surfaces could not endure isothermal aging (Figure 5.9) as well as cycling (Figure 5.17), thermal resistance increased significantly upon these reliability testing, which indicates an inefficient thermal joint. Results suggests that the diffusion barrier layer does not help in improving the thermal performance of alloys. In addition, substrate-alloy interactions (which is primarily diffusion and interfacial reaction) makes the thermal joint more reliable.

In phase 2 testing, when the alloys were placed between different surfaces (copper and nickel), all the alloys survived high temperature aging at 130^{o}C for 3,000 hours (Figure 5.18) and thermal cycling from -40^{o}C TO +80^{o}C for 1,500 cycles (3,000 hours) (Figure 5.19) without significant thermal performance degradation, which indicates the reliability of alloys at the interface between dissimilar materials. Phase 3 reliability tests include highly accelerated stress testing, HAST at 85^{o}C and 85% RH and thermal cycling from -40^{o}C to +125^{o}C of alloys between bare copper surfaces. HAST tests showed that the alloys were able to withstand as long as 2,016 hours (84 days) without significant increase in thermal resistance, which ensures the stability of the LMAs at a high humidity and hot environment. Thermal cycling tests also showed that the

alloys are capable of surviving large number of cycles. All these reliability tests confirm the stability of LMAs as TIMs in a harsh environment.

In conclusion, LMAs are environment and health-friendly unless they contain any mercury, lead or cadmium. In addition, they are easy to apply and commercially available thus manufacturing at high volume would not be an issue. Many widely used commercial TIMs are greases or highly solid-loaded pastes that have a high viscosity and in some cases shear-harden, which makes these types of TIMs more difficult to apply. LMAs are not only more compliant and less viscous but do not shear-harden. Furthermore, LMAs are cost-effective compared to other TIMs. As LMAs are thin liquids in molten form, only a very small amount (6-9 mg/cm^2) is required to wet the mating surfaces, which makes an LMA interface at least 25% cheaper compared to commercial high viscosity greases. However, care must be taken when LMAs are applied at the interface. By choosing a proper substrate-alloy combination, the LMA interface can be made highly reliable.

6.1 Future works

In this work, LMAs are found to be effective when applied between the bare copper and copper-nickel interfaces. In actual processor-heat sink application, the LMAs are usually placed between the die/chip (which is usually made of silicon) and heat sink (which is usually made of copper). Even though it is presumed that LMAs will continue to perform reliably between dissimilar material joints, however, further tests are required to investigate the performance of LMA as TIMs in actual application. Based on the observation, scope for the future work and directions are suggested

- In-situ thermal performance of LMAs in actual processor-heat sink application.

- Reliability testing (high temperature aging, thermal cycling, exposure to humidity) of LMAs at the processor-heat sink interface.
- Identify the intermetallic compounds that form at the interface by scanning electron microscopy or x-ray diffraction techniques.

Bibliography

[1] Prasher, Ravi. "Thermal interface materials: historical perspective, status, and future directions." *Proceedings of the IEEE* 94.8 (2006): 1571-1586.

[2] Gwinn, Joshua P., and R. L. Webb. "Performance and testing of thermal interface materials." *Microelectronics Journal* 34.3 (2003): 215-222

[3] Frank P. Incropera, David P. Dewitt, Theodore L. Bergman, and Adrienne S. Lavine. .*Fundamentals of heat and mass transfer*. 6th edition, John Wiley & Sons, 2007.

[4] Martin, Y., and Kessel, T.V. "High performance Liquid Metal Thermal Interface for Large Volume Production." *IMAPS Thermal and Power Management, San Jose CA* (2007).

[5] Pfahl, Bob, Haley Fu, and Chuck Richardson. "Highlights of iNEMI 2013 technology roadmaps." *Electronic Manufacturing Technology Symposium (IEMT), 2012 35th IEEE/CPMT International*. IEEE, 2012.

[6] Mahajan, R., Nair, R., Wakharkar, V., Swan, J., Tang, J., and Vandentop, G. "Emerging Drirections for Packaging Technologies." *Intel Technology Journal* 6.2 (2002): 62-75.

[7] Wasniewski, Joseph R., David H. Altman, Stephen L. Hodson, Timothy S. Fisher, Anuradha Bulusu, Samuel Graham, and Baratunde A. Cola. "Characterization of metallically bonded carbon nanotube-based thermal interface materials using a high accuracy 1D steady-state technique." *Journal of Electronic Packaging* 134.2 (2012): 020901.

[8] Roy, Chandan K., Sushil Bhavnani, Michael C. Hamilton, R. Wayne Johnson, Jonathan L. Nguyen, Roy W. Knight, and Daniel K. Harris."Investigation into the application of low melting temperature alloys as wet thermal interface materials." *International Journal of Heat and Mass Transfer* 85 (2015): 996-1002.

[9] Chung, D. D. L. "Materials for thermal conduction." *Applied Thermal Engineering* 21.16 (2001): 1593-1605.

[10] Rauch, Bob. "Understanding the performance characteristics of phase-change thermal interface materials." *Thermal and Thermomechanical Phenomena in Electronic Systems, 2000. ITHERM 2000. The Seventh Intersociety Conference on*. Vol. 1. IEEE, 2000.

[11] Blazej, D. "Thermal Interface Materials." *Electronics Cooling*. 9.4 (2003): 14-20.

[12] Roy, Chandan K., Sushil Bhavnani, Mike Hamilton, Wayne R. Johnson, Roy W. Knight, and Daniel K. Harris."Performance of Low Melt Alloys as Thermal Interface Materials." *31st Semiconductor Thermal Measurement and Management Symposium (SEMI-THERM) 2015, IEEE*, 2015

[13] Roy, Chandan K., Sushil Bhavnani, Mike Hamilton, Wayne R. Johnson, Roy W. Knight, and Daniel K. Harris. "Application of Low Melt Alloys as Compliant Thermal Interface Materials: A Study of Performance and Degradation under Thermal Duress." *Electronics Cooling*. June, 2015: 26-31

[14] Prasher, Ravi S., and James C. Matayabas Jr. "Thermal contact resistance of cured gel polymeric thermal interface material." *Components and Packaging Technologies, IEEE Transactions on* 27.4 (2004): 702-709.

[15] Samson E., Sridhar V. Machiroutu, Je-Young Chang, Ishmael Santos, Jim Hermerding, Ashay Dani, Ravi Prasher, and David W. Song. "Some thermal technology and thermal management

considerations in the design of next generation Intel Centrino Mobile Technology platforms." *Intel Technology Journal* 9.1, 2005.

[16] Sarvar, Farhad, David C. Whalley, and Paul P. Conway. "Thermal interface materials-A review of the state of the art." *Electronics Systemintegration Technology Conference, 2006. 1st*. Vol. 2. IEEE, 2006.

[17] Xu, Jun, and Timothy S. Fisher. "Enhancement of thermal interface materials with carbon nanotube arrays." *International Journal of Heat and Mass Transfer*49.9 (2006): 1658-1666.

[18] Cross, Robert, Baratunde A. Cola, Timothy Fisher, Xianfan Xu, Ken Gall, and Samuel Graham. "A metallization and bonding approach for high performance carbon nanotube thermal interface materials." *Nanotechnology*21.44 (2010): 445705.

[19] Tong, Tao, Yang Zhao, Lance Delzeit, Ali Kashani, M. Meyyappan, and Arun Majumdar. "Dense vertically aligned multiwalled carbon nanotube arrays as thermal interface materials." *Components and Packaging Technologies, IEEE Transactions on* 30.1 (2007): 92-100.

[20] Hu, Xuejiao, Linan Jiang, and Kenneth E. Goodson. "Thermal conductance enhancement of particle-filled thermal interface materials using carbon nanotube inclusions." *Thermal and Thermomechanical Phenomena in Electronic Systems, 2004. ITHERM'04. The Ninth Intersociety Conference on*. IEEE, 2004.

[21] Choi, S. U. S., Z. G. Zhang, Wu Yu, F. E. Lockwood, and E. A. Grulke. "Anomalous thermal conductivity enhancement in nanotube suspensions." *Applied physics letters* 79.14 (2001): 2252-2254.

[22] Fabris, Drazen, Michael Rosshirt, Christopher Cardenas, Patrick Wilhite, Toshishige Yamada, and Cary Y. Yang. "Application of carbon nanotubes to thermal interface materials." *Journal of Electronic Packaging* 133.2 (2011): 020902.

[23] Nan, Ce-Wen, Gang Liu, Yuanhua Lin, and Ming Li. "Interface effect on thermal conductivity of carbon nanotube composites." *Applied Physics Letters* 85.16 (2004): 3549-3551.

[24] Goyal, Vivek, and Alexander A. Balandin. "Thermal properties of the hybrid graphene-metal nano-micro-composites: applications in thermal interface materials." *Applied Physics Letters* 100.7 (2012): 073113.

[25] Shahil, Khan MF, and Alexander A. Balandin. "Graphene–multilayer graphene nanocomposites as highly efficient thermal interface materials." *Nano letters*12.2 (2012): 861-867.

[26] Berber, Savas, Young-Kyun Kwon, and David Tománek. "Unusually high thermal conductivity of carbon nanotubes." *Physical review letters* 84.20 (2000): 4613.

[27] Zhu, Lingbo, Dennis W. Hess, and C. P. Wong. "Assembling carbon nanotube films as thermal interface materials." *Electronic Components and Technology Conference, 2007. ECTC'07. Proceedings. 57th*. IEEE, 2007.

[28] Barako, Michael T., Yuan Gao, Amy M. Marconnet, Mehdi Asheghi, and Kenneth E. Goodson. "Solder-bonded carbon nanotube thermal interface materials." *Thermal and Thermomechanical Phenomena in Electronic Systems (ITherm), 2012 13th IEEE Intersociety Conference on*. IEEE, 2012.

[29] Peacock, Melissa A., Chandan K. Roy, Michael C. Hamilton, R. Wayne Johnson, Roy W. Knight, and Daniel K. Harris. "Characterization of transferred vertically aligned carbon

nanotubes arrays as thermal interface materials." *International Journal of Heat and Mass Transfer* 97 (2016): 94-100.

[30] Hone, J., M. C. Llaguno, M. J. Biercuk, A. T. Johnson, B. Batlogg, Z. Benes, and J. E. Fischer."Thermal properties of carbon nanotubes and nanotube-based materials." *Applied Physics A* 74.3 (2002): 339-343.

[31] Cook, R. S., K. H. Token, and R. L. Calkins. "A novel concept for reducing thermal contact resistance." *Journal of Spacecraft and Rockets* 21.1 (1984): 122-124.

[32] Webb, Ralph L., and Joshua P. Gwinn. "Low melting point thermal interface material." *Thermal and Thermomechanical Phenomena in Electronic Systems, 2002. ITHERM 2002. The Eighth Intersociety Conference on*. IEEE, 2002.

[33] Macris, Chris G., Thomas R. Sanderson, Robert G. Ebel, Christopher B. Leyerle, and Enerdyne Solutions. "Performance, reliability, and approaches using a low melt alloy as a thermal interface material." *Proceedings IMAPS*. 2004.

[34] Hill, Richard F., and Jason L. Strader. "Practical utilization of low melting alloy thermal interface materials." *Semiconductor Thermal Measurement and Management Symposium, 2006 IEEE Twenty-Second Annual IEEE*. IEEE, 2006.

[35] Carlberg, Björn, Teng Wang, Yifeng Fu, Johan Liu, and Dongkai Shangguan."Nanostructured polymer-metal composite for thermal interface material applications." *Electronic Components and Technology Conference, 2008. ECTC 2008. 58th*. IEEE, 2008.

[36] Hamdan, A., A. McLanahan, R. Richards, and C. Richards. "Characterization of a liquid–metal microdroplet thermal interface material." *Experimental Thermal and Fluid Science* 35.7 (2011): 1250-1254

[37] Yang, E., Hongyan Guo, Jingdong Guo, Jianku Shang, and Mingguang Wang. "Thermal Performance of Low-Melting-Temperature Alloy Thermal Interface Materials." *Acta Metallurgica Sinica (English Letters)* 27.2 (2014): 290-294.

[38] Shaddock, David, Stanton Weaver, Ioannis Chasiotis, Binoy Shah, and Dalong Zhong. "Development of a compliant nanothermal interface material." *ASME 2011 Pacific Rim Technical Conference and Exhibition on Packaging and Integration of Electronic and Photonic Systems*. American Society of Mechanical Engineers, 2011.

[39] Luo, Xin, Yong Zhang, Carl Zandén, Murali Murugesan, Yu Cao, Lilei Ye, and Johan Liu. "Novel thermal interface materials: boron nitride nanofiber and indium composites for electronics heat dissipation applications." *Journal of Materials Science: Materials in Electronics* 25.5 (2014): 2333-2338.

[40] Wikipedia contributors. "Kopp's law." Wikipedia, The Free Encyclopedia, 22 Nov. 2015. Web. 6 Apr. 2016.

[41] "TCi Thermal Conductivity Analyzer." *How It Works*. C-Therm. Web. 06 Apr. 2016.

[42] Sofia, John W. "Analysis of thermal transient data with synthesized dynamic models for semiconductor devices." *Components, Packaging, and Manufacturing Technology, Part A, IEEE Transactions on* 18.1 (1995): 39-47.

[43] Cola, Baratunde A., Jun Xu, Changrui Cheng, Xianfan Xu, Timothy S. Fisher, and Hanping Hu. "Photoacoustic characterization of carbon nanotube array thermal interfaces." *Journal of applied physics* 101.5 (2007): 054313.

[44] McNamara, Andrew J., Yogendra Joshi, and Zhuomin M. Zhang. "Characterization of nanostructured thermal interface materials–a review."*International Journal of Thermal Sciences* 62 (2012): 2-11.

[45] Kohli, Punit, Martin Sobczak, Jeff Bowin, and Michael Matthews. "Advanced thermal interface materials for enhanced flip chip BGA." *Electronic Components and Technology Conference, 2001. Proceedings., 51st*. IEEE, 2001.

[46] ASTM standard D5470, 2012," Standard Test Method for Thermal Transmission Properties of Thermally Conductive Electrical Insulation Materials", ASTM international, West Conshohocken, PA, 2012, DOI: 10.1520/D5470-12, www.astm.org .

[47] Analysis Tech. *Material Thermal Testers: TIM Tester 1400 Specifications*. 2012. 18 April 2014.

[48] Liu, Tingyi, Prosenjit Sen, and Chang-Jin Kim. "Characterization of nontoxic liquid-metal alloy galinstan for applications in microdevices."*Microelectromechanical Systems, Journal of* 21.2 (2012): 443-450.

[49] DeVoto, Douglas, Paul Paret, Mark Mihalic, Sreekant Narumanchi, Avram Bar-Cohen, and Kaiser Matin. "Thermal performance and reliability characterization of bonded interface materials (BIMs)." *Thermal and Thermomechanical Phenomena in Electronic Systems (ITherm), 2014 IEEE Intersociety Conference on*. IEEE, 2014.

[50] Kim, Dae-Gon, Jeong-Won Yoon, Chang-Youl Lee, and Seung-Boo Jung. "Reaction Diffusion and Formation of Cu11In9 and In27Ni10 Phases in the Couple of Indium-Substrates." *Materials Transactions* 44.1 (2003): 72-77.

[51] Roy, Chandan K., Sushil Bhavnani, Michael C. Hamilton, R. Wayne Johnson, Roy W. Knight, and Daniel K. Harris. "Accelerated aging and thermal cycling of low melting temperature alloys as wet thermal interface materials." *Microelectronics Reliability* 55.12 (2015): 2698-2704.

[52] Ancharov, A. I., T. F. Grigoryeva, A. P. Barinova, and V. V. Boldyrev. "Interaction between copper and gallium." *Russian Metallurgy (Metally)* 2008.6 (2008): 475-479.

[53] Schmetterer, Clemens, Hans Flandorfer, Christian L. Lengauer, Jean-Pierre Bros, and Herbert Ipser. "The system Ga–Ni: A new investigation of the Ga-rich part." *Intermetallics* 18.2 (2010): 277-285.

[54] Roy, Chandan K., Sushil Bhavnani, Michael C. Hamilton, R. Wayne Johnson, Roy W. Knight, and Daniel K. Harris "Durability of low melt alloys as thermal interface materials." *J. Electron. Packag* 138.1 (2016): doi: 10.1115/1.4032462.

[55] Roy, Chandan K., Sushil Bhavnani, Michael C. Hamilton, R. Wayne Johnson, Roy W. Knight, and Daniel K. Harris "Thermal performance of low melting temperature alloys at the interface between dissimilar materials." *Applied Thermal Engineering* 99 (2016): 72-79

Appendix

Simulation data for calculation of Probe disturbance

Probe angle (Degree)	Probe location *l* (mm)	TIM top surface T_{max} (^oC)	TIM top surface T_{min} (^oC)	ΔT_{upper} (T_{max}-T_{min}) (^oC)	ΔT_{TIM} (^oC)	Disturbance $\Delta T_{upper}/ \Delta T_{TIM}$ (%)
0	0.8	27.0157	26.9142	0.1015	0.2322	43.71
	1.6	27.0198	26.9806	0.0392	0.2321	16.89
	2.4	26.9732	26.9381	0.0351	0.2313	15.17
90	0.8	27.2242	26.696	0.5282	0.2325	227.18
	1.6	27.271	27.0065	0.2645	0.2358	112.17
	2.4	27.0216	26.8521	0.1695	0.2309	73.41
180	0.8	27.2098	26.6843	0.5255	0.2322	226.31
	1.6	27.0971	26.8393	0.2578	0.2319	111.17
	2.4	27.0352	26.8596	0.1756	0.2313	75.92

Thermal resistance calculation

Sample thermal resistance calculation for Cu/In-Bi-Sn/Cu (sample 1 in Figure 5.1)

Thermistor readings, T_1=68.65ºC and T_2=64.71ºC

Heat flux, q"= 40.92W/cm^2

Probe location, *l*=0.16 cm (1.6 mm)

Thermal conductivity of copper alloy 110, k =3.88W/cmºC

Solve for ΔT using the equation presented in equation 3-8 gives,

$$\Delta T = T_{s1} - T_{s2} = T_1 - T_2 - \frac{2q''l}{k} = 68.65^oC - 64.71^oC - \frac{2*40.92\frac{W}{cm^2}*0.16\ cm}{3.88\frac{W}{cm^oC}} = 0.57\ ^oC.$$

Now, thermal resistance of the LMA TIM is calculated as

$$R_{th} = \frac{\Delta T}{q''} = \frac{0.57\ ^oC}{40.92\ \frac{W}{cm^2}} = 0.014\ cm^2{}^oC/W.$$